

# Equilibrium transport with time-inconsistent costs: An application to matching problems in the job market

Erhan Bayraktar \*      Bingyan Han †

August 27, 2024

## Abstract

Given two probability measures on sequential data, we investigate the transport problem with time-inconsistent preferences in a discrete-time setting. Motivating examples are nonlinear objectives, state-dependent costs, and regularized optimal transport with general  $f$ -divergence. Under the bicausal constraint, we introduce the concept of equilibrium transport. Existence is proved in the semi-discrete Markovian case and the continuous non-Markovian case with strict quasiconvexity, while uniqueness also holds in the second case. We apply our framework to study inertia of two job markets, top-ranking executives and academia. The empirical analysis shows that a job market with stronger inertia is less efficient. The University of California (UC) postdoc job market has the strongest inertia even than that of executives, while there is no evidence of inertia in the UC faculty job market.

**Keywords:** Dynamic programming; time-inconsistent costs; bicausal optimal transport; job market

## 1 Introduction

Optimal transport (OT) is a method for quantifying the discrepancy between two probability distributions. The origins of OT can be traced back to Monge’s mass transfer problem in the 18th century. However, it was not until the advent of linear programming in the mid 20th century that OT was revitalized by Kantorovich. Brenier (1991) and Gangbo and McCann (1996) provided new insights into OT through the lens of convex analysis and geometry. Nowadays, OT is recognized as an interdisciplinary tool with a wide range of applications in fields such as mathematics (Villani, 2009), machine learning (Arjovsky et al., 2017; Peyré and Cuturi, 2019), statistics (Torous et al., 2021), distributionally robust optimization (Blanchet and Murthy, 2019; Gao and Kleywegt, 2022; Mohajerin Esfahani and Kuhn, 2018), and quantitative economics (Galichon, 2016; Gabaix and Landier, 2008).

While most literature on OT has focused on static data without a chronological structure, temporal data are ubiquitous in finance, statistics, and optimization. To address this, Lassalle (2013) introduced causal optimal transport (COT), which imposes a causality constraint on the transport plans between discrete stochastic processes. In a less formal sense, COT requires that

---

\*Department of Mathematics, University of Michigan, Ann Arbor, Email: erhan@umich.edu.

†Thrust of Financial Technology, The Hong Kong University of Science and Technology (Guangzhou), Email: bingyanhan@hkust-gz.edu.cn.

when the past of one process,  $X$ , is given, the past of another process,  $Y$ , should be independent of the future of  $X$  under the transport plan. COT has found applications in mathematical finance (Backhoff-Veraguas et al., 2020), video modeling (Xu et al., 2020), mean-field games (Acciaio et al., 2021; Backhoff-Veraguas and Zhang, 2023), and stochastic optimization (Pflug and Pichler, 2012, 2014; Acciaio et al., 2020).

When making decisions over time, humans often exhibit time inconsistency, where the optimal plan at the present moment is not followed in the future. To address this, consistent planning is suggested as a remedy by Strotz (1955). Time inconsistency is observed in non-exponential discounting (Strotz, 1955; Laibson, 1997), prospect theory (Kahneman and Tversky, 1979), gambling behaviors (Barberis, 2012), and mean-variance portfolio selection (Basak and Chabakauri, 2010). Mathematical models with time inconsistency include variants of portfolio selection (Björk and Murgoci, 2014; Björk et al., 2014, 2017; Han et al., 2021; Kováčová and Rudloff, 2021), optimal stopping (Bayraktar et al., 2021; Pichler et al., 2022), robust decision-making (Epstein and Ji, 2022), probability distortion (Ma et al., 2021), and risk measures in Pflug and Pichler (2014, Chapter 5) and Föllmer and Schied (2011, Chapter 11).

In this paper, we generalize the classic Monge-Kantorovich problem to a dynamic setting with time-inconsistent costs. Suppose transport plans are bicausal in the sense that two processes are causal with respect to each other. The cost function is allowed to include time-inconsistent preferences such as nonlinear objectives and state dependence. Moreover, we notice that regularization with general  $f$ -divergence (Bayraktar et al., 2022; Taşkesen et al., 2023; González-Sanz and Nutz, 2024) can also be a new source of time inconsistency. To address the self-contradictory behavior and the violation of dynamic programming principle (henceforth DPP), we adopt the subgame Nash equilibria solution as in Björk and Murgoci (2014); Basak and Chabakauri (2010). This concept, given formally in Definition 2.2, is well-defined and easy to understand in a discrete-time setting.

Our main technical contribution lies in characterizing equilibrium transport in Definition 2.2 with an extended DPP framework. Lemma 3.3 and Theorem 3.5 establish the existence of equilibrium transport under a semi-discrete setting with Markovian dynamics. The assumptions imposed in Theorem 3.5 are comparable to the classic assumptions in Villani (2009, Theorem 4.1) and straightforward to verify. Our proof involves refining the Polish topology recursively, drawing on Kechris (2012, Theorem 13.11). Several fundamental claims need to be checked carefully under the refined topology. A crucial topological result is that the weak topology on  $\Pi(\mu(dx_{t+1}|x_t), \nu(dy_{t+1}|y_t))$  relies solely on the Borel structure, rather than the topological one. Our proof technique is still new in the well-studied literature on measurable selection and DPP. Theorem 4.5 proves the existence and uniqueness of parametric couplings in a continuous, non-Markovian setting under a strict quasiconvexity assumption, leveraging Berge’s maximum theorem. Section 5.2 provides a concrete example illustrating Theorem 4.5. In contrast to the existence of equilibrium controls (Bayraktar and Han, 2023), the proof techniques in this paper are tailored for OT and rely heavily on the topological and Borel structures of probability spaces.

Our framework introduces a novel methodology with broad interdisciplinary applications. We provide two illustrative examples in Section 5 and conduct an empirical study in two job markets in Sections 7 and 8:

- (1) The first example in Section 5.1 explores dynamic matching between supply and demand types with a mean-variance objective. The types are horizontally differentiated, where closer type matches result in lower costs. Equilibrium transport may either increase or decrease the probability of mismatches, depending on the current state. Numerically, finding an equilibrium transport is more straightforward than determining a pre-committed OT, as the former is a local optimizer and suitable for parallelized algorithms. The subsequent example in Sec-

tion 5.2 involving Gaussian data has explicit and unique equilibrium parametric transport, while the pre-committed optimal parametric transport is not unique.

- (2) In the empirical study, we investigate positive assortative matching (PAM) in the executive job market (Gabaix and Landier, 2008), which suggests that larger firms should hire more talented top executives and offer higher salaries. However, empirical data sometimes deviate from the expected firm size-wage relationship, leading us to investigate why PAM may not always apply. We conjecture that various factors, such as regulatory constraints, financial performance momentum, and status quo bias, incentivize firms to maintain the previous firm-wage matching, irrespective of the PAM principle. Section 6 introduces a novel job market model incorporating a state-dependent term to capture the persistence or inertia in maintaining previous matching, enabling a quantification of the underlying motivations shaping labor market dynamics.

In Sections 7 and 8, we observe that a job market is less efficient when its inertia represented by state dependence is stronger. Notably, industries like Consumer Discretionary, Real Estate, and Information Technology show weak correlations between net sales and wages over the past five years, coinciding with higher levels of inertia. Furthermore, our analysis extends to the academic job market within the University of California (UC) system. In Section 8, we highlight the consistent alignment of faculty wages in Business, Economics, and Engineering departments with U.S. News rankings, without any inertia effects. However, median wages of postdocs from all departments are highly inconsistent with university rankings. The postdoc job market demonstrates even stronger inertia compared with top executives in any industry, a phenomenon often overlooked in literature.

- (3) We provide practical techniques to improve robustness, such as a data-driven clustering method detailed in Section 7.2.1 and a model validation process utilizing synthetic data and bootstrapping in Section 7.2.3. These approaches guarantee the resilience of our results against the noise in net sales and wage data. The Python code is accessible on the GitHub repository: <https://github.com/hanbingyan/equitrans>.

The rest of the paper is organized as follows. We introduce the usual weak topology and bicausal OT in Sections 1.1 and 1.2. Section 2 presents motivations for equilibrium transport and characterization in the discrete case. Section 3 considers the semi-discrete and Markovian case. Section 4 presents the continuous and non-Markovian case. Section 5 gives two illustrative examples. Section 6 introduces a new job market model with inertia measured by state dependence. Sections 7 and 8 apply the model to executive and academic job markets. Technical proofs are deferred to Section A in the e-companion. Sections B and C in the e-companion give some supplementary Tables and Figures.

## 1.1 Notation and the usual weak topology

Denote the finite number of periods as  $T$ . For each  $t \in \{1, \dots, T\}$ , consider a Polish (complete, separable, and metrizable) space  $(\mathcal{X}_t, \mathcal{T}_{\mathcal{X}_t})$ , where  $\mathcal{X}_t$  is a closed (but not necessarily bounded) subset of  $\mathbb{R}^d$ .  $\mathcal{X}_t$  is interpreted as the range of the process at time  $t$ . Let  $C(\mathcal{X}_t; \mathcal{T}_{\mathcal{X}_t})$  be the set of continuous functions  $f : (\mathcal{X}_t, \mathcal{T}_{\mathcal{X}_t}) \rightarrow (\mathbb{R}, \mathcal{T}_{\mathbb{R}})$ , where  $\mathbb{R}$  is always equipped with the usual topology  $\mathcal{T}_{\mathbb{R}}$ .  $C_b(\mathcal{X}_t; \mathcal{T}_{\mathcal{X}_t})$  is the set of continuous and bounded functions. Denote  $\mathcal{B}(\mathcal{T}_{\mathcal{X}_t})$  as the Borel  $\sigma$ -algebra of the topological space  $(\mathcal{X}_t, \mathcal{T}_{\mathcal{X}_t})$ .

In this paper, we always endow the product space with the product topology.  $\mathcal{X}_{1:T} := \mathcal{X}_1 \times \dots \times \mathcal{X}_T$  is a closed subset of  $\mathbb{R}^{T \times d}$  with the product topology  $\mathcal{T}_{\mathcal{X}} := \prod_{t=1}^T \mathcal{T}_{\mathcal{X}_t}$ , which is also Polish.

With some abuse of notation, we simply write  $\mathcal{X}$  while we mean  $\mathcal{X}_{1:T}$ . By Kallenberg (2021, Lemma 1.2), the Borel  $\sigma$ -algebra of the product space satisfies  $\mathcal{B}(\mathcal{X}) = \mathcal{B}(\mathcal{X}_1) \otimes \cdots \otimes \mathcal{B}(\mathcal{X}_T)$ .

Denote the set of all Borel probability measures on  $\mathcal{X}$  as  $\mathcal{P}(\mathcal{X})$ . As in Bertsekas and Shreve (1978, Section 7.4.2) and Parthasarathy (2005, Section II.6), the usual weak topology is defined as follows. For a given  $\varepsilon > 0$ ,  $\mu \in \mathcal{P}(\mathcal{X})$ , and  $f \in C_b(\mathcal{X}; \mathcal{T}_{\mathcal{X}})$ , define the subset of  $\mathcal{P}(\mathcal{X})$  as

$$V(\mu; f, \varepsilon) := \left\{ \mu' \in \mathcal{P}(\mathcal{X}) : \left| \int f d\mu - \int f d\mu' \right| < \varepsilon \right\}.$$

Consider the collection of these subsets as

$$V[C_b(\mathcal{X}; \mathcal{T}_{\mathcal{X}})] := \{V(\mu; f, \varepsilon) : \varepsilon > 0, \mu \in \mathcal{P}(\mathcal{X}), f \in C_b(\mathcal{X}; \mathcal{T}_{\mathcal{X}})\}.$$

We endow  $\mathcal{P}(\mathcal{X})$  with  $\mathcal{V}[C_b(\mathcal{X}; \mathcal{T}_{\mathcal{X}})]$ , the weakest topology on  $\mathcal{P}(\mathcal{X})$  which contains the collection  $V[C_b(\mathcal{X}; \mathcal{T}_{\mathcal{X}})]$ . By Parthasarathy (2005, Theorems 6.2 and 6.5),  $(\mathcal{P}(\mathcal{X}), \mathcal{V}[C_b(\mathcal{X}; \mathcal{T}_{\mathcal{X}})])$  is a Polish topological space if and only if  $(\mathcal{X}, \mathcal{T}_{\mathcal{X}})$  is so.

In the OT theory, we need to consider another closed set  $\mathcal{Y} = \mathcal{Y}_{1:T} = \mathcal{Y}_1 \times \dots \times \mathcal{Y}_T$ . We also equip each factor space  $\mathcal{Y}_t$  with a Polish topology  $\mathcal{T}_{\mathcal{Y}_t}$  and other notations are introduced similarly as in the counterparts for  $\mathcal{X}$ .

For notational convenience, we interpret  $\mathcal{X}_{1:t}$ ,  $\mathcal{X}_{1:t} \times \mathcal{Y}_{1:t}$ , and other similar terms as the product of factor spaces with indices in  $1, \dots, t$ . For a Borel probability measure  $\mu$  on temporal data, we denote  $\mu(dx_{t+1:T}|x_{1:t})$  as a regular conditional probability kernel of  $x_{t+1:T}$  given  $x_{1:t}$ , which is uniquely determined in a suitable way (Bogachev, 2007, Theorem 10.4.14 and Corollary 10.4.17). When there is no confusion, we also write the kernel as  $\mu^t$  for simplicity. If  $\mu$  is a finite discrete measure, we sometimes use  $\mu(x_{t+1:T}|x_{1:t})$ , which omits the differential, as the conditional probability at the atom  $x_{t+1:T}$  given  $x_{1:t}$ . The initial state at time 0 is always fixed.

We emphasize that metrics and Wasserstein distances are introduced for the continuous case in Section 4 only. The semi-discrete case in Section 3 does not rely on a specific choice of the metric.

## 1.2 Bicausal optimal transport

There is a vast literature on the OT theory and its applications (Villani, 2009; Kuhn et al., 2019; Blanchet et al., 2021). However, the previous works have been focusing on data without the time dimension. Motivated by the ubiquitous role of temporal data in OR/MS, finance, and economics, a new notion of adapted Wasserstein distance or causal optimal transport (COT) has been proposed to compare distributions on temporal data (Lassalle, 2013; Backhoff-Veraguas et al., 2017). We present a brief review in this subsection.

Consider two probability measures  $\mu \in \mathcal{P}(\mathcal{X})$  and  $\nu \in \mathcal{P}(\mathcal{Y})$ . Denote  $\Pi(\mu, \nu)$  as the set of all the couplings that admit  $\mu$  and  $\nu$  as marginals. Suppose transporting one unit of mass from  $x$  to  $y$  incurs a cost of  $c(x, y)$ . A generic OT problem is formulated as

$$\mathcal{W}(\mu, \nu) := \inf_{\pi \in \Pi(\mu, \nu)} \int_{\mathcal{X} \times \mathcal{Y}} c(x, y) \pi(dx, dy).$$

If the data have a temporal structure as  $x = (x_1, \dots, x_t, \dots, x_T)$  and  $y = (y_1, \dots, y_t, \dots, y_T)$ , not all couplings  $\pi \in \Pi(\mu, \nu)$  will make sense. A natural requirement of the transport plan  $\pi(x, y)$  should be the non-anticipative condition. Informally speaking, if the past of  $x$  is given, then the past of  $y$  should be independent of the future of  $x$  under the measure  $\pi$ . Mathematically, it means a transport plan  $\pi$  should satisfy

$$\pi(dy_t|x_{1:T}) = \pi(dy_t|x_{1:t}), \quad t = 1, \dots, T-1, \quad \pi\text{-a.s.} \quad (1.1)$$

The property (1.1) is known as the causality condition from  $x$  to  $y$  and the transport plan satisfying (1.1) is called *causal* by Lassalle (2013). It can be interpreted by the equivalent formulation:  $y_t = F_t(x_{1:t}, U_t)$ ,  $\forall t \in 1, \dots, T$ , for some measurable functions  $F_t$  and uniform random variables  $U_t$ . Crucially,  $U_t$  is independent of  $x_{1:T}$ , but the  $\{U_t\}_{t=1}^T$  need not to be independent of each other; see Kallenberg (2021, Theorem 8.17) and Backhoff-Veraguas et al. (2017).

If (1.1) holds when we exchange the positions of  $x$  and  $y$ , then the transport plan is called bicausal. Denote  $\Pi_{bc}(\mu, \nu)$  as the set of all bicausal transport plans between  $\mu$  and  $\nu$ . The bicausal OT problem considers the optimization over  $\Pi_{bc}(\mu, \nu)$  only:

$$\mathcal{W}_{bc}(\mu, \nu) := \inf_{\pi \in \Pi_{bc}(\mu, \nu)} \int_{\mathcal{X} \times \mathcal{Y}} c(x, y) \pi(dx, dy). \quad (1.2)$$

For applications of (bi)causal OT, see Backhoff-Veraguas et al. (2020); Xu et al. (2020); Acciaio et al. (2021); Pflug and Pichler (2012); Acciaio et al. (2020) for an incomplete list.

In this paper, we consider two probability measures  $\mu$  and  $\nu$  with symmetric positions and focus on the bicausal transport plans only. For a given transport plan  $\pi \in \Pi(\mu, \nu)$ , we can decompose  $\pi$  in terms of successive regular kernels:

$$\pi(dx_{1:T}, dy_{1:T}) = \bar{\pi}(dx_1, dy_1) \prod_{s=1}^{T-1} \pi(dx_{s+1}, dy_{s+1} | x_{1:s}, y_{1:s}). \quad (1.3)$$

By Backhoff-Veraguas et al. (2017, Proposition 5.1),  $\pi$  is a bicausal transport plan if and only if

- (1)  $\bar{\pi} \in \Pi(p_*^1 \mu, p_*^1 \nu)$ , and
- (2) for each  $t = 1, \dots, T - 1$  and  $\pi$ -almost every path  $(x_{1:t}, y_{1:t})$ , the following condition holds:

$$\pi(dx_{t+1}, dy_{t+1} | x_{1:t}, y_{1:t}) \in \Pi(\mu(dx_{t+1} | x_{1:t}), \nu(dy_{t+1} | y_{1:t})).$$

$p_*^1 \mu$  (resp.  $p_*^1 \nu$ ) is the pushforward of  $\mu$  (resp.  $\nu$ ) by the projection  $p^1$  onto the first coordinate.

## 2 Equilibrium transport

Time-consistent problems satisfy the Bellman equation. If a solution is optimal on the time interval  $\{t, \dots, T - 1\}$ , then it is also optimal on any subinterval  $\{s, \dots, T - 1\}$  with  $s \geq t$ . However, there are various time-inconsistent preferences (Strotz, 1955; Kahneman and Tversky, 1979; Laibson, 1997; Basak and Chabakauri, 2010). In this context, we present three instances where time inconsistency arises in the bicausal OT problem, with the regularization case being particularly noteworthy and previously unnoticed.

### 2.1 Motivation

#### 2.1.1 Regularized bicausal OT

In practice, continuous densities are approximated by empirical measures with finite supports. The computational burden of discrete OT can be high, then regularization is adopted in implementation (Cuturi, 2013; Pichler and Weinhardt, 2022; Eckstein and Pammer, 2024; González-Sanz and Nutz, 2024). The discrete bicausal OT with regularization is

$$\inf_{\pi \in \Pi_{bc}(\mu, \nu)} \langle c(x_{1:T}, y_{1:T}), \pi(x_{1:T}, y_{1:T}) \rangle_F + \left\langle f \left( \frac{\pi(x_{1:T}, y_{1:T})}{\mu(x_{1:T}) \otimes \nu(y_{1:T})} \right), \mu(x_{1:T}) \otimes \nu(y_{1:T}) \right\rangle_F \quad (2.1)$$

for a convex function  $f$ . The last term is known as the  $f$ -divergence. Here,

$$\langle c(x_{1:T}, y_{1:T}), \pi(x_{1:T}, y_{1:T}) \rangle_F = \sum_{x_{1:T} \in \mathcal{X}, y_{1:T} \in \mathcal{Y}} c(x_{1:T}, y_{1:T}) \pi(x_{1:T}, y_{1:T}),$$

which sums over all paths. The arguments  $(x_{1:T}, y_{1:T})$  in  $\langle c(x_{1:T}, y_{1:T}), \pi(x_{1:T}, y_{1:T}) \rangle_F$  should be interpreted as dummy variables similar in the integral (1.2).  $\mu \otimes \nu$  is the independent coupling and  $\frac{\pi}{\mu \otimes \nu}$  is interpreted as an element-wise division.

A popular choice of  $f(\cdot)$  is the Kullback–Leibler (KL) divergence given by  $f(x) = x \ln(x)$ . In this case, the regularized objective (2.1) is still time-consistent. Indeed, the KL divergence is separable in the sense that

$$\begin{aligned} & \text{KL}(\pi(x_{1:T}, y_{1:T}) \| \mu(x_{1:T}) \otimes \nu(y_{1:T})) \\ &= \left\langle \ln \left( \frac{\pi(x_{1:T}, y_{1:T})}{\mu(x_{1:T}) \otimes \nu(y_{1:T})} \right), \pi(x_{1:T}, y_{1:T}) \right\rangle_F \\ &= \left\langle \left\langle \ln \left( \frac{\pi(x_T, y_T | x_{1:T-1}, y_{1:T-1})}{\mu(x_T | x_{1:T-1}) \otimes \nu(y_T | y_{1:T-1})} \right), \pi(x_T, y_T | x_{1:T-1}, y_{1:T-1}) \right\rangle_F \right. \\ & \quad \left. + \ln \left( \frac{\pi(x_{1:T-1}, y_{1:T-1})}{\mu(x_{1:T-1}) \otimes \nu(y_{1:T-1})} \right), \pi(x_{1:T-1}, y_{1:T-1}) \right\rangle_F. \end{aligned} \quad (2.2)$$

For simplicity, we denote the successive regular kernels of  $\pi(x_{1:T}, y_{1:T})$  as  $\{\bar{\pi}, \pi_1, \dots, \pi_{T-1}\}$ . For example,  $\pi_{T-1} = \pi(x_T, y_T | x_{1:T-1}, y_{1:T-1})$ . The second equality (2.2) shows that the optimization over  $\pi_{T-1}$  is only determined by the first term. We can repeat the decomposition on the second term recursively over time. The classic DPP is applicable in this setting. If  $\{\pi_t^*, \dots, \pi_{T-1}^*\}$  is optimal on the interval  $\{t, \dots, T-1\}$ , then  $\{\pi_s^*, \dots, \pi_{T-1}^*\}$  is also optimal on the subinterval  $\{s, \dots, T-1\}$  with  $s > t$ .

However, the entropic regularization can be numerically unstable and fails to preserve transport plan sparsity, prompting exploration of alternative choices for  $f(\cdot)$  as discussed in Bayraktar et al. (2022). Notably, Taşkesen et al. (2023, Proposition 3.5 and Theorem 3.7) proved that some  $f$ -divergence regularization in the primal problem is equivalent to the so-called smooth  $c$ -transform in the dual problem.

Some non-separable examples with time inconsistency are

- (1) Squared Hellinger distance:  $f(x) = (1 - \sqrt{x})^2$ . The  $f$ -divergence term becomes

$$\left\langle f \left( \frac{\pi(x_{1:T}, y_{1:T})}{\mu(x_{1:T}) \otimes \nu(y_{1:T})} \right), \mu(x_{1:T}) \otimes \nu(y_{1:T}) \right\rangle_F = 2 - 2 \left\langle \sqrt{\pi(x_{1:T}, y_{1:T})}, \sqrt{\mu(x_{1:T}) \otimes \nu(y_{1:T})} \right\rangle_F.$$

- (2) Le Cam distance:  $f(x) = \frac{(x-1)^2}{2x+2}$  and

$$\left\langle f \left( \frac{\pi(x_{1:T}, y_{1:T})}{\mu(x_{1:T}) \otimes \nu(y_{1:T})} \right), \mu(x_{1:T}) \otimes \nu(y_{1:T}) \right\rangle_F = \frac{1}{2} \sum_{x_{1:T}, y_{1:T}} \frac{[\pi(x_{1:T}, y_{1:T}) - \mu(x_{1:T}) \otimes \nu(y_{1:T})]^2}{\pi(x_{1:T}, y_{1:T}) + \mu(x_{1:T}) \otimes \nu(y_{1:T})}.$$

The summation is over all possible paths  $x_{1:T}$  and  $y_{1:T}$ .

- (3) Jensen-Shannon divergence:  $f(x) = x \ln\left(\frac{2x}{x+1}\right) + \ln\left(\frac{2}{x+1}\right)$ , and

$$\text{JS}(\mathbb{P}, \mathbb{Q}) = \text{KL} \left( \mathbb{P} \left\| \frac{\mathbb{P} + \mathbb{Q}}{2} \right. \right) + \text{KL} \left( \mathbb{Q} \left\| \frac{\mathbb{P} + \mathbb{Q}}{2} \right. \right),$$

with  $\mathbb{P} = \pi$ ,  $\mathbb{Q} = \mu \otimes \nu$  is the independent coupling.

Under these specifications, the objective is no longer separable and the DPP is violated. The cost functional at time  $t$  is given by

$$J(x_{1:t}, y_{1:t}; \pi) = \langle c(x_{1:T}, y_{1:T}), \pi(x_{t+1:T}, y_{t+1:T} | x_{1:t}, y_{1:t}) \rangle_F \quad (2.3)$$

$$+ \left\langle f \left( \frac{\pi(x_{t+1:T}, y_{t+1:T} | x_{1:t}, y_{1:t})}{\mu(x_{t+1:T} | x_{1:t}) \otimes \nu(y_{t+1:T} | y_{1:t})} \right), \mu(x_{t+1:T} | x_{1:t}) \otimes \nu(y_{t+1:T} | y_{1:t}) \right\rangle_F.$$

When the iterated expectation relationship (or tower property) fails, a global OT plan on  $\{t, \dots, T-1\}$  may not be optimal for the subproblems on  $\{t+1, \dots, T-1\}$ . The intuition is that we may sacrifice the optimality on the subinterval  $\{t+1, \dots, T-1\}$  to attain better solutions on  $\{t, \dots, T-1\}$ . Nevertheless, an agent can still choose to ignore time inconsistency and follow the global optimizer at time 0 irrevocably. However, he should recognize that the “today self” and “future selves” have an intertemporal conflict with the “optimal” plan (Strotz, 1955).

**Remark 2.1.** *This paper focuses on existence and uniqueness of solutions introduced in Definition 2.2. Convergence of numerical algorithms for the transport problem with time-inconsistent costs remains an open problem. Notably, even in the static case with quadratic regularization, this problem has only been examined in a recent work by González-Sanz and Nutz (2024).*

### 2.1.2 Nonlinear objectives

With a nonlinear function  $G$ , suppose the agent would like to minimize the transport cost given by

$$\inf_{\pi \in \Pi_{bc}(\mu, \nu)} G \left( \int h(x_{1:T}, y_{1:T}) \pi(dx_{1:T}, dy_{1:T}) \right).$$

An illustrative example is

$$\inf_{\pi \in \Pi_{bc}(\mu, \nu)} \left( \int h(x_{1:T}, y_{1:T}) \pi(dx_{1:T}, dy_{1:T}) - m \right)^2.$$

The agent wants to match the expected value of  $h(\cdot, \cdot)$  to a given level of  $m$ . Time inconsistency appears since the tower property fails for the objective.

### 2.1.3 State-dependent preference

For a fixed  $t = 0, \dots, T-1$ , consider an objective functional

$$J(x_{1:t}, y_{1:t}; \pi) = \int c(x_t, y_t, x_{1:T}, y_{1:T}) \pi(dx_{t+1:T}, dy_{t+1:T} | x_{1:t}, y_{1:t}). \quad (2.4)$$

The cost  $c$  has four arguments. The first  $(x_t, y_t)$  is state-dependent and plays a different role than the counterpart in  $x_{1:T}$  and  $y_{1:T}$ . That is, for a different time  $s \neq t$ , the integrand becomes  $c(x_s, y_s, x_{1:T}, y_{1:T})$ . Therefore, the integrand is different when the time changes and it leads to time inconsistency.

A classic example is non-exponential discounting (Strotz, 1955; Laibson, 1997). At time  $t$ , consider

$$\inf_{\pi \in \Pi_{bc}(\mu(dx_{t+1:T} | x_{1:t}), \nu(dy_{t+1:T} | y_{1:t}))} \int \sum_{s=t+1}^T \varphi(s-t) c(x_s, y_s) \pi(dx_{t+1:T}, dy_{t+1:T} | x_{1:t}, y_{1:t}), \quad (2.5)$$

where  $\varphi(\cdot)$  is a discounting function besides the power function. Note that the form (2.5) can be reformulated into (2.4) by redefining a new  $\tilde{x}_t = (t, x_t)$ . Since transitions of time are deterministic, the reformulation does not change the conditional probability kernels.

## 2.2 Definition of equilibrium transport

To handle time inconsistency and define a reasonable concept of “optimal” solutions, we should consider consistent plans that the agent can follow, instead of the pre-committed solutions. The agent who is aware of time inconsistency should keep in mind that the objectives in the future are different. Inspired by the concept of subgame perfect Nash equilibrium, several works (Strotz, 1955; Björk and Murgoci, 2014; Björk et al., 2017) propose to reformulate the problem as a non-cooperative game between agents at time  $t + 1, \dots, T - 1$  that are incarnations of the agent at time  $t$ , that is, a game between the current self and the future selves. An equilibrium solution, denoted as  $\{\pi_t^*, \dots, \pi_{T-1}^*\}$  in a discrete-time setting, should satisfy the following property: If ourselves in the future time  $t + 1, \dots, T - 1$  stick with  $\{\pi_{t+1}^*, \dots, \pi_{T-1}^*\}$ , then it is optimal for us at the current time  $t$  to adopt  $\pi_t^*$ . This backward recursive definition guarantees that the agent at each time  $t$  will not deviate from  $\pi_t^*$ .

Inspired by the above discussion, we define the equilibrium transport as follows. We refer to a transport plan  $\pi$  by its successive regular kernels  $\{\bar{\pi}, \pi_1, \dots, \pi_{T-1}\}$  in (1.3). At time  $t \in \{0, \dots, T-1\}$ , denote a generic cost functional as  $J(x_{1:t}, y_{1:t}; \pi)$ , which implies that the current path is  $(x_{1:t}, y_{1:t})$  and the agent uses the transport plan  $\pi$  in time  $t, \dots, T - 1$ .

**Definition 2.2.** Consider a given bicausal transport plan  $\pi^*$  with successive regular kernels  $\{\bar{\pi}^*, \pi_1^*, \dots, \pi_{T-1}^*\}$ .

1. For any  $t = 1, \dots, T - 1$  and  $\pi^*$ -almost every path  $(x_{1:t}, y_{1:t})$ , consider any transport plan  $\gamma \in \Pi(\mu(dx_{t+1}|x_{1:t}), \nu(dy_{t+1}|y_{1:t}))$ . When  $t = 0$ , we adopt the convention that  $\mathcal{X}_0$  and  $\mathcal{Y}_0$  are singletons and consider  $\bar{\gamma} \in \Pi(p_*^1 \mu, p_*^1 \nu)$ .
2. Define a perturbed transport plan  $\pi^{t,\gamma}$  as

$$\pi^{t,\gamma}(dx_{t+1:T}, dy_{t+1:T}|x_{1:t}, y_{1:t}) = \gamma(dx_{t+1}, dy_{t+1}|x_{1:t}, y_{1:t}) \prod_{s=t+1}^{T-1} \pi^*(dx_{s+1}, dy_{s+1}|x_{1:s}, y_{1:s}).$$

Then  $\pi^*$  is a subgame perfect Nash equilibrium bicausal transport plan if for every  $t = 0, \dots, T - 1$  and  $\pi^*$ -almost every  $(x_{1:t}, y_{1:t})$ , we have

$$\inf_{\gamma \in \Pi(\mu(dx_{t+1}|x_{1:t}), \nu(dy_{t+1}|y_{1:t}))} J(x_{1:t}, y_{1:t}; \pi^{t,\gamma}) = J(x_{1:t}, y_{1:t}; \pi^{t,*}),$$

where

$$\pi^{t,*}(dx_{t+1:T}, dy_{t+1:T}|x_{1:t}, y_{1:t}) = \prod_{s=t}^{T-1} \pi^*(dx_{s+1}, dy_{s+1}|x_{1:s}, y_{1:s}).$$

We call  $\pi^*$  an equilibrium transport for simplicity. If  $\pi^*$  exists, define the equilibrium value function  $V$  as

$$V_t(x_{1:t}, y_{1:t}) = J(x_{1:t}, y_{1:t}; \pi^{t,*}).$$

## 2.3 The discrete case

To understand Definition 2.2 with an example, we revisit the regularized objective (2.3) and characterize an equilibrium transport as follows. If time moves to  $t + 1$ , the cost functional is given

by

$$J(x_{1:t+1}, y_{1:t+1}; \pi) = \langle c(x_{1:T}, y_{1:T}), \pi(x_{t+2:T}, y_{t+2:T} | x_{1:t+1}, y_{1:t+1}) \rangle_F \\ + \left\langle f \left( \frac{\pi(x_{t+2:T}, y_{t+2:T} | x_{1:t+1}, y_{1:t+1})}{\mu(x_{t+2:T} | x_{1:t+1}) \otimes \nu(y_{t+2:T} | y_{1:t+1})} \right), \mu(x_{t+2:T} | x_{1:t+1}) \otimes \nu(y_{t+2:T} | y_{1:t+1}) \right\rangle_F.$$

If all agents at time  $t + 1, \dots, T - 1$  adopt the equilibrium transport  $\pi^*$ , then

$$J(x_{1:t+1}, y_{1:t+1}; \pi^*) = V_{t+1}(x_{1:t+1}, y_{1:t+1}).$$

Next, we argue by backward induction and consider the subproblem at time  $t$  with a perturbed transport plan  $\pi^{t,\gamma} = \pi^*(x_{t+2:T}, y_{t+2:T} | x_{1:t+1}, y_{1:t+1})\gamma(x_{t+1}, y_{t+1})$ . We have

$$J(x_{1:t}, y_{1:t}; \pi^{t,\gamma}) = \langle c(x_{1:T}, y_{1:T}), \pi^*(x_{t+2:T}, y_{t+2:T} | x_{1:t+1}, y_{1:t+1})\gamma(x_{t+1}, y_{t+1}) \rangle_F \\ + \left\langle f \left( \frac{\pi^*(x_{t+2:T}, y_{t+2:T} | x_{1:t+1}, y_{1:t+1})\gamma(x_{t+1}, y_{t+1})}{\mu(x_{t+1:T} | x_{1:t}) \otimes \nu(y_{t+1:T} | y_{1:t})} \right), \mu(x_{t+1:T} | x_{1:t}) \otimes \nu(y_{t+1:T} | y_{1:t}) \right\rangle_F.$$

Therefore, combining the two equations, we obtain the following recursive relationship between  $J(x_{1:t}, y_{1:t}; \pi^{t,\gamma})$  and  $J(x_{1:t+1}, y_{1:t+1}; \pi^*)$ :

$$J(x_{1:t}, y_{1:t}; \pi^{t,\gamma}) = \langle J(x_{1:t+1}, y_{1:t+1}; \pi^*), \gamma(x_{t+1}, y_{t+1}) \rangle_F \\ - \left\langle f \left( \frac{\pi^*(x_{t+2:T}, y_{t+2:T} | x_{1:t+1}, y_{1:t+1})}{\mu(x_{t+2:T} | x_{1:t+1}) \otimes \nu(y_{t+2:T} | y_{1:t+1})} \right), \mu(x_{t+2:T} | x_{1:t+1}) \otimes \nu(y_{t+2:T} | y_{1:t+1})\gamma(x_{t+1}, y_{t+1}) \right\rangle_F \\ + \left\langle f \left( \frac{\pi^*(x_{t+2:T}, y_{t+2:T} | x_{1:t+1}, y_{1:t+1})\gamma(x_{t+1}, y_{t+1})}{\mu(x_{t+1:T} | x_{1:t}) \otimes \nu(y_{t+1:T} | y_{1:t})} \right), \mu(x_{t+1:T} | x_{1:t}) \otimes \nu(y_{t+1:T} | y_{1:t}) \right\rangle_F.$$

By Definition 2.2, if all agents at time  $t + 1, \dots, T - 1$  adopt the equilibrium transport  $\{\pi_{t+1}^*, \dots, \pi_{T-1}^*\}$ , then it is also optimal for the agent at time  $t$  to follow  $\pi_t^*$ . Therefore, the recursive relationship leads to the following equation for the value function:

$$V_t(x_{1:t}, y_{1:t}) = \inf_{\gamma \in \Pi(\mu(x_{t+1} | x_{1:t}), \nu(y_{t+1} | y_{1:t}))} \left[ \langle V_{t+1}(x_{1:t+1}, y_{1:t+1}), \gamma(x_{t+1}, y_{t+1}) \rangle_F \\ - \left\langle f \left( \frac{\pi^*(x_{t+2:T}, y_{t+2:T} | x_{1:t+1}, y_{1:t+1})}{\mu(x_{t+2:T} | x_{1:t+1}) \otimes \nu(y_{t+2:T} | y_{1:t+1})} \right), \mu(x_{t+2:T} | x_{1:t+1}) \otimes \nu(y_{t+2:T} | y_{1:t+1})\gamma(x_{t+1}, y_{t+1}) \right\rangle_F \\ + \left\langle f \left( \frac{\pi^*(x_{t+2:T}, y_{t+2:T} | x_{1:t+1}, y_{1:t+1})\gamma(x_{t+1}, y_{t+1})}{\mu(x_{t+1:T} | x_{1:t}) \otimes \nu(y_{t+1:T} | y_{1:t})} \right), \mu(x_{t+1:T} | x_{1:t}) \otimes \nu(y_{t+1:T} | y_{1:t}) \right\rangle_F \right].$$

We follow Björk and Murgoci (2014); Björk et al. (2017) and call the recursive relationship of the value function  $V_t$  above the extended dynamic programming (DP) equation. Since the problem is finite and discrete, the infimum over  $\gamma$  is attained and induces the conditional kernel  $\pi_t^*$  of an equilibrium transport. Moreover, there can be multiple equilibrium transport plans, since the extended DP equation may have more than one optimizer. The value function is continuous automatically under the discrete topology. For the discrete case with general nonlinear and state-dependent objectives, see Remark 4.8 in Section 4.2.

As a side remark, if we consider the regularized objective (2.3) with continuous measures  $\mu$  and/or  $\nu$  instead, the usual weak topology in Section 1.1 is not strong enough to prove the continuity of value function. Even convergence of probabilities under Wasserstein distance does not necessarily lead to convergence under  $f$ -divergence, including Jensen-Shannon, KL, reverse KL, total variation, and other divergences. See Arjovsky et al. (2017, Example 1). Since the continuity of value function is needed for the recursion, we can only show the existence of equilibrium transport in the discrete case for the regularized objective (2.3) under the current weak topology.

### 3 The semi-discrete and Markovian case

In this section, we work with topological spaces without fixing any particular metrics. Lemma 3.3 and Theorem 3.5 provide the existence of equilibrium transport when  $\mathcal{X}$  is a finite discrete set with the discrete topology and  $\mathcal{Y}$  can be a general closed set in  $\mathbb{R}^{T \times d}$ . The current formulation is already computationally challenging. Indeed, Taşkesen et al. (2023, Theorem 2.2) showed that the computational complexity of the Wasserstein distance between a discrete probability measure supported on two points and the Lebesgue measure on the standard hypercube is already #P-hard.

Suppose the nonlinear and state-dependent objective is given by

$$J(x_t, y_t; \pi) := \int \sum_{k=t+1}^T c_k(x_t, y_t, x_k, y_k) \pi(dx_{t+1:T}, dy_{t+1:T} | x_t, y_t) + G\left(x_t, y_t, \int h(x_T, y_T) \pi(dx_T, dy_T | x_t, y_t)\right). \quad (3.1)$$

The function  $h$  only depends on  $(x_T, y_T)$ . The cost function  $c$  is separable and given by

$$c(w, v, x_{1:T}, y_{1:T}) := \sum_{k=1}^T c_k(w, v, x_k, y_k),$$

where  $w$  and  $v$  capture the state dependence on  $x$  and  $y$ . The first two terms in  $G(x_t, y_t, \cdot)$  are also state-dependent.

By convention, we interpret  $\mathcal{X}_0$  and  $\mathcal{Y}_0$  as singletons.

**Assumption 3.1.** (1) For each  $t \in \{1, \dots, T\}$ ,  $\mathcal{X}_t$  is a non-empty finite discrete set equipped with the discrete topology  $\mathcal{T}_{\mathcal{X}_t}$ . And  $\mathcal{X}$  is endowed with the product discrete topology.

(2) For each  $k \in \{1, \dots, T\}$  and  $i \in \{0, \dots, T\}$ ,  $c_k(x_i, y_i, x_k, y_k) : (\mathcal{X}_i \times \mathcal{Y}_i \times \mathcal{X}_k \times \mathcal{Y}_k, \mathcal{T}_{\mathcal{X}_i} \times \mathcal{T}_{\mathcal{Y}_i} \times \mathcal{T}_{\mathcal{X}_k} \times \mathcal{T}_{\mathcal{Y}_k}) \rightarrow (\mathbb{R}, \mathcal{T}_{\mathbb{R}})$  is continuous and bounded. Hence, when  $i = k$ ,  $c_k(x_k, y_k, x_k, y_k)$  is  $\mathcal{T}_{\mathcal{X}_k} \times \mathcal{T}_{\mathcal{Y}_k}$ -continuous and bounded.

(3)  $h(x_T, y_T) : (\mathcal{X}_T \times \mathcal{Y}_T, \mathcal{T}_{\mathcal{X}_T} \times \mathcal{T}_{\mathcal{Y}_T}) \rightarrow (\mathbb{R}, \mathcal{T}_{\mathbb{R}})$  is continuous and bounded.

(4) For each  $t \in \{0, \dots, T\}$ ,  $G(x_t, y_t, g) : (\mathcal{X}_t \times \mathcal{Y}_t \times \mathbb{R}, \mathcal{T}_{\mathcal{X}_t} \times \mathcal{T}_{\mathcal{Y}_t} \times \mathcal{T}_{\mathbb{R}}) \rightarrow (\mathbb{R}, \mathcal{T}_{\mathbb{R}})$  is continuous and bounded.

**Assumption 3.2.** For each  $t \in \{1, \dots, T-1\}$ ,

(1) the regular conditional kernels of  $\mu$  and  $\nu$  are Markovian and denoted as  $\mu(dx_{t+1}|x_t)$  and  $\nu(dy_{t+1}|y_t)$ .

(2)  $\nu(dy_{t+1}|y_t) : (\mathcal{Y}_t, \mathcal{T}_{\mathcal{Y}_t}) \rightarrow (\mathcal{P}(\mathcal{Y}_{t+1}), \mathcal{V}[C_b(\mathcal{Y}_{t+1}; \mathcal{T}_{\mathcal{Y}_{t+1}})])$  is Borel measurable.

Here, the Markov property means that the kernels depend on the current  $x_t$  (or  $y_t$ ) instead of the whole path  $x_{1:t}$  (or  $y_{1:t}$ ). We note that  $\mu(dx_{t+1}|x_t)$  is continuous with respect to the discrete topology.

Under the current formulation, the extended DP equation is also Markovian:

$$\begin{aligned}
V_t(x_t, y_t) = \inf_{\gamma \in \Pi(\mu(dx_{t+1}|x_t), \nu(dy_{t+1}|y_t))} & \left[ \int \left( c_{t+1}(x_t, y_t, x_{t+1}, y_{t+1}) + V_{t+1}(x_{t+1}, y_{t+1}) \right) \gamma(dx_{t+1}, dy_{t+1}) \right. \\
& - \int G(x_{t+1}, y_{t+1}, g_{t+1}(x_{t+1}, y_{t+1})) \gamma(dx_{t+1}, dy_{t+1}) \\
& + G\left(x_t, y_t, \int g_{t+1}(x_{t+1}, y_{t+1}) \gamma(dx_{t+1}, dy_{t+1})\right) \\
& - \int \sum_{k=t+2}^T b_k(x_{t+1}, y_{t+1}, x_{t+1}, y_{t+1}) \gamma(dx_{t+1}, dy_{t+1}) \\
& \left. + \int \sum_{k=t+2}^T b_k(x_t, y_t, x_{t+1}, y_{t+1}) \gamma(dx_{t+1}, dy_{t+1}) \right]. \tag{3.2}
\end{aligned}$$

In this equation,

- (a) the boundary condition for  $V$  is

$$V_T(x_T, y_T) = G(x_T, y_T, h(x_T, y_T));$$

- (b) let  $\pi^*(dx_{t+1}, dy_{t+1}|x_t, y_t)$  denote an optimizer for the equation (3.2) at time  $t$ . Concatenate these kernels to obtain

$$\pi^*(dx_{t+1:T}, dy_{t+1:T}|x_t, y_t) = \prod_{s=t}^{T-1} \pi^*(dx_{s+1}, dy_{s+1}|x_s, y_s); \tag{3.3}$$

- (c) the function sequences  $g_{t+1}$  and  $b_k$  in (3.2) are given by

$$\begin{aligned}
g_{t+1}(x_{t+1}, y_{t+1}) & := \int h(x_T, y_T) \pi^*(dx_T, dy_T|x_{t+1}, y_{t+1}), \\
b_k(w, v, x_{t+1}, y_{t+1}) & := \int c_k(w, v, x_k, y_k) \pi^*(dx_k, dy_k|x_{t+1}, y_{t+1}),
\end{aligned}$$

with  $\pi^*(dx_k, dy_k|x_{t+1}, y_{t+1})$  obtained by backward induction using (3.3). Here, the time  $t \in \{0, \dots, T-2\}$  and the index  $k \in \{t+2, \dots, T\}$ . The state-dependent terms  $w \in \mathcal{X}_i$  and  $v \in \mathcal{Y}_i$ , with  $i \in \{0, \dots, t+1\}$ .

There is an essential difficulty to prove the existence of equilibrium transport. Recall the Borel space framework in Bertsekas and Shreve (1978, Chapters 7 and 8) for stochastic optimal control. The model treated there has Borel state, control, and disturbance spaces; see Bertsekas and Shreve (1978, Definition 8.1). The existence of optimal policies relies on measurable selection theorems. The optimizer usually has weaker properties compared with the objective function. For example, if the objective is lower semicontinuous (l.s.c.), then an optimizer, if it exists, is Borel measurable (Bertsekas and Shreve, 1978, Proposition 7.33). If the objective is lower semianalytic, then an  $\varepsilon$ -optimizer is universally measurable (Bertsekas and Shreve, 1978, Proposition 7.50). However, the extended DP equation introduces auxiliary functions  $g_{t+1}$  and  $b_k$ , tied to the optimizer, and thus inheriting the weaker properties. Consequently, demonstrating the existence of an equilibrium via a recursive application of measurable selection becomes challenging.

Our main idea to prove Lemma 3.3 is the Borel measurable selection theorem (Brown and Purves, 1973) but with a careful treatment of the Polish topology (Kechris, 2012, Theorem 13.11).

The proof is given in Section A.1 of the e-companion. Kechris (2012, Theorem 13.11) shows that there is a finer Polish topology with the same Borel sets, such that a Borel function is continuous under the finer topology. We apply this technique recursively. However, one has to be careful to verify that several fundamental claims are still valid under the new topology:

- (1) Tightness of transport plans (Villani, 2009, Lemma 4.4) uses the fact that the topology on  $\mathcal{X}_{t+1} \times \mathcal{Y}_{t+1}$  is a product topology. But Kechris (2012, Theorem 13.11) does not guarantee that the refined topology on  $\mathcal{X}_{t+1} \times \mathcal{Y}_{t+1}$  is still a product topology in general. Therefore, we imposed that  $\mathcal{X}_{t+1}$  is equipped with the discrete topology and refine the topology on  $\mathcal{Y}_{t+1}$ . The Markov property is imposed for a similar reason, to ensure that  $\mathcal{Y}_{t+1:T}$  has a product topology after applying the refining technique.
- (2) Recall that compact Hausdorff topologies  $\mathcal{T}$  are both minimal Hausdorff and maximal compact (Steen and Seebach, 1978, Section I.3, p.25). In other words, no topology strictly smaller than  $\mathcal{T}$  can be Hausdorff and no topology strictly larger than  $\mathcal{T}$  can be compact. Consequently, it is crucial to emphasize that  $\Pi(\mu(dx_{t+1}|x_t), \nu(dy_{t+1}|y_t))$  remains compact after refining the Polish topology. Indeed, the weak topology on  $\Pi(\mu(dx_{t+1}|x_t), \nu(dy_{t+1}|y_t))$  only depends on the Borel structure of  $\mathcal{X}_{t+1}$  and  $\mathcal{Y}_{t+1}$ , instead of the topological one. It means that if we replace the topologies on  $\mathcal{X}_{t+1}$  and  $\mathcal{Y}_{t+1}$  with new ones having the same Borel sets, then the weak topology on  $\Pi(\mu(dx_{t+1}|x_t), \nu(dy_{t+1}|y_t))$  is unchanged. This technical topological result is also observed in Beiglböck and Pratelli (2012, Lemma 2.3 and Remark 2.4).

To the best of our knowledge, the refining topology technique is still new in the established literature on measurable selection and DP, dating back to Brown and Purves (1973); Bertsekas and Shreve (1978).

**Lemma 3.3.** *Suppose Assumptions 3.1 and 3.2 hold. Then for  $t \in \{0, \dots, T-1\}$ , there exists a Borel measurable optimizer  $\pi^*(dx_{t+1}, dy_{t+1}|x_t, y_t)$  for (3.2). Moreover,  $\pi^*$  defined recursively by (3.3) is an equilibrium transport in the sense of Definition 2.2. The value function  $V_t(x_t, y_t)$  in (3.2) is Borel measurable in  $(x_t, y_t)$ . Moreover, there exists a finer Polish topology such that  $\pi^*(dx_{t+1}, dy_{t+1}|x_t, y_t)$  and  $V_t(x_t, y_t)$  are continuous in  $(x_t, y_t)$ .*

Note that for  $t \in \{0, \dots, T-2\}$ ,

$$V_{t+1}(x_{t+1}, y_{t+1}) = \sum_{k=t+2}^T b_k(x_{t+1}, y_{t+1}, x_{t+1}, y_{t+1}) + G(x_{t+1}, y_{t+1}, g_{t+1}(x_{t+1}, y_{t+1})).$$

Then the extended DP equation (3.2) reduces to

$$\begin{aligned} V_t(x_t, y_t) = \inf_{\gamma \in \Pi(\mu(dx_{t+1}|x_t), \nu(dy_{t+1}|y_t))} & \left[ \int c_{t+1}(x_t, y_t, x_{t+1}, y_{t+1}) \gamma(dx_{t+1}, dy_{t+1}) \right. \\ & + G\left(x_t, y_t, \int g_{t+1}(x_{t+1}, y_{t+1}) \gamma(dx_{t+1}, dy_{t+1})\right) \\ & \left. + \int \sum_{k=t+2}^T b_k(x_t, y_t, x_{t+1}, y_{t+1}) \gamma(dx_{t+1}, dy_{t+1}) \right]. \end{aligned} \quad (3.4)$$

The original expression (3.2) demonstrates the derivation of the value function  $V_t$  from  $V_{t+1}$ , establishing a recursive connection that aligns closely with Björk and Murgoci (2014). Under the continuity assumption, the proof of Lemma 3.3 can rely on (3.2) and the reduction (3.4) is not

needed. However, when the costs are l.s.c. only, it becomes unclear whether (3.2) can maintain the l.s.c. property and the reduction (3.4) is needed. Both (3.2) and (3.4) are used to give more intuitive proofs.

**Assumption 3.4.** (1) *Assumption 3.1 (1) holds.*

(2) *For each  $k \in \{1, \dots, T\}$  and  $i \in \{0, \dots, T\}$ ,  $c_k(x_i, y_i, x_k, y_k) : (\mathcal{X}_i \times \mathcal{Y}_i \times \mathcal{X}_k \times \mathcal{Y}_k, \mathcal{T}_{\mathcal{X}_i} \times \mathcal{T}_{\mathcal{Y}_i} \times \mathcal{T}_{\mathcal{X}_k} \times \mathcal{T}_{\mathcal{Y}_k}) \rightarrow (\mathbb{R}, \mathcal{T}_{\mathbb{R}})$  is l.s.c. and bounded from below. Hence, when  $i = k$ ,  $c_k(x_k, y_k, x_k, y_k)$  is  $\mathcal{T}_{\mathcal{X}_k} \times \mathcal{T}_{\mathcal{Y}_k}$ -l.s.c. and bounded from below.*

(3)  *$h(x_T, y_T) : (\mathcal{X}_T \times \mathcal{Y}_T, \mathcal{T}_{\mathcal{X}_T} \times \mathcal{T}_{\mathcal{Y}_T}) \rightarrow (\mathbb{R}, \mathcal{T}_{\mathbb{R}})$  is l.s.c. and bounded from below.*

(4) *For each  $t \in \{0, \dots, T\}$ ,  $G(x_t, y_t, g) : (\mathcal{X}_t \times \mathcal{Y}_t \times \mathbb{R}, \mathcal{T}_{\mathcal{X}_t} \times \mathcal{T}_{\mathcal{Y}_t} \times \mathcal{T}_{\mathbb{R}}) \rightarrow (\mathbb{R}, \mathcal{T}_{\mathbb{R}})$  is l.s.c. and  $G(x_t, y_t, \cdot)$  is nondecreasing for each  $(x_t, y_t)$ .*

Theorem 3.5 extends Lemma 3.3 to l.s.c. costs. Hence, Theorem 3.5 is comparable to the classic existence of an optimal coupling (Villani, 2009, Theorem 4.1). Moreover, it is direct to verify the additional assumptions such as  $G(x_t, y_t, \cdot)$  is nondecreasing for each  $(x_t, y_t)$ .

**Theorem 3.5.** *Suppose Assumptions 3.2 and 3.4 hold. Then for  $t \in \{0, \dots, T-1\}$ , there exists a Borel measurable optimizer  $\pi^*(dx_{t+1}, dy_{t+1}|x_t, y_t)$  for (3.2) or equivalently (3.4). Moreover,  $\pi^*$  defined recursively by (3.3) is an equilibrium transport in the sense of Definition 2.2. The value function  $V_t(x_t, y_t)$  in (3.2) is Borel measurable in  $(x_t, y_t)$ . Moreover, there exists a finer Polish topology such that  $\pi^*(dx_{t+1}, dy_{t+1}|x_t, y_t)$  is continuous in  $(x_t, y_t)$  and  $V_t(x_t, y_t)$  is l.s.c. in  $(x_t, y_t)$ .*

## 4 Continuous and non-Markovian cases with parametric couplings

### 4.1 Metric spaces and Wasserstein distances

For generic probability measures and unbounded cost functions, metric spaces are needed for growth rate conditions; see Lemma A.4 in the e-companion. Consider  $\mathcal{X}$  and  $\mathcal{Y}$  with the Euclidean topology. Given a fixed  $p \in [1, \infty)$ , introduce the metric as  $d_{\mathcal{X}}(x_{1:T}, x'_{1:T}) = \left[ \sum_{t=1}^T d_{\mathcal{X}_t}(x_t, x'_t)^p \right]^{1/p}$  for  $x, x' \in \mathcal{X}$ , where  $d_{\mathcal{X}_t}(x_t, x'_t) := |x_t - x'_t|$ . The Wasserstein space of order  $p$  is given by

$$\mathcal{P}_p(\mathcal{X}) := \left\{ \mu \in \mathcal{P}(\mathcal{X}) \mid \int_{\mathcal{X}} d_{\mathcal{X}}(x_{1:T}, \bar{x}_{1:T})^p \mu(dx) < \infty \right\}$$

for some fixed  $\bar{x}_{1:T} \in \mathcal{X}$ . We always equip  $\mathcal{P}_p(\mathcal{X})$  with the Wasserstein distance of order  $p$ :

$$W_p(\mu, \mu') = \left( \inf_{\gamma \in \Pi(\mu, \mu')} \int_{\mathcal{X} \times \mathcal{X}} d_{\mathcal{X}}(x, x')^p \gamma(dx, dx') \right)^{1/p}. \quad (4.1)$$

Let

$$C_p(\mathcal{X}) := \left\{ f \in C(\mathcal{X}) \mid \exists \text{ constant } C > 0, |f(x)| \leq C(1 + d_{\mathcal{X}}(x, \bar{x})^p) \right\}$$

be the set of continuous functions from  $\mathcal{X}$  to  $\mathbb{R}$  with a growth rate of order  $p$  in  $d_{\mathcal{X}}(x, \bar{x})$ . Consider a sequence of probability measures  $\{\mu^k\}_{k \in \mathbb{N}}$  in  $\mathcal{P}_p(\mathcal{X})$  and  $\mu$  another probability measure in  $\mathcal{P}_p(\mathcal{X})$ . Recall that  $\mu^k$  converges weakly in  $\mathcal{P}_p(\mathcal{X})$  to  $\mu$  means that  $\mu^k$  converges to  $\mu$  in the usual weak convergence and  $\int d_{\mathcal{X}}(x, \bar{x})^p \mu^k(dx) \rightarrow \int d_{\mathcal{X}}(x, \bar{x})^p \mu(dx)$ ; see Villani (2009, Definition 6.7). By Villani (2009, Theorem 6.8),  $W_p(\mu^k, \mu) \rightarrow 0$  is equivalent to  $\mu^k$  converges weakly in  $\mathcal{P}_p(\mathcal{X})$  to  $\mu$ .

Similarly, we can replace  $(\mathcal{X}, d_{\mathcal{X}})$  with any metric space  $(\mathcal{S}, d_{\mathcal{S}})$  that is Polish and define  $\mathcal{P}_p(\mathcal{S})$  and  $C_p(\mathcal{S})$  accordingly. For example,  $\mathcal{S} = \mathcal{X}_{t+1}$  or  $\mathcal{S} = \mathcal{X}_{t+1} \times \mathcal{Y}_{t+1}$ . In particular, we denote the metric for  $\mathcal{X} \times \mathcal{Y}$  as

$$d((x, y), (\bar{x}, \bar{y})) = [d_{\mathcal{X}}(x, \bar{x})^p + d_{\mathcal{Y}}(y, \bar{y})^p]^{1/p}.$$

## 4.2 Parametric couplings

For each time  $t \in \{0, \dots, T-1\}$ , we use  $\gamma(dx_{t+1}, dy_{t+1} | \theta_{t+1})$  to model elements in a subset of  $\mathcal{P}_p(\mathcal{X}_{t+1} \times \mathcal{Y}_{t+1})$ . Suppose the parameter  $\theta_{t+1}$  is in a Polish topological vector space  $(\Theta_{t+1}, \mathcal{T}_{\Theta_{t+1}})$  with a complete compatible metric  $d_{\Theta_{t+1}}$ . The parametric model  $\gamma$  may not enumerate every element in  $\mathcal{P}_p(\mathcal{X}_{t+1} \times \mathcal{Y}_{t+1})$  and can be regarded as a form of dimension reduction. For example, the agent may want to narrow down the candidate couplings and consider specific parametric distributions only. The dual potential functions are commonly modeled by neural networks, which provide a parametric form for the couplings if regularization is also considered; see Seguy et al. (2018, Equation (8)). Another method in Delon and Desolneux (2020) restricts to Gaussian mixtures models as the couplings. Parametric methods can reduce the computational burden while sacrifice the accuracy. If we take  $\Theta_{t+1} = \mathcal{P}_p(\mathcal{X}_{t+1} \times \mathcal{Y}_{t+1})$ , it collapses to the classic formulation. We term the parametric kernel as the parametric transport (coupling) and the concatenation is denoted as

$$\gamma(dx_{t+1:T}, dy_{t+1:T} | \theta_{t+1:T}) := \prod_{s=t}^{T-1} \gamma(dx_{s+1}, dy_{s+1} | \theta_{s+1}). \quad (4.2)$$

Consider a general nonlinear and state-dependent objective which is not necessarily separable:

$$\begin{aligned} J(x_{1:t}, y_{1:t}; \theta_{t+1:T}) &:= \int c(x_t, y_t, x_{1:T}, y_{1:T}) \gamma(dx_{t+1:T}, dy_{t+1:T} | \theta_{t+1:T}) \\ &\quad + G\left(x_t, y_t, \int h(x_{1:T}, y_{1:T}) \gamma(dx_{t+1:T}, dy_{t+1:T} | \theta_{t+1:T})\right). \end{aligned} \quad (4.3)$$

The minimization is over  $\theta_{t+1:T}$ , which should satisfy the bicausal constraints  $\gamma(dx_{t+1:T}, dy_{t+1:T} | \theta_{t+1:T}) \in \Pi_{bc}(\mu(dx_{t+1:T} | x_{1:t}), \nu(dy_{t+1:T} | y_{1:t}))$ .

We impose the following assumptions on the objective and probability measures.

**Assumption 4.1.** (1) For each  $t \in \{0, \dots, T\}$ ,  $c(x_t, y_t, x_{1:T}, y_{1:T}) \in C_p(\mathcal{X}_{1:T} \times \mathcal{Y}_{1:T})$ .

(2)  $h(\cdot, \cdot)$  is continuous and

$$|h(x_{1:T}, y_{1:T})| \leq C(1 + d((x_{1:T}, y_{1:T}), (\bar{x}_{1:T}, \bar{y}_{1:T}))^{1/r})$$

for some constant  $r > 0$  satisfying  $1/r \leq p$ .

(3) For each  $t \in \{0, \dots, T\}$ ,  $G(x_t, y_t, g) : (\mathcal{X}_t \times \mathcal{Y}_t \times \mathbb{R}, \mathcal{T}_{\mathcal{X}_t} \times \mathcal{T}_{\mathcal{Y}_t} \times \mathcal{T}_{\mathbb{R}}) \rightarrow (\mathbb{R}, \mathcal{T}_{\mathbb{R}})$  is continuous and  $|G(x_t, y_t, g)| \leq C[1 + |g|^{pr} + d((x_t, y_t), (\bar{x}_t, \bar{y}_t))^p]$ .

**Assumption 4.2.** (1) For each  $t \in \{0, \dots, T-1\}$ ,  $x_{1:t} \mapsto \mu(dx_{t+1:T} | x_{1:t})$  is continuous with respect to metric  $d_{\mathcal{X}}$  on the domain  $\mathcal{X}_{1:t}$  and the  $W_p$  metric on the range  $\mathcal{P}_p(\mathcal{X}_{t+1})$ .

(2) For each  $t \in \{0, \dots, T-1\}$  and constant  $a \in \{1/r, p\}$ , where the constant  $r > 0$  is the same as in Assumption 4.1,

$$\int_{\mathcal{X}_{t+1:T}} d_{\mathcal{X}}(x_{1:T}, \bar{x}_{1:T})^a \mu(dx_{t+1:T} | x_{1:t}) \leq C[1 + d_{\mathcal{X}}(x_{1:t}, \bar{x}_{1:t})^a].$$

Same assumptions on  $\nu$  hold with the metric  $d_{\mathcal{Y}}$ .

Assumption 4.2(2) is used in (A.5) for the growth rate.  
Introduce the correspondence  $D_t : \mathcal{X}_{1:t} \times \mathcal{Y}_{1:t} \rightarrow \Theta_{t+1}$  as

$$(x_{1:t}, y_{1:t}) \mapsto \{\theta_{t+1} \in \Theta_{t+1} | \gamma(dx_{t+1}, dy_{t+1} | \theta_{t+1}) \in \Pi(\mu(dx_{t+1} | x_{1:t}), \nu(dy_{t+1} | y_{1:t}))\}. \quad (4.4)$$

We use a notation  $\rightarrow$  to highlight that the correspondence maps a point to a subset.  
The equilibrium parametric transport is characterized by:

$$V_t(x_{1:t}, y_{1:t}) = \inf_{\theta_{t+1} \in D_t(x_{1:t}, y_{1:t})} f(x_{1:t}, y_{1:t}, \theta_{t+1}), \quad (4.5)$$

where

$$\begin{aligned} f(x_{1:t}, y_{1:t}, \theta_{t+1}) := & G\left(x_t, y_t, \int g_{t+1}(x_{1:t+1}, y_{1:t+1}) \gamma(dx_{t+1}, dy_{t+1} | \theta_{t+1})\right) \\ & + \int b_{t+1}(x_t, y_t, x_{1:t+1}, y_{1:t+1}) \gamma(dx_{t+1}, dy_{t+1} | \theta_{t+1}). \end{aligned} \quad (4.6)$$

In this equation,

- (a) the boundary condition for  $V$  is

$$V_T(x_{1:T}, y_{1:T}) = c(x_T, y_T, x_{1:T}, y_{1:T}) + G(x_T, y_T, h(x_{1:T}, y_{1:T}));$$

- (b) denote an optimizer for the equation (4.5) at time  $t$  as  $\theta_{t+1}^*(x_{1:t}, y_{1:t})$ . It yields the equilibrium parametric kernels in the sense of Definition 2.2 when kernels are restricted in the parametric spaces:

$$\gamma(dx_{t+1:T}, dy_{t+1:T} | \theta_{t+1:T}^*(x_{1:t}, y_{1:t})) = \prod_{s=t}^{T-1} \gamma(dx_{s+1}, dy_{s+1} | \theta_{s+1}^*(x_{1:s}, y_{1:s})); \quad (4.7)$$

- (c) the function sequences  $g_{t+1}$  and  $b_{t+1}$  in (4.5) are given by

$$\begin{aligned} g_{t+1}(x_{1:t+1}, y_{1:t+1}) & := \int h(x_{1:T}, y_{1:T}) \gamma(dx_{t+2:T}, dy_{t+2:T} | \theta_{t+2:T}^*(x_{1:t+1}, y_{1:t+1})), \\ b_{t+1}(w, v, x_{1:t+1}, y_{1:t+1}) & := \int c(w, v, x_{1:T}, y_{1:T}) \gamma(dx_{t+2:T}, dy_{t+2:T} | \theta_{t+2:T}^*(x_{1:t+1}, y_{1:t+1})), \end{aligned}$$

with  $\gamma(dx_{t+2:T}, dy_{t+2:T} | \theta_{t+2:T}^*(x_{1:t+1}, y_{1:t+1}))$  in (4.7) and  $\theta_{i+1}^*(x_{1:i}, y_{1:i})$ ,  $i = t+1, \dots, T-1$ , are obtained by backward induction using (4.5).

Recall that a function  $f : \mathcal{S} \rightarrow \mathbb{R}$  defined on a convex subset  $\mathcal{S}$  of a real vector space is quasiconvex if for all  $s, s' \in \mathcal{S}$  and  $\lambda \in [0, 1]$ , we have  $f(\lambda s + (1-\lambda)s') \leq \max\{f(s), f(s')\}$ . If furthermore  $f(\lambda s + (1-\lambda)s') < \max\{f(s), f(s')\}$  for all  $s \neq s'$  and  $\lambda \in (0, 1)$ , then  $f$  is strictly quasiconvex. Every convex function is quasiconvex. Besides, we recall the definition of upper and lower hemicontinuity:

**Definition 4.3.** (Charalambos and Aliprantis, 2013, Definition 17.2) A correspondence  $\varphi : X \rightarrow Y$  between topological spaces is:

- upper hemicontinuous at the point  $x$  if for every neighborhood  $U$  of  $\varphi(x)$ , there is a neighborhood  $V$  of  $x$  such that  $z \in V$  implies  $\varphi(z) \subset U$ .

- lower hemicontinuous at  $x$  if for every open set  $U$  that meets  $\varphi(x)$  (i.e.  $\varphi(x) \cap U \neq \emptyset$ ), there is a neighborhood  $V$  of  $x$  such that  $z \in V$  implies  $\varphi(z) \cap U \neq \emptyset$ .
- continuous at  $x$  if it is both upper and lower hemicontinuous at  $x$ .

**Assumption 4.4.** For each  $t \in \{0, \dots, T-1\}$ ,

- (1)  $\gamma(dx_{t+1}, dy_{t+1} | \theta_{t+1}) : (\Theta_{t+1}, d_{\Theta_{t+1}}) \rightarrow \mathcal{P}_p(\mathcal{X}_{t+1} \times \mathcal{Y}_{t+1})$  is continuous;
- (2)  $D_t$  in (4.4) is a continuous correspondence and  $D_t(x_{1:t}, y_{1:t})$  is non-empty, convex, and compact, under the product topology  $\mathcal{T}_{\mathcal{X}_{1:t}} \times \mathcal{T}_{\mathcal{Y}_{1:t}} \times \mathcal{T}_{\Theta_{t+1}}$ ;
- (3) for an arbitrary path  $(x_{1:t}, y_{1:t}) \in \mathcal{X}_{1:t} \times \mathcal{Y}_{1:t}$ , we have  $f(x_{1:t}, y_{1:t}, \theta_{t+1})$  in (4.6) strictly quasi-convex in  $\theta_{t+1} \in \Theta_{t+1}$ .

We apply a version of Berge's maximum theorem with strict quasiconcavity, see Sundaram (1996, Theorem 9.14 and Corollary 9.20) or Charalambos and Aliprantis (2013, Theorem 17.31), to prove existence and uniqueness of the equilibrium parametric transport. The proof is given in Section A.2.

**Theorem 4.5.** Suppose Assumptions 4.1, 4.2, and 4.4 hold. Then for each  $t \in \{0, \dots, T-1\}$ ,

- (a) there is a continuous and unique optimizer,  $\theta_{t+1}^*(x_{1:t}, y_{1:t}) : (\mathcal{X}_{1:t} \times \mathcal{Y}_{1:t}, d) \rightarrow (\Theta_{t+1}, d_{\Theta_{t+1}})$ , for the extended DP equation (4.5);
- (b) the equilibrium parametric kernel

$$\gamma(dx_{t+1:T}, dy_{t+1:T} | \theta_{t+1:T}^*(x_{1:t}, y_{1:t})) : (\mathcal{X}_{1:t} \times \mathcal{Y}_{1:t}, d) \rightarrow \mathcal{P}_p(\mathcal{X}_{t+1:T} \times \mathcal{Y}_{t+1:T})$$

in (4.7) is continuous and unique;

- (c) the corresponding value function  $V_t$  satisfies (4.5) and  $V_t \in C_p(\mathcal{X}_{1:t} \times \mathcal{Y}_{1:t})$ .

**Remark 4.6.**  $\theta_{t+1}^*$  is unique among all correspondences, including functions, with graphs that are subsets of the graph of  $D_t$ . If the objective  $f(x_{1:t}, y_{1:t}, \theta_{t+1})$  satisfies the quasiconvexity but not strictly in Assumption 4.4 (3), we could also include a regularization term on  $\theta_{t+1}$  directly, such as  $|\theta_{t+1}|^2$ . If the regularization term is  $\mathcal{T}_{\Theta_{t+1}}$ -continuous, then it can be treated similarly by Theorem 4.5.

It is direct to recover the classic formulation when the correspondence

$$D_t(x_{1:t}, y_{1:t}) = \Pi(\mu(dx_{t+1}|x_{1:t}), \nu(dy_{t+1}|y_{1:t}))$$

by setting  $\Theta_{t+1} = \mathcal{P}_p(\mathcal{X}_{t+1} \times \mathcal{Y}_{t+1})$ ,  $t \in \{0, \dots, T-1\}$ .

**Corollary 4.7.** Suppose

- (1) Assumptions 4.1 and 4.2 hold;
- (2)  $\Theta_{t+1} = \mathcal{P}_p(\mathcal{X}_{t+1} \times \mathcal{Y}_{t+1})$ ,  $t \in \{0, \dots, T-1\}$ ;
- (3) for each given  $t \in \{0, \dots, T-1\}$  and an arbitrary path  $(x_{1:t}, y_{1:t}) \in \mathcal{X}_{1:t} \times \mathcal{Y}_{1:t}$ , suppose  $f(x_{1:t}, y_{1:t}, \gamma)$  in (4.6) is strictly quasiconvex in any

$$\gamma(dx_{t+1}, dy_{t+1}) \in \Pi(\mu(dx_{t+1}|x_{1:t}), \nu(dy_{t+1}|y_{1:t})).$$

Then for each  $t \in \{0, \dots, T-1\}$ ,

- (a) there is a continuous and unique optimizer,  $\pi^*(dx_{t+1}, dy_{t+1}|x_{1:t}, y_{1:t}) : (\mathcal{X}_{1:t} \times \mathcal{Y}_{1:t}, d) \rightarrow \mathcal{P}_p(\mathcal{X}_{t+1} \times \mathcal{Y}_{t+1})$ , for the extended DP equation (4.5);
- (b) the equilibrium transport  $\pi^*(dx_{t+1:T}, dy_{t+1:T}|x_{1:t}, y_{1:t}) : (\mathcal{X}_{1:t} \times \mathcal{Y}_{1:t}, d) \rightarrow \mathcal{P}_p(\mathcal{X}_{t+1:T} \times \mathcal{Y}_{t+1:T})$  in (4.7), is continuous and unique;
- (c) the corresponding value function  $V_t$  satisfies (4.5) and  $V_t \in C_p(\mathcal{X}_{1:t} \times \mathcal{Y}_{1:t})$ .

**Remark 4.8.** For the special case that  $\mu$  and  $\nu$  are discrete measures with finite supports, the extended DPP is straightforward. When  $\mathcal{X}$  and  $\mathcal{Y}$  are equipped with discrete topology, the value function  $V_t(x_{1:t}, y_{1:t})$  in (4.5) and the correspondence  $D_t$  in (4.4) are continuous automatically. There exists an equilibrium transport  $\pi^*$  which may not be unique. The strict quasiconvexity is not needed for the existence. However, we can regard probability masses as parameters and obtain the uniqueness if strict quasiconvexity holds.

## 5 Illustrative examples

### 5.1 Dynamic matching under a mean-variance objective

Inspired by Hu and Zhou (2022), we examine an example from operations management involving the matching of supply  $x$  with demand  $y$ . Consider two supply types and two demand types, with type labels  $\mathcal{X}_t = \{0, 1\}$  and  $\mathcal{Y}_t = \{0, 1\}$ , respectively. In each period, supply and demand of different types arrive randomly:  $x_{1:T} \sim \mu$  and  $y_{1:T} \sim \nu$ . The supply and demand types exhibit idiosyncratic taste towards one another, where matching closer types incurs lower costs. They are known as horizontally differentiated demand and supply types (Hu and Zhou, 2022, Section 4). A practical example is a ride-hailing platform, where types are determined by the locations of riders and drivers, and closer matches result in reduced costs.

The one-period cost matrix  $f(x_t, y_t)$  is presented in Table 1.

	$x = 0$	$x = 1$
$y = 0$	1.0	2.0
$y = 1$	2.0	0.0

Table 1: One-period cost matrix of supply/demand matching

The total cost over  $T$  periods is given by  $c(x_{1:T}, y_{1:T}) = \sum_{t=1}^T \beta^t f(x_t, y_t)$ , where  $\beta \in [0, 1]$  acts as a discount factor. In the multi-period matching, bicausality is a natural requirement, meaning that no future information can be utilized. The agent aims to find a bicausal matching plan  $\pi$  that minimizes both cost and variance:

$$\inf_{\pi \in \Pi_{bc}(\mu, \nu)} \mathbb{E}_\pi [c(x_{1:T}, y_{1:T})] + \gamma \text{Var}_\pi [c(x_{1:T}, y_{1:T})]. \quad (5.1)$$

Here, constant  $\gamma > 0$  represents the tolerance level for variance.

As an illustration, we consider a scenario where the number of periods  $T = 2$ , the discount factor  $\beta = 1$ , and the marginals  $\mu$  and  $\nu$  are given as follows:

$$\begin{aligned} \mu(x_1) &= 0.1\delta_0 + 0.9\delta_1, & \mu(x_2|x_1 = 0) &= 0.8\delta_0 + 0.2\delta_1, & \mu(x_2|x_1 = 1) &= 0.2\delta_0 + 0.8\delta_1, \\ \nu(y_1) &= 0.5\delta_0 + 0.5\delta_1, & \nu(y_2|y_1 = 0) &= 0.9\delta_0 + 0.1\delta_1, & \nu(y_2|y_1 = 1) &= 0.1\delta_0 + 0.9\delta_1. \end{aligned} \quad (5.2)$$

Here,  $\delta_i$  represents the Dirac measure at type  $i$ . The transition kernels are designed in a way that the next type is more likely to be the same as the previous one.

The pre-committed solution to (5.1), denoted as  $\pi^{pre}$ , is given by

$$\begin{aligned}\pi^{pre}(x_1, y_1) &= 0.1\delta_{(0,0)} + 0.4\delta_{(1,0)} + 0.5\delta_{(1,1)}, \\ \pi^{pre}(x_2, y_2|x_1 = 0, y_1 = 0) &= 0.8\delta_{(0,0)} + 0.1\delta_{(1,0)} + 0.1\delta_{(1,1)}, \\ \pi^{pre}(x_2, y_2|x_1 = 1, y_1 = 0) &= 0.2\delta_{(0,0)} + 0.7\delta_{(1,0)} + 0.1\delta_{(1,1)}, \\ \pi^{pre}(x_2, y_2|x_1 = 1, y_1 = 1) &= 0.2\delta_{(0,1)} + 0.1\delta_{(1,0)} + 0.7\delta_{(1,1)}.\end{aligned}\tag{5.3}$$

Similarly,  $\delta_{(i,j)}$  is the Dirac measure at  $(x_2, y_2) = (i, j)$ . The corresponding mean and variance of the cost are calculated as:

$$\mathbb{E}_{\pi^{pre}} [c(x_{1:2}, y_{1:2})] = 1.94 \quad \text{and} \quad \text{Var}_{\pi^{pre}} [c(x_{1:2}, y_{1:2})] = 2.6164.\tag{5.4}$$

Consequently, the optimal value of the objective in (5.1) amounts to 4.5564.

In contrast, the equilibrium transport  $\pi^*$  is given as follows:

$$\begin{aligned}\pi^*(x_1, y_1) &= 0.1\delta_{(0,0)} + 0.4\delta_{(1,0)} + 0.5\delta_{(1,1)}, \\ \pi^*(x_2, y_2|x_1 = 0, y_1 = 0) &= 0.8\delta_{(0,0)} + 0.1\delta_{(1,0)} + 0.1\delta_{(1,1)}, \\ \pi^*(x_2, y_2|x_1 = 1, y_1 = 0) &= 0.1\delta_{(0,0)} + 0.1\delta_{(0,1)} + 0.8\delta_{(1,0)}, \\ \pi^*(x_2, y_2|x_1 = 1, y_1 = 1) &= 0.1\delta_{(0,0)} + 0.1\delta_{(0,1)} + 0.8\delta_{(1,1)}.\end{aligned}\tag{5.5}$$

The corresponding value of the objective in (5.1) is 5.0519, with the mean and variance given by

$$\mathbb{E}_{\pi^*} [c(x_{1:2}, y_{1:2})] = 1.91 \quad \text{and} \quad \text{Var}_{\pi^*} [c(x_{1:2}, y_{1:2})] = 3.1419.\tag{5.6}$$

We have the following comments on this example:

- (1) The pairs (0, 1) and (1, 0) are referred to as mismatches. Compared with the pre-committed OT, the equilibrium transport can increase or decrease the probabilities of mismatches in  $(x_2, y_2)$ , depending on the previous state  $(x_1, y_1)$ . Specifically, when  $(x_1, y_1) = (1, 0)$ , the total probability for  $(x_2, y_2) = (0, 1)$  and  $(x_2, y_2) = (1, 0)$  increases from 0.7 to 0.9. Conversely, when  $(x_1, y_1) = (1, 1)$ , this sum decreases from 0.3 to 0.1. Structural properties of equilibrium transport become more complex due to the dependence on the temporal structures of the marginals  $\mu$  and  $\nu$ , a challenge not encountered in the static formulation (Boerma et al., 2023) or the infinite horizon setting (Shimer and Smith, 2000).
- (2) Both the pre-committed OT (5.3) and the equilibrium transport (5.5) are not Monge maps. In the discrete setting, it is common to split probability masses, see also Boerma et al. (2023, Section 3.1). Exploring the denseness of specific Monge maps for the equilibrium transport presents another intriguing and demanding task, extending the previous research by Schrott et al. (2023).
- (3) Regarding computational algorithms, the optimization problem (5.1) is not a linear program due to the presence of variance operator. While solvers like Gurobi can efficiently address this specific example, the general problem can be challenging because of the nonlinear  $G$ . In contrast to Eckstein and Pammer (2024); González-Sanz and Nutz (2024), different methodologies are needed for algorithm design and convergence analysis. Despite this, identifying an equilibrium transport is easier than obtaining a pre-committed OT, given its local optimization nature and the possibility of solving sub-problems (4.5) across states in parallel.

## 5.2 Gaussian data

It is rare for continuous OT problems to have explicit solutions, even in the single-period case. One exception is the Gaussian distribution (Givens and Shortt, 1984; Gunasingam and Wong, 2024). As an explicit example illustrating Theorem 4.5, we consider  $\mu$  and  $\nu$  as Gaussian distributions with linear dynamics:

$$\begin{aligned}x_{t+1} &= x_t + \lambda_t, & \lambda_t &\sim N(0, 1), \\y_{t+1} &= y_t + \eta_t, & \eta_t &\sim N(0, 1).\end{aligned}$$

For simplicity, suppose  $x_t \in \mathbb{R}$  and  $y_t \in \mathbb{R}$  are one-dimensional. The white Gaussian noise process  $\{\lambda_t\}$  consists of standard normal random variables that are independent of each other. Impose the same condition on  $\{\eta_t\}$ .

Consider a two-period problem with a nonlinear and state-dependent objective:

$$\left(x_0 y_0 - \int x_2 y_2 \pi(dx_2, dy_2 | x_0, y_0)\right)^2. \quad (5.7)$$

The initial states  $x_0$  and  $y_0$  are fixed as constants.

We assume that the agent considers only normal distribution as couplings. At time  $t = 1$ , the agent seeks an optimal coupling which is a bivariate normal distribution  $\gamma(dx_2, dy_2 | \theta_2)$  with marginals  $x_2 \sim N(x_1, 1)$  and  $y_2 \sim N(y_1, 1)$  and  $\theta_2 \in [-1, 1]$  as the correlation between  $x_2$  and  $y_2$ . Since the first term in the square is state-dependent, the objective at time 1 is

$$\left(x_1 y_1 - \int x_2 y_2 \gamma(dx_2, dy_2 | \theta_2)\right)^2.$$

Recalling  $f$  in (4.6), we have  $f(x_1, y_1, \theta_2) = (x_1 y_1 - \theta_2 \times 1 \times 1 - x_1 y_1)^2 = \theta_2^2$ , which is strictly quasiconvex in  $\theta_2 \in [-1, 1]$ . For other conditions in Assumptions 4.1, 4.2, and 4.4, we take  $1/r = 2$  and  $p = 4$  as the growth rate. Assumptions 4.1 and 4.2 are satisfied.  $\gamma(dx_2, dy_2 | \theta_2)$  is continuous in  $\theta_2$  with the Wasserstein distance of order 4, by properties of the normal distribution and Villani (2009, Theorem 6.8). Clearly, the correspondence  $D_1 : (x_1, y_1) \rightarrow [-1, 1]$  satisfies Assumption 4.4 (2). Theorem 4.5 shows that  $\theta_2^*(x_1, y_1) = 0$  is the unique optimizer at time 1. Similarly,  $\theta_1^*(x_0, y_0) = 0$ , which is also unique. In this case, the restriction on normal couplings is not too restrictive since it gives a value function equal to zero.

Consider the agent who ignores time inconsistency and minimizes the objective (5.7) at time 0 only. Any constant  $(\theta_1, \theta_2)$  with  $\theta_2 + \theta_1 = 0$  is an optimizer for  $(x_0 y_0 - \int x_2 y_2 \pi(dx_2, dy_2 | x_0, y_0))^2 = (\theta_2 + \theta_1)^2$ . However, for nonzero  $\theta_1$ , the agent at time 1 will find that it is optimal to deviate from  $\theta_2 = -\theta_1$ . Therefore, it is possible to have a unique equilibrium parametric transport but multiple globally optimal parametric transports.

## 6 A job market model with inertia

### 6.1 Matching as an OT problem

To motivate our equilibrium transport job market model, we first review the connection between a chief executive officer (CEO) compensation model in Gabaix and Landier (2008) and the classic OT problem, following Galichon (2016, Chapter 4).

Gabaix and Landier (2008) considered a matching problem between firms and potential managers. Consider the static setting with  $T = 1$  for simplicity. Assume there are the same number

of managers and firms, represented by scalar characteristics  $x \sim \mu$  and  $y \sim \nu$ , respectively. The manager of type  $x$  can generate earnings of  $\Phi(x, y)$  for the firm of type  $y$ . Suppose the manager of type  $x$  receives a salary of  $\psi(x)$ . The firm  $y$  chooses the optimal manager that maximizes the earnings after deducting the wage:

$$\sup_{x \in \mathcal{X}} \Phi(x, y) - \psi(x). \quad (6.1)$$

Denote the optimal value in (6.1) as  $\phi(y)$  for each  $y \in \mathcal{Y}$ . The pair  $(\psi, \phi)$  is a solution to the following problem:

$$\inf_{\psi(x) + \phi(y) \geq \Phi(x, y)} \int_{\mathcal{X}} \psi(x) \mu(dx) + \int_{\mathcal{Y}} \phi(y) \nu(dy). \quad (6.2)$$

The Kantorovich duality shows that (6.2) is the dual for the primal problem:

$$\sup_{\pi \in \Pi(\mu, \nu)} \int_{\mathcal{X} \times \mathcal{Y}} \Phi(x, y) \pi(dx, dy). \quad (6.3)$$

It gives a clear connection between the CEO compensation problem in Gabaix and Landier (2008) and the OT problem. Gabaix and Landier (2008) aim to determine the function  $\psi(x)$  for salaries, with a critical assumption that the function  $\Phi(x, y)$  is supermodular: If  $\bar{x} \geq \underline{x}$  and  $\bar{y} \geq \underline{y}$ , then  $\Phi(\bar{x}, \bar{y}) + \Phi(\underline{x}, \underline{y}) \geq \Phi(\bar{x}, \underline{y}) + \Phi(\underline{x}, \bar{y})$ . Examples include the Cobb-Douglas function  $x^a y^b$ ,  $a, b > 0$  and  $-|x - y|^p$ ,  $p \geq 1$ . Consequently, the total earnings are higher when managers of higher types are matched with firms of higher types and the lower types with the lower types. Formally, Galichon (2016, Theorem 4.3) shows that if  $\Phi(x, y)$  is supermodular, then the primal problem (6.3) has a *comonotone* solution (Galichon, 2016, Definition 4.1). This concept is known by various names such as positive assortative matching (PAM), monotone rearrangement, Fréchet–Hoeffding coupling, quantile transform, or Knothe–Rosenblatt coupling (Villani, 2009, Chapter 1, p.17). The time-dependent version is studied in Backhoff-Veraguas et al. (2017, Theorem 2.9).

In Gabaix and Landier (2008), the variables  $x$  and  $y$  are interpreted as manager talents and firm sizes. An important conclusion is that larger firms should employ more talented managers and offer higher salaries. In the competitive equilibrium, the ranks of CEO talents and equilibrium compensations align, as shown in Gabaix and Landier (2008, Equation (5)).

## 6.2 The strengths and weaknesses of positive assortative matching

We can compare this theoretical conclusion in Gabaix and Landier (2008) with the empirical data. Indeed, Roberts’ law (Gabaix and Landier, 2008) states that CEO compensation is roughly proportional to (firm size) $^\kappa$ , with a typical empirical exponent  $\kappa \simeq 1/3$ . However, empirical data from executive job markets do not always show a perfect employer-employee correspondence. Figure 1 plots the wages and net sales data for the Industrials sector in the fiscal year of 2021. A power-law relationship holds approximately, but some big firms deviate from the Roberts’ law and underpay their managers. These empirical observations reveal that the supermodular surplus function  $\Phi(x, y)$  requires adjustments, which motivates our formulation in a dynamic setting.

## 6.3 Matching with a state-dependent preference

Consider a time horizon of  $T$  years, where we observe a time series of employer characteristics  $(x_1, \dots, x_t, \dots, x_T) \sim \mu$ . If employers prioritize profitability, we use the net sale ranks of employers as  $x$ . Sales data tend to be more stable than stock market values. If employers are universities, then rankings are readily available. For employees, commonly used characteristics include talent and salary, while talent is not observable. In this paper, we use the ranks of salaries after clustering

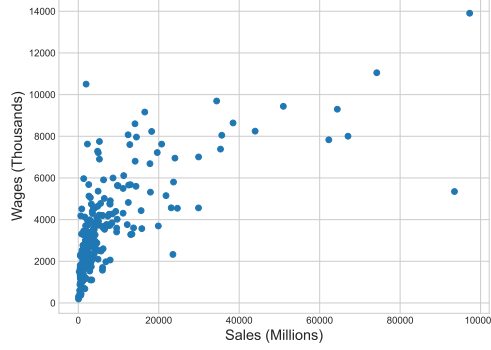


Figure 1: Sale-wage relationship in the Industrials sector in the fiscal year of 2021.

as the types of employees, with a distribution  $\nu$ . This choice is motivated by the fact that talents and equilibrium compensations share the same ranks in the competitive equilibrium as derived in Gabaix and Landier (2008).

Employers and employees are in symmetric positions when choosing each other. If the PAM holds perfectly, then the optimal employer-employee matching should assign the employer ranked number  $n$  with the employee ranked number  $n$ . Denote  $x_t$  as the rank of employers and  $y_t$  as the rank of employees at time  $t$ . The ranks  $x_t$  and  $y_t$  have the same range since the numbers of employers and employees are equal. With a discount factor  $\beta \in [0, 1]$ , a multi-period model motivated by the PAM is

$$\inf_{\pi \in \Pi_{bc}(\mu, \nu)} \int \sum_{t=1}^T \beta^t |x_t - y_t| \pi(dx_{1:T}, dy_{1:T}). \quad (6.4)$$

To be consistent with our previous formulations (3.1) and (4.6), we consider minimization instead of maximization as in (6.3). In contrast to the Cobb-Douglas function, the absolute value  $|x - y|$  does not involve any hyperparameters.

As mentioned above, some high-ranked firms pay less to executives and some industries are less consistent with the Roberts' law. We conjecture that there are incentives to maintain the original matching, regardless of its efficiency. For example, there may be implicit benefits to continuing to work for the same company, particularly if an employee is the founder. Additionally, employers may want to preserve the previous ranking of wages among their peers. We attempt to quantify this conjecture and refine the benchmark model (6.4) using the equilibrium transport method. For any time  $t > 1$ , we introduce a new term to reduce the cost if we keep similar matching and modify the objective (6.4) to

$$\inf_{\pi \in \Pi_{bc}(\mu^t, \nu^t)} \int \left[ -\alpha e^{-\frac{|x_{t+1}-x_t|+|y_{t+1}-y_t|}{\tau}} + \sum_{s=t+1}^T \beta^s |x_s - y_s| \right] \pi(dx_{t+1:T}, dy_{t+1:T} | x_{1:t}, y_{1:t}). \quad (6.5)$$

$\Pi_{bc}(\mu^t, \nu^t)$  uses simplified notations  $\mu^t = \mu(dx_{t+1:T} | x_{1:t})$  and  $\nu^t = \nu(dy_{t+1:T} | y_{1:t})$ .  $\alpha$  is a constant to be determined and  $\tau > 0$  is a scaling constant. We call the first term the state-dependent preference function. We consider an exponential function for a fast decay when  $(x_{t+1}, y_{t+1})$  deviates from the previous  $(x_t, y_t)$ . If we interpret  $0/0 = 0$  and set  $\tau = 0$ , the state-dependent function also includes the indicator function  $\mathbf{1}_{\{x_{t+1}=x_t, y_{t+1}=y_t\}}$  as a special case. The motivation for the state-dependent term can be further explained as follows:

- (1) Federal securities laws require disclosure of compensation paid to high-ranking executives of public companies. These companies are typically required to provide a Summary Compensation Table with executive compensation for the past *three* fiscal years <sup>[1]</sup> in their annual financial statement files (usually annual proxy statements). This requirement is intended to help stakeholders better understand year-over-year changes in compensation. As such, the state-dependent term reflects the concerns and practices of stakeholders and regulators.
- (2) Commonly, the current firm-wage matching depends on previous ones for financial reasons. For example, executive compensation programs in public companies often have several components, such as an annual base salary, an annual cash incentive, and long-term equity awards. The base salary tends to remain stable over time, while cash incentives and long-term equity awards are often linked to financial performance, such as annual sales, revenues, and market values. These factors can exhibit momentum and depend on past performance. Our state-dependent term captures this potential dependence on the previous firm-wage matching.
- (3) From a psychological and behavioral perspective, this specification also aligns with the *status quo bias* if  $\alpha > 0$ . People prefer to keep their current state. The employer may maintain a similar compensation rank among peers in the same industry. The employee may not resign and find a new job even if he/she is underpaid, possibly due to the status quo bias and relocation costs.

Overall, the state-dependent term with  $\alpha > 0$  is a form of persistence or inertia to favor matching pairs close to the previous pair  $(x_t, y_t)$ . In contrast, the PAM favors pairs with  $x_{t+1} = y_{t+1}$  regardless of previous states.

The problem (6.5) becomes state-dependent and thus is time-inconsistent. Since we consider  $x$  and  $y$  as ranks, the extended DP equation in the discrete case is sufficient. Denoting the equilibrium transport plan for a given  $\alpha$  as  $\pi(\alpha)$ , we can calculate the classic Wasserstein distance  $\mathcal{W}(\pi(\alpha), \pi_r)$  between  $\pi(\alpha)$  and the observed actual transport plan (matching)  $\pi_r$ :

$$\mathcal{W}(\pi(\alpha), \pi_r) := \inf_{\gamma \in \Pi(\pi(\alpha), \pi_r)} \int (|x_t - x'_t| + |y_t - y'_t|) d\gamma. \quad (6.6)$$

By varying  $\alpha$ , we can find  $\alpha$  minimizing  $\mathcal{W}(\pi(\alpha), \pi_r)$ . When the optimal  $\alpha$  is negative, it indicates that the data prefer to deviate from the previous matching, while a positive value of  $\alpha$  indicates that the data tend to maintain the previous matching.

In the next two sections, we investigate the inertia, measured by state dependence, of two job markets: top-ranking executives and academia (faculty and postdocs). The choice of these markets is mainly due to the availability of data. We examine the inertia measure  $\alpha$  and link it with the efficiency of job markets.

## 7 Executive job market

### 7.1 Overview

We focus on a five-year time horizon 2017 – 2021. The net sales data are from Compustat and the executive compensation information is from Execucomp. With the data cleaning procedure in Section B.1, our final sample consists of 790 firms, with a total market value of 61.7 trillion U.S. dollars in 2021. 396 firms are S&P 500 components. Table 8 in the e-companion presents the

---

<sup>1</sup><https://www.sec.gov/answers/execcomp.htm>

Sector	10	15	20	25	30	35	40	45	50	55	60
Spearman	0.72	0.793	0.752	0.515	0.755	0.768	0.745	0.646	0.75	0.871	0.559
Kendall	0.543	0.598	0.564	0.362	0.571	0.587	0.579	0.475	0.564	0.692	0.388

Table 2: Spearman and Kendall rank correlation between net sales and compensations in five years.

descriptive statistics for the data. Firms are classified into different industries using the Global Industry Classification Standard (GICS).

The first question we address is which industries are more aligned with the Roberts’ law, such that larger firms pay higher salaries to executives. To answer this question, we calculate the Spearman’s (Spearman, 1904) and Kendall’s (Kendall, 1938) rank correlations between net sales and compensations in Table 2. We find that the Consumer Discretionary (GICS Code 25), Real Estate (GICS Code 60), and Information Technology (GICS Code 45) industries are the top three sectors with weak correlations between net sales and wages. The Utilities industry (GICS Code 55) has the highest correlation.

Next, we examine the potential connection between the sale-wage correlation and inertia. In the following sections, we calibrate the optimal value of  $\alpha$  and find that the inertia is stronger when the relationship between sales and wages is weaker.

For clarity, we define an efficient job market as follows.

**Definition 7.1.** *A job market is said to be more efficient if the sale-wage correlation is higher. We call this correlation as the efficiency coefficient.*

Section 7.2 explains our choice of the statistical methods and Section 7.3 reports the main results.

## 7.2 Estimation methodology

### 7.2.1 Number of clusters

Ranks are discrete data that are suitable for discrete OT. However, the smallest number of firms in a single industry, as shown in Table 8, is 30. If we use the original ranks as the variables  $x_t$  and  $y_t$ , a large amount of data would be needed to estimate the transition probability matrices  $\mu(dx_{t+1}|x_t)$  and  $\nu(dy_{t+1}|y_t)$ . This is unrealistic, as the earliest wage data in Execucomp is primarily from 1992. In addition, transitions of original ranks can be noisy and sensitive to fluctuations in the data. There is also a practical concern about the computational burden of a large transport plan matrix.

Therefore, we aggregate data into several clusters with orders. There are two questions to consider in this process: the number of clusters and whether to use even-sized or uneven-sized clusters. As for the first question, the number of clusters cannot be too small or too large. A small number of clusters fails to capture the variations in the data. If we use only one cluster, all industries would perfectly match firms with wages. On the other hand, using too many clusters leads to the problems discussed above. There is no theoretical result on the optimal number of clusters. Backhoff-Veraguas et al. (2022, Definition 1.2) suggests using  $N^{1/(T+1)}$  clusters, where  $N$  is the number of time series. However, this result is only valid for  $N \rightarrow \infty$ , and would be too small when there are only a few data points. Given these difficulties, we suggest a practical and data-driven rule for determining the number of clusters.

For simplicity, we will use the same number of clusters for each industry to ensure fairness when comparing cross-sectional differences. The main feature we want to preserve after clustering is the relationship between sales and wages. Clusters are ordered and sales/wages in the same cluster are

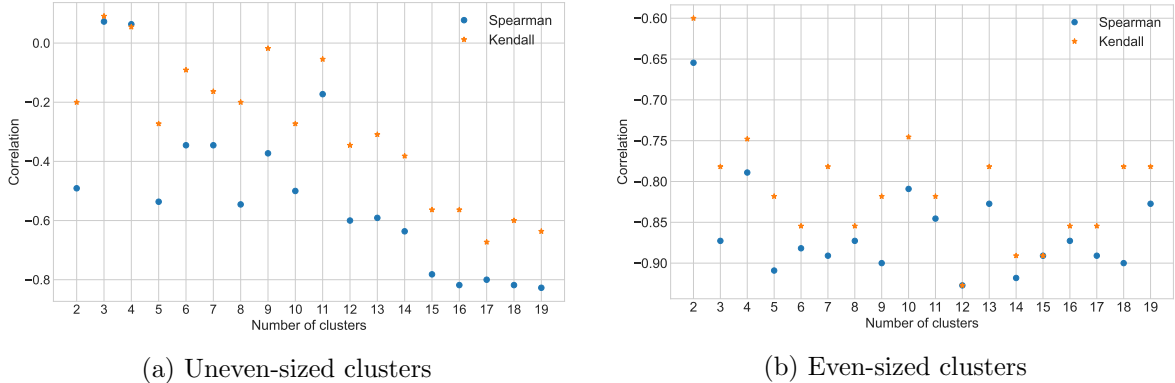


Figure 2: Selection for the optimal number of clusters.

assigned with the same rank. Denote the sale and wage cluster ranks for the firm  $i$  at time  $t$  as  $x_t^i$  and  $y_t^i$ , respectively. We call the mean absolute value of the difference in wage and sale ranks, that is,

$$\frac{1}{NT} \sum_{i=1}^N \sum_{t=1}^T |x_t^i - y_t^i|,$$

the *sale-wage discrepancy* for this industry. If the number of clusters is chosen appropriately, the sale-wage discrepancy should be bigger for sectors with lower sale-wage efficiency reported in Table 2. In other words, if we calculate the correlation between the sale-wage discrepancy and the sale-wage efficiency, we should prefer the number of clusters that generates strong negative correlations.

Figure 2 shows the correlations between the sale-wage discrepancy and efficiency using different numbers of clusters. The clusters are uneven in size in Figure 2a and even in size in Figure 2b. The uneven clusters are determined using the Jenks optimization method (Jenks, 1967) and the original values of wages and log values of sales. One advantage of uneven clusters is that the correlation is roughly monotonic with the number of clusters, as shown in Figure 2a. However, a disadvantage is that a large number of clusters is required to achieve a low, negative correlation, which is impractical due to the small amount of data. Even-sized clusters with ranks as the input, shown in Figure 2b, can achieve a low correlation with a relatively small number of clusters. Figure 2 reports both Kendall’s and Spearman’s rank correlations. We choose the first number of clusters that has a correlation less than  $-0.8$ . Based on Figure 2b, the suitable number of clusters is 5 or 6, depending on the type of the correlation used. As a robustness check, we also report the results using seven clusters in the e-companion.

### 7.2.2 Estimation of transition matrices

After determining the number of clusters, we estimate the conditional probability kernels which are transition matrices of ranks. We impose the following assumption to further simplify the model specification.

**Assumption 7.2.** *The conditional kernels  $\mu(dx_{t+1}|x_{1:t})$  and  $\nu(dy_{t+1}|y_{1:t})$  are Markov and time-homogeneous. That is,  $\mu(dx_{t+1}|x_{1:t}) = \mu(dx_{t+1}|x_t)$  and is the same for any  $t = 1, \dots, T - 1$ . The same condition holds for  $\nu(dy_{t+1}|y_{1:t})$  as well.*

To improve the accuracy of these estimates, we use wage-sale data spanning from 2010 to 2021 for the 790 firms considered in Table 8. We allow the planner to use all available data from 2010

to the final year of 2021 in the estimation process, in order to provide a larger pool of data. The transition matrices are calculated based on the frequencies of observed transitions between ranks over the years. Estimation results are given in Section B of the e-companion.

The transitions between ranks are crucial for our analysis. In the extreme case,  $x_{t+1} = x_t$  and  $y_{t+1} = y_t$  with probability one, that is, transition matrices are identity matrices. Then the state-dependent term will have no impact on the transport plans, because the marginal constraints have determined the matching already. There is no freedom to alter firm-wage pairs over time when rank transitions are forbidden. However, as long as transitions are not deterministic, we can capture  $\alpha$  with enough data.

### 7.2.3 Model validation

To stabilize the calibration, we adopt two additional methods. First, as our real dataset is of limited size, we use the re-sampling technique (bootstrapping) to generate a larger dataset by drawing with replacement from the real samples. Second, in practice, there are only a few non-zero entries in the one-period transport plans  $\pi_t$ . However, after multiplying the one-period transport plans as in equation (1.3) to obtain  $\pi(\alpha)$ , there are many paths of  $(x_{1:T}, y_{1:T})$  with very small probabilities. To speed up the calculation of the Wasserstein distance  $\mathcal{W}(\pi(\alpha), \pi_r)$  in (6.6) and amplify the impact of  $\alpha$ , we restrict the domain of  $\pi(\alpha)$  to a set of paths with an equal size of the bootstrap samples and the highest probabilities.

In our model, several approximations and hyperparameters may cause systematic bias, including the number of clusters, estimation errors in the transition matrices, the choice of the state-dependent preference function, the size of the bootstrap samples, and the restriction of  $\pi(\alpha)$  on paths with the highest probabilities. To address concerns about potential bias in our model, we propose to first apply it to synthetic data consisting only of perfectly matched sale-wage pairs. That is, firms ranked number  $n$  always pay wages ranked number  $n$ . In this case,  $x_t = y_t$  for all time points  $1 \leq t \leq T$ . Ideally, we would expect to observe the optimal value of  $\alpha$  to be close to zero in this scenario. There are several advantages to this validation procedure. First, it allows us to test whether the framework is functioning correctly in the simplest possible case. Second, it provides a method for selecting appropriate hyperparameters such that the benchmark outcome is close to zero. Finally, we can use the outcome of this analysis to correct any systematic bias in the model.

## 7.3 Results

Consider the number of clusters as 6 and the preference function as the indicator function. We divided the ranks by the number of clusters  $n$ , such that  $x_t$  and  $y_t$  are in  $[0, 1 - 1/n]$ , with 0 representing the highest rank. The candidate values for  $\alpha$  are discrete and evenly spaced as  $\{-1.5, -1.44, \dots, 0, \dots, 1.44, 1.5\}$ , with a step size of 0.06. The discount factor is set to  $\beta = 0.9$ . We ran the calibration with ten simulation instances. The size of both the synthetic and bootstrap samples is set to 500. We restricted the domain of  $\pi(\alpha)$  to 500 paths with the highest probabilities. The first row of Table 3, named as benchmark  $\alpha$ , presents the mean values of the optimal  $\alpha$  with synthetic perfectly matched data. In most sectors, the optimal benchmark  $\alpha$  is close to zero. Moreover, we observe that the model is biased toward the negative values of  $\alpha$ . Next, we feed the model with bootstrap samples from the real dataset. The row labeled “raw  $\alpha$ ” in Table 3 reports the optimal  $\alpha$  obtained from the resampled real data. Most of these values shift to the positive direction. Sector 50 obtains a smaller value due to a small fluctuation in the Wasserstein distance. The last row in Table 3 calculates the difference between the raw and benchmark  $\alpha$ . Overall, there is a state-dependent effect or inertia in most industries, regardless of whether the raw  $\alpha$  or the

Sector	10	15	20	25	30	35	40	45	50	55	60
Benchmark $\alpha$	-0.084	-0.06	-0.06	-0.084	-0.042	-0.114	-0.288	-0.096	-0.258	-0.12	-0.06
Raw $\alpha$	0.438	0.006	0.276	0.522	0.054	0.03	-0.048	0.66	-0.384	0.018	0.702
Adjusted $\alpha$	0.522	0.066	0.336	0.606	0.096	0.144	0.24	0.756	-0.126	0.138	0.762

Table 3: Mean values of the optimal  $\alpha$  in ten simulations. The number of clusters is set as 6. If there are multiple optimal  $\alpha$ , we choose the one that is closest to zero.

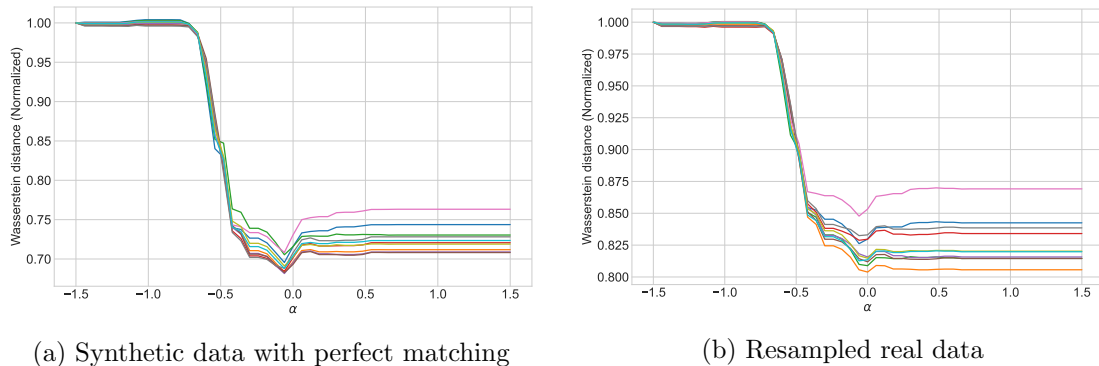


Figure 3: Calibration curves for Materials sector (GICS Code 15). Ten curves in each subplot represent ten independent simulations.

adjusted  $\alpha$  is used.

To understand the impact of  $\alpha$  on the Wasserstein distance  $\mathcal{W}(\pi(\alpha), \pi_r)$  between the model-implied and empirical transport plans, we consider the Materials and the Real Estate sectors as examples. Figures 3 and 4 depict the calibration curves with  $\alpha$  as the horizontal axis and  $\mathcal{W}(\pi(\alpha), \pi_r)$  in (6.6) (normalized) as the vertical axis. The Wasserstein distance is divided by  $\mathcal{W}(\pi(-1.5), \pi_r)$  such that all curves start from 1 when  $\alpha = -1.5$ . There are ten curves in each subplot, representing ten simulation instances with independent bootstrap samples. When comparing the results in Figures 3a and 3b for the Materials sector (GICS Code 15), we find that the shape of the calibration curves does not change significantly when perfectly matched data are replaced by the resampled real data. This suggests that the Materials sector does not exhibit a significant state-dependent phenomenon or inertia in sale-wage pairs. However, in the Real Estate sector, we find that the inertia is strong. The optimal  $\alpha$  shifts significantly toward positive values in Figure 4b, in contrast to the synthetic perfectly matched data in Figure 4a.

### Main observation

The central message of this section is that sectors with less efficient job markets tend to exhibit a higher level of inertia. This assertion has been supported by the negative correlations between the optimal  $\alpha$  in Table 3 and the sale-wage efficiency coefficient in Table 2. Table 4 shows that the correlation values are generally less than  $-0.6$  and statistically significant at the 5% level. Job markets with stronger inertia are less likely to embrace the PAM and adapt to change. Thus, there is a negative relationship between job market efficiency and inertia within a dynamic framework. In Section B.3 of the e-companion, we conduct a robustness check with different numbers of clusters and obtain similar conclusions.

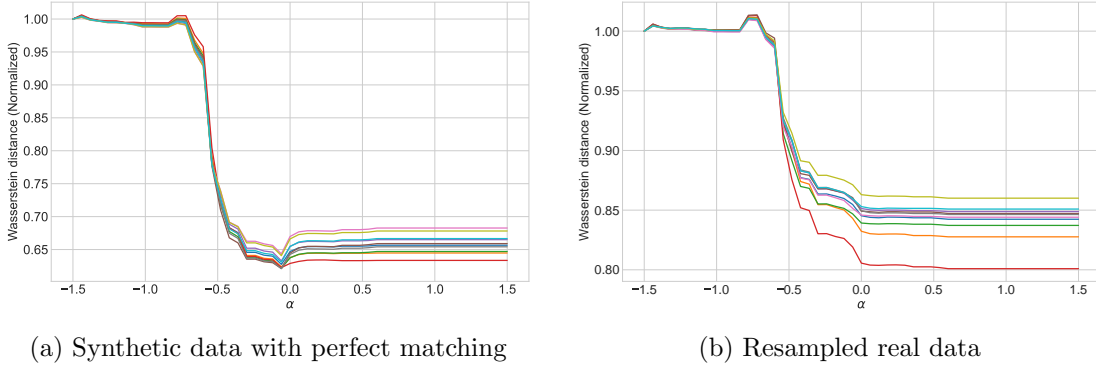


Figure 4: Calibration curves for Real Estate sector (GICS Code 60). Ten curves in each subplot represent ten independent simulations.

Correlation	Spearman ( $p$ -value)	Kendall ( $p$ -value)
Raw $\alpha$	-0.645 (0.032)	-0.600 (0.010)
Adjusted $\alpha$	-0.773 (0.005)	-0.600 (0.010)

Table 4: The relation between job market efficiency and the inertia effect. The correlations are between the optimal  $\alpha$  in Table 3 and the sale-wage efficiency coefficient in Table 2. The number of clusters is 6.

## 8 Academic job market

### 8.1 Overview

In contrast to the executive job market, the academic job market received less attention in the literature. Our analysis fills this gap using the University of California (UC) compensation data from the Government Compensation in California website [2] for the period of 2017 – 2021. The dataset includes total annual wages for various positions. In our analysis, we focus on four specific full-time positions: “Prof-Ay-B/E/E”, “Assoc Prof-Ay-B/E/E”, “Asst Prof-Ay-B/E/E”, and “Postdoc-Employee”. “AY” is short for Academic Year and “B/E/E” means Business/Economics/Engineering. In our current dataset, these three areas are reported jointly. The employees under the “Postdoc-Employee” title are from all departments. These full-time positions may provide a better representation of compensation levels than part-time positions. Tables 13 – 16 in the e-companion present the summary statistics of salaries in 2017 – 2021 for nine universities in the UC system, except UC San Francisco since it focuses on medical research and does not have faculty in the B/E/E departments. These tables also include the number of employees under each job title for 2021 only.

In assessing university quality, we utilize the U.S. News rankings, based on historical data compiled by Andrew G. Reiter [3]. While acknowledging the methodological limitations of university rankings, particularly the subjectivity of reputational assessments, our focus is specifically on the rankings of nine universities within the UC system. It is important to highlight that faculty salaries contribute to these rankings but carry a weight of only 7% [4]. Therefore, the ranks of faculty wages and university rankings do not align automatically. To determine the annual pay levels at each

<sup>2</sup><https://publicpay.ca.gov/Reports/RawExport.aspx>

<sup>3</sup><https://andyreiter.com/datasets/>

<sup>4</sup>More details in the article at <https://www.usnews.com/education/best-colleges/articles/how-us-news-calculated-the-rankings>

Position	Professor	Associate Professor	Assistant Professor	Postdoc
Spearman	0.78	0.747	0.868	0.403
Kendall	0.616	0.585	0.707	0.298

Table 5: Correlations between university rankings and wages in 2017–2021.

university, we calculate a single value by first ranking all wage observations among a given year and job title, and then selecting the median rank as a measure of compensation levels. This method mitigates the impact of outliers in the data.

Table 5 presents Spearman’s and Kendall’s rank correlations between university rankings and wages in 2017 – 2021. Salaries for B/E/E assistant professors are more consistent with university rankings, compared with executives in most sectors. However, postdoc salaries do not show a strong positive correlation with university rankings. It is the lowest among all job positions and business sectors analyzed in this paper. This pattern motivates us to examine whether the inertia in postdoc salaries is also stronger.

## 8.2 Number of clusters and estimation of transition matrices

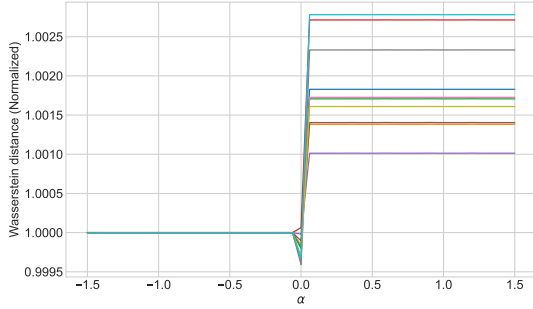
To determine the number of clusters for our analysis, we consider the U.S. News rankings and domain knowledge, as the small number of universities in our dataset (nine) makes it difficult to use the criterion applied to the executive data. We find that there are usually two universities with closely ranked positions, with the top two universities in the UC system ranking around the 20th place among national universities (and sometimes tied). The other universities tend to rank around the 30th, 40th, 80th, and 90th places. Based on these observations, we set the number of clusters to five, with two universities in each of the top four clusters and one university in the last cluster. Estimation results of the transition matrices are given in Figures 8 and 9 of the e-companion.

## 8.3 Results

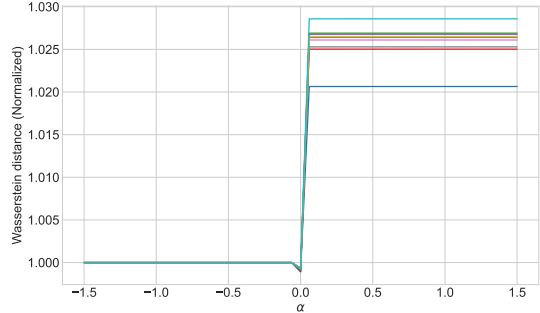
Since the number of universities in our dataset is much smaller than the number of firms, we set the size of our bootstrap samples to 200 for each simulation. We use the state-dependent preference function with  $\tau = 1$  and  $\alpha \in \{-1.5, -1.44, \dots, 0, \dots, 1.44, 1.5\}$  evenly spaced with a step size of 0.06.

Using the B/E/E Professors data, Figure 5 plots the Wasserstein distance between the model-implied transport plan  $\pi(\alpha)$  and the empirical transport plan  $\pi_r$ . The Wasserstein distance is divided by  $\mathcal{W}(\pi(-1.5), \pi_r)$  such that all curves start from 1 when  $\alpha = -1.5$ . As a validation test and benchmark, Figure 5a calibrates  $\alpha$  to synthetic data with perfect matching and plots curves from ten simulation instances. It shows that the optimal  $\alpha$  is zero and there is no evidence of inertia when synthetic data with perfect matching are used. In contrast, Figure 5b shows the results using bootstrap samples. The optimal  $\alpha$  is still zero across different simulation runs, indicating that the real data for the professor category are very similar to the perfectly matched synthetic data. Table 6 reports the mean values of optimal  $\alpha$  across these ten simulations.

We observe similar curves for associate professors and assistant professors. Their wages are also highly matched with university rankings, with no significant evidence of inertia. We report the mean values of the optimal  $\alpha$  in Table 6 and show the calibration curves in Figures 11 – 10, deferred to the e-companion.



(a) Synthetic data with perfect matching

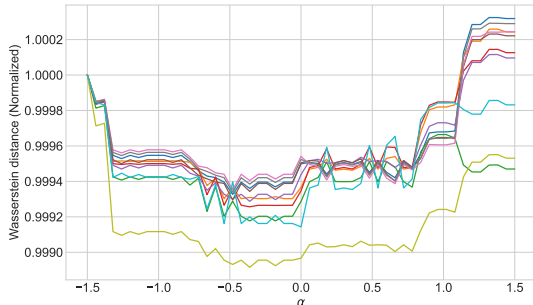


(b) Resampled real data

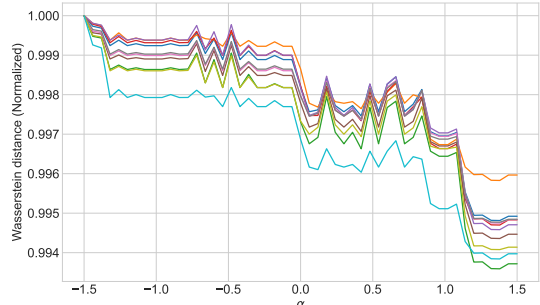
Figure 5: Calibration curves for B/E/E professors. In each subplot, ten curves represent individual calibrations with ten independent sampled data.

### Main observation

In contrast, we observe strong inertia in the salary data for postdocs. Figure 6a demonstrates the effectiveness of our framework by showing that the optimal  $\alpha$  is close to zero when using synthetic perfectly matched data. However, when we use the bootstrap samples, the trend in the calibration curves changes significantly. Figure 6b shows that the optimal  $\alpha$  exceeds 1, indicating strong inertia in the postdoc salary data. This effect is also stronger than in the executive data. The wages of postdocs do not match the rankings of universities. In the past five years from 2017 to 2021, UC Berkeley has paid lower median salaries to postdocs, compared with UCLA and several other universities in the UC system, as shown in Table 16. However, the difference in postdoc wages is small. Additionally, the change in Wasserstein distance is also small, mainly because the university wage data, with only nine observations, have a simpler structure than the executive data.



(a) Synthetic data with perfect matching



(b) Resampled real data

Figure 6: Calibration curves for postdocs.

Figure 6 also shows that the Wasserstein distance curves can be noisy when  $\alpha$  varies. To estimate the optimal  $\alpha$  robustly, we filter the original curves using the one-dimensional total variation denoising algorithm (Condat, 2013). This algorithm is suitable for signals with piecewise constant behaviors. Table 6 reports the mean optimal  $\alpha$  calculated from the filtered data. There is no significant evidence of inertia in wages for faculty. In contrast, the effect of inertia is very strong in the postdoc sector.

Position	Professor	Associate Professor	Assistant Professor	Postdoc
Benchmark $\alpha$	0.0	-0.06	-0.06	0.0
Raw $\alpha$	0.0	-0.06	-0.06	1.194
Adjusted $\alpha$	0.0	0.0	0.0	1.194

Table 6: Mean values of optimal  $\alpha$  after total variation filtering.

We test the connection between the inertia and university ranking-wage correlations, summarized in Table 7. Correlations in Table 7 are negative, showing that when the inertia is stronger, wages are less matched with university rankings. However, the power of our tests is low since only four types of jobs are considered.

Correlation	Spearman ( $p$ -value)	Kendall ( $p$ -value)
Raw $\alpha$	-0.632 (0.368)	-0.548 (0.279)
Adjusted $\alpha$	-0.775 (0.225)	-0.707 (0.180)

Table 7: Correlations between optimal  $\alpha$  and the ranking-wage dependence.

## 8.4 Discussions on relevant literature

Several alternative matching methods have been proposed in the literature, including search frictions (Shimer and Smith, 2000) and composite sorting (Boerma et al., 2023). When applying these frameworks to the academic job market, certain assumptions require careful consideration. The composite sorting model suggests that firms can mitigate mismatch costs through technology investments when a worker is underqualified. However, it remains debatable whether a university would invest in an underqualified researcher. Conversely, it seems more plausible that a university might offer amenities to attract overqualified researchers. Shimer and Smith (2000) posit that matching is both time-consuming and haphazard, but given the small size of the academic job market, this issue may not be significant. It is worth noting that our model could be integrated with Boerma et al. (2023) and/or Shimer and Smith (2000) to better explain wage dispersion, as these formulations do not account for the inertia caused by state dependence.

## Acknowledgment

The authors express gratitude to the anonymous referees and editors for their valuable comments and suggestions that have greatly improved this manuscript. Erhan Bayraktar is partially supported by the National Science Foundation under grant DMS-2106556 and by the Susan M. Smith chair. Bingyan Han is partially supported by The Hong Kong University of Science and Technology (Guangzhou) Start-up Fund G0101000197 and the Guangzhou-HKUST(GZ) Joint Funding Program (No. 2024A03J0630). This work was partially conducted when Bingyan Han was a post-doctoral researcher in the Department of Mathematics at the University of Michigan. He expresses gratitude to the University of Michigan for providing support and an atmosphere conducive to this work.

## References

Acciaio, B., Backhoff-Veraguas, J., and Jia, J. (2021). Cournot–Nash equilibrium and optimal transport in a dynamic setting. *SIAM Journal on Control and Optimization*, 59(3):2273–2300.

- Acciaio, B., Backhoff-Veraguas, J., and Zalashko, A. (2020). Causal optimal transport and its links to enlargement of filtrations and continuous-time stochastic optimization. *Stochastic Processes and their Applications*, 130(5):2918–2953.
- Arjovsky, M., Chintala, S., and Bottou, L. (2017). Wasserstein generative adversarial networks. In *International Conference on Machine Learning*, pages 214–223. PMLR.
- Backhoff-Veraguas, J., Bartl, D., Beiglböck, M., and Eder, M. (2020). Adapted Wasserstein distances and stability in mathematical finance. *Finance and Stochastics*, 24(3):601–632.
- Backhoff-Veraguas, J., Bartl, D., Beiglböck, M., and Wiesel, J. (2022). Estimating processes in adapted Wasserstein distance. *The Annals of Applied Probability*, 32(1):529–550.
- Backhoff-Veraguas, J., Beiglbock, M., Lin, Y., and Zalashko, A. (2017). Causal transport in discrete time and applications. *SIAM Journal on Optimization*, 27(4):2528–2562.
- Backhoff-Veraguas, J. and Zhang, X. (2023). Dynamic Cournot-Nash equilibrium: The non-potential case. *Mathematics and Financial Economics*, 17(2):153–174.
- Barberis, N. (2012). A model of casino gambling. *Management Science*, 58(1):35–51.
- Basak, S. and Chabakauri, G. (2010). Dynamic mean-variance asset allocation. *The Review of Financial Studies*, 23(8):2970–3016.
- Bayraktar, E., Eckstein, S., and Zhang, X. (2022). Stability and sample complexity of divergence regularized optimal transport. *arXiv preprint arXiv:2212.00367*.
- Bayraktar, E. and Han, B. (2023). Existence of Markov equilibrium control in discrete time. *SIAM Journal on Financial Mathematics*, 14(4):SC60–SC71.
- Bayraktar, E., Zhang, J., and Zhou, Z. (2021). Equilibrium concepts for time-inconsistent stopping problems in continuous time. *Mathematical Finance*, 31(1):508–530.
- Beiglböck, M., Jourdain, B., Margheriti, W., and Pammer, G. (2022). Approximation of martingale couplings on the line in the adapted weak topology. *Probability Theory and Related Fields*, 183(1):359–413.
- Beiglböck, M. and Pratelli, A. (2012). Duality for rectified cost functions. *Calculus of Variations and Partial Differential Equations*, 45:27–41.
- Bertsekas, D. and Shreve, S. E. (1978). *Stochastic Optimal Control: The Discrete-time Case*. Academic Press.
- Björk, T., Khapko, M., and Murgoci, A. (2017). On time-inconsistent stochastic control in continuous time. *Finance and Stochastics*, 21(2):331–360.
- Björk, T. and Murgoci, A. (2014). A theory of Markovian time-inconsistent stochastic control in discrete time. *Finance and Stochastics*, 18(3):545–592.
- Björk, T., Murgoci, A., and Zhou, X. Y. (2014). Mean–variance portfolio optimization with state-dependent risk aversion. *Mathematical Finance*, 24(1):1–24.
- Blanchet, J. and Murthy, K. (2019). Quantifying distributional model risk via optimal transport. *Mathematics of Operations Research*, 44(2):565–600.

- Blanchet, J., Murthy, K., and Nguyen, V. A. (2021). Statistical analysis of Wasserstein distributionally robust estimators. In *Tutorials in Operations Research: Emerging Optimization Methods and Modeling Techniques with Applications*, pages 227–254. INFORMS.
- Boerma, J., Tsyvinski, A., Wang, R., and Zhang, Z. (2023). Composite sorting. *arXiv preprint arXiv:2303.06701*.
- Bogachev, V. I. (2007). *Measure Theory*, volume II. Springer Science & Business Media.
- Brenier, Y. (1991). Polar factorization and monotone rearrangement of vector-valued functions. *Communications on Pure and Applied Mathematics*, 44(4):375–417.
- Brown, L. D. and Purves, R. (1973). Measurable selections of extrema. *The Annals of Statistics*, pages 902–912.
- Charalambos, D. and Aliprantis, B. (2013). *Infinite Dimensional Analysis: A Hitchhiker’s Guide*. Springer.
- Condat, L. (2013). A direct algorithm for 1-D total variation denoising. *IEEE Signal Processing Letters*, 20(11):1054–1057.
- Cuturi, M. (2013). Sinkhorn distances: Lightspeed computation of optimal transport. *Advances in Neural Information Processing Systems*, 26.
- Delon, J. and Desolneux, A. (2020). A Wasserstein-type distance in the space of Gaussian mixture models. *SIAM Journal on Imaging Sciences*, 13(2):936–970.
- Eckstein, S. and Pammer, G. (2024). Computational methods for adapted optimal transport. *The Annals of Applied Probability*, 34(1A):675–713.
- Epstein, L. G. and Ji, S. (2022). Optimal learning under robustness and time-consistency. *Operations Research*, 70(3):1317–1329.
- Föllmer, H. and Schied, A. (2011). *Stochastic Finance: An Introduction in Discrete Time*. Walter de Gruyter.
- Gabaix, X. and Landier, A. (2008). Why has CEO pay increased so much? *The Quarterly Journal of Economics*, 123(1):49–100.
- Galichon, A. (2016). *Optimal Transport Methods in Economics*. Princeton University Press.
- Gangbo, W. and McCann, R. J. (1996). The geometry of optimal transportation. *Acta Mathematica*, 177(2):113–161.
- Gao, R. and Kleywegt, A. (2022). Distributionally robust stochastic optimization with Wasserstein distance. *Mathematics of Operations Research*.
- Givens, C. R. and Shortt, R. M. (1984). A class of Wasserstein metrics for probability distributions. *Michigan Mathematical Journal*, 31(2):231–240.
- González-Sanz, A. and Nutz, M. (2024). Quantitative convergence of quadratically regularized linear programs. *arXiv preprint arXiv:2408.04088*.
- Gunasingam, M. and Wong, T.-K. L. (2024). Adapted optimal transport between Gaussian processes in discrete time. *arXiv preprint arXiv:2404.06625*.

- Han, B., Pun, C. S., and Wong, H. Y. (2021). Robust state-dependent mean–variance portfolio selection: A closed-loop approach. *Finance and Stochastics*, 25(3):529–561.
- Hu, M. and Zhou, Y. (2022). Dynamic type matching. *Manufacturing & Service Operations Management*, 24(1):125–142.
- Jenks, G. F. (1967). The data model concept in statistical mapping. *International Yearbook of Cartography*, 7:186–190.
- Kahneman, D. and Tversky, A. (1979). Prospect theory: An analysis of decision under risk. *Econometrica*, 47(2):263–292.
- Kallenberg, O. (2021). *Foundations of Modern Probability*. Springer Science & Business Media. The third edition.
- Kechris, A. (2012). *Classical Descriptive Set Theory*, volume 156. Springer Science & Business Media.
- Kendall, M. G. (1938). A new measure of rank correlation. *Biometrika*, 30(1/2):81–93.
- Kováčová, G. and Rudloff, B. (2021). Time consistency of the mean-risk problem. *Operations research*, 69(4):1100–1117.
- Kuhn, D., Esfahani, P. M., Nguyen, V. A., and Shafieezadeh-Abadeh, S. (2019). Wasserstein distributionally robust optimization: Theory and applications in machine learning. In *Operations research & management science in the age of analytics*, pages 130–166. INFORMS.
- Laibson, D. (1997). Golden eggs and hyperbolic discounting. *The Quarterly Journal of Economics*, 112(2):443–478.
- Lassalle, R. (2013). Causal transference plans and their Monge-Kantorovich problems. *arXiv preprint arXiv:1303.6925*.
- Ma, J., Wong, T.-K. L., and Zhang, J. (2021). Time-consistent conditional expectation under probability distortion. *Mathematics of Operations Research*, 46(3):1149–1180.
- Mohajerin Esfahani, P. and Kuhn, D. (2018). Data-driven distributionally robust optimization using the Wasserstein metric: Performance guarantees and tractable reformulations. *Mathematical Programming*, 171(1):115–166.
- Neufeld, A. and Sester, J. (2021). On the stability of the martingale optimal transport problem: A set-valued map approach. *Statistics & Probability Letters*, 176:109131.
- Parthasarathy, K. R. (2005). *Probability Measures on Metric Spaces*, volume 352. American Mathematical Soc.
- Peyré, G. and Cuturi, M. (2019). Computational optimal transport: With applications to data science. *Foundations and Trends® in Machine Learning*, 11(5-6):355–607.
- Pflug, G. C. and Pichler, A. (2012). A distance for multistage stochastic optimization models. *SIAM Journal on Optimization*, 22(1):1–23.
- Pflug, G. C. and Pichler, A. (2014). *Multistage Stochastic Optimization*, volume 1104. Springer.

- Pichler, A., Liu, R. P., and Shapiro, A. (2022). Risk-averse stochastic programming: Time consistency and optimal stopping. *Operations Research*, 70(4):2439–2455.
- Pichler, A. and Weinhardt, M. (2022). The nested Sinkhorn divergence to learn the nested distance. *Computational Management Science*, 19(2):269–293.
- Schrott, S., Beiglböck, M., and Pammer, G. (2023). Denseness of biadapted Monge mappings. *Annales de l’Institut Henri Poincaré-Probabilités et Statistiques*.
- Seguy, V., Damodaran, B. B., Flamary, R., Courty, N., Rolet, A., and Blondel, M. (2018). Large-scale optimal transport and mapping estimation. In *International Conference on Learning Representations*, pages 1–15.
- Shimer, R. and Smith, L. (2000). Assortative matching and search. *Econometrica*, 68(2):343–369.
- Spearman, C. (1904). The proof and measurement of association between two things. *The American Journal of Psychology*, 15(1):72–101.
- Steen, L. A. and Seebach, J. A. (1978). *Counterexamples in Topology*. Springer.
- Strotz, R. (1955). Myopia and inconsistency in dynamic utility maximization. *Review of Economic Studies*, 23(3):165–180.
- Sundaram, R. K. (1996). *A First Course in Optimization Theory*. Cambridge University Press.
- Taşkesen, B., Shafieezadeh-Abadeh, S., and Kuhn, D. (2023). Semi-discrete optimal transport: Hardness, regularization and numerical solution. *Mathematical Programming*, 199(1-2):1033–1106.
- Taylor, L. A. (2013). CEO wage dynamics: Estimates from a learning model. *Journal of Financial Economics*, 108(1):79–98.
- Torous, W., Gunsilius, F., and Rigollet, P. (2021). An optimal transport approach to causal inference. *arXiv preprint arXiv:2108.05858*.
- Villani, C. (2009). *Optimal Transport: Old and New*, volume 338. Springer.
- Xu, T., Li, W. K., Munn, M., and Acciaio, B. (2020). COT-GAN: Generating sequential data via causal optimal transport. *Advances in Neural Information Processing Systems*, 33:8798–8809.

## A Proofs of results

### A.1 The semi-discrete and Markovian case

We need several auxiliary results to study the continuity. Lemmas A.1 and A.2 do not rely on any particular choice of the metric.

**Lemma A.1.** *Suppose*

- (1)  $(\mathcal{X}_t, \mathcal{T}_{\mathcal{X}_t})$ ,  $(\mathcal{X}_{t+1}, \mathcal{T}_{\mathcal{X}_{t+1}})$ ,  $(\mathcal{Y}_t, \mathcal{T}_{\mathcal{Y}_t})$ ,  $(\mathcal{Y}_{t+1}, \mathcal{T}_{\mathcal{Y}_{t+1}})$  are Polish topological spaces and the product spaces between them are endowed with product topologies;

- (2) the stochastic kernels  $\mu(dx_{t+1}|x_t) : (\mathcal{X}_t, \mathcal{T}_{\mathcal{X}_t}) \rightarrow (\mathcal{P}(\mathcal{X}_{t+1}), \mathcal{V}[C_b(\mathcal{X}_{t+1}; \mathcal{T}_{\mathcal{X}_{t+1}})])$  and  $\nu(dy_{t+1}|y_t) : (\mathcal{Y}_t, \mathcal{T}_{\mathcal{Y}_t}) \rightarrow (\mathcal{P}(\mathcal{Y}_{t+1}), \mathcal{V}[C_b(\mathcal{Y}_{t+1}; \mathcal{T}_{\mathcal{Y}_{t+1}})])$  are continuous.

Denote a correspondence as

$$D : (\mathcal{X}_t \times \mathcal{Y}_t, \mathcal{T}_{\mathcal{X}_t} \times \mathcal{T}_{\mathcal{Y}_t}) \rightarrow (\mathcal{P}(\mathcal{X}_{t+1} \times \mathcal{Y}_{t+1}), \mathcal{V}[C_b(\mathcal{X}_{t+1} \times \mathcal{Y}_{t+1}; \mathcal{T}_{\mathcal{X}_{t+1}} \times \mathcal{T}_{\mathcal{Y}_{t+1}})])$$

that maps  $(x_t, y_t) \mapsto \Pi(\mu(dx_{t+1}|x_t), \nu(dy_{t+1}|y_t))$ .

Then  $D$  is upper hemicontinuous and  $D(x_t, y_t)$  is non-empty, convex, and compact. Moreover,  $D$  has a closed graph under the product topology  $\mathcal{T}_{\mathcal{X}_t} \times \mathcal{T}_{\mathcal{Y}_t} \times \mathcal{V}[C_b(\mathcal{X}_{t+1} \times \mathcal{Y}_{t+1}; \mathcal{T}_{\mathcal{X}_{t+1}} \times \mathcal{T}_{\mathcal{Y}_{t+1}})]$ .

*Proof.*  $\Pi(\mu(dx_{t+1}|x_t), \nu(dy_{t+1}|y_t))$  is non-empty since the independent coupling belongs to this set. This set is convex. Indeed, if  $\gamma^1, \gamma^2 \in \Pi(\mu(dx_{t+1}|x_t), \nu(dy_{t+1}|y_t))$ , then  $\lambda\gamma^1 + (1-\lambda)\gamma^2$ ,  $\lambda \in [0, 1]$  is also a probability measure with marginals  $\mu(dx_{t+1}|x_t)$  and  $\nu(dy_{t+1}|y_t)$ .

Since Polish spaces are second countable, first countable, and metrizable, we can apply Charalambos and Aliprantis (2013, Theorem 17.20). We only need to show that if a sequence  $\{(x_t^n, y_t^n, \gamma^n)\}$  is in the graph of  $D$  and  $(x_t^n, y_t^n) \rightarrow (x_t, y_t)$  under  $\mathcal{T}_{\mathcal{X}_t} \times \mathcal{T}_{\mathcal{Y}_t}$ , then the sequence  $\{\gamma^n\}$  has a limit point in  $\Pi(\mu(dx_{t+1}|x_t), \nu(dy_{t+1}|y_t))$ .

We have assumed  $\mu(dx_{t+1}|x_t)$  and  $\nu(dy_{t+1}|y_t)$  are continuous with the usual weak convergence. Thus, by Prokhorov's theorem,  $\{\mu(dx_{t+1}|x_t^n)\}_{n=1}^\infty$  and  $\{\nu(dy_{t+1}|y_t^n)\}_{n=1}^\infty$  are tight. The set of couplings  $\Pi(\{\mu(dx_{t+1}|x_t^n)\}_{n=1}^\infty, \{\nu(dy_{t+1}|y_t^n)\}_{n=1}^\infty)$  is also tight by Villani (2009, Lemma 4.4), where we emphasize that the product topology  $\mathcal{T}_{\mathcal{X}_{t+1}} \times \mathcal{T}_{\mathcal{Y}_{t+1}}$  is imposed. Indeed, Villani (2009, Lemma 4.4) relies on the fact that, if  $A \subset \mathcal{X}_{t+1}$  and  $B \subset \mathcal{Y}_{t+1}$  are compact, then  $A \times B$  is compact under the product topology  $\mathcal{T}_{\mathcal{X}_{t+1}} \times \mathcal{T}_{\mathcal{Y}_{t+1}}$ .

Since  $\{\gamma^n\}_{n=1}^\infty$  is in  $\Pi(\{\mu(dx_{t+1}|x_t^n)\}_{n=1}^\infty, \{\nu(dy_{t+1}|y_t^n)\}_{n=1}^\infty)$ , we can apply Prokhorov's theorem again. A subsequence  $\{\gamma^{n_k}\}_{k=1}^\infty$  converges weakly in the usual sense to some  $\gamma$ . We show  $\gamma \in \Pi(\mu(dx_{t+1}|x_t), \nu(dy_{t+1}|y_t))$ . Denote the projection operator on the first and second component as  $p_{\mathcal{X}} : \mathcal{X}_{t+1} \times \mathcal{Y}_{t+1} \rightarrow \mathcal{X}_{t+1}$  and  $p_{\mathcal{Y}} : \mathcal{X}_{t+1} \times \mathcal{Y}_{t+1} \rightarrow \mathcal{Y}_{t+1}$ . With the product topology, these projection operators are continuous. Hence, if  $f(x_{t+1})$  is a  $\mathcal{T}_{\mathcal{X}_{t+1}}$ -continuous function, then  $f \circ p_{\mathcal{X}}$  is  $\mathcal{T}_{\mathcal{X}_{t+1}} \times \mathcal{T}_{\mathcal{Y}_{t+1}}$ -continuous. Therefore, we have

$$\gamma^{n_k} \circ p_{\mathcal{X}}^{-1} \rightarrow \gamma \circ p_{\mathcal{X}}^{-1}, \quad \gamma^{n_k} \circ p_{\mathcal{Y}}^{-1} \rightarrow \gamma \circ p_{\mathcal{Y}}^{-1} \text{ weakly for } k \rightarrow \infty.$$

Since the marginals satisfy  $\gamma^{n_k} \circ p_{\mathcal{X}}^{-1} = \mu(dx_{t+1}|x_t^{n_k})$  and  $\gamma^{n_k} \circ p_{\mathcal{Y}}^{-1} = \nu(dy_{t+1}|y_t^{n_k})$ , together with  $\mu(dx_{t+1}|x_t^{n_k}) \rightarrow \mu(dx_{t+1}|x_t)$ ,  $\nu(dy_{t+1}|y_t^{n_k}) \rightarrow \nu(dy_{t+1}|y_t)$  weakly for  $k \rightarrow \infty$ , we obtain  $\gamma \circ p_{\mathcal{X}}^{-1} = \mu(dx_{t+1}|x_t)$  and  $\gamma \circ p_{\mathcal{Y}}^{-1} = \nu(dy_{t+1}|y_t)$ . Therefore,  $\gamma \in \Pi(\mu(dx_{t+1}|x_t), \nu(dy_{t+1}|y_t))$ .

By Charalambos and Aliprantis (2013, Theorem 17.20),  $D$  is upper hemicontinuous and compact-valued. By Charalambos and Aliprantis (2013, Theorem 17.10) and Polish spaces are Hausdorff,  $D$  has a closed graph.  $\square$

**Lemma A.2.** Consider Polish topological spaces  $(\mathcal{S}_1, \mathcal{T}_{\mathcal{S}_1})$ ,  $(\mathcal{S}_2, \mathcal{T}_{\mathcal{S}_2})$ , and  $(\mathcal{S}_3, \mathcal{T}_{\mathcal{S}_3})$ . Suppose

- (1) the stochastic kernel  $\gamma(ds_2|s_1) : (\mathcal{S}_1, \mathcal{T}_{\mathcal{S}_1}) \rightarrow (\mathcal{P}(\mathcal{S}_2), \mathcal{V}[C_b(\mathcal{S}_2; \mathcal{T}_{\mathcal{S}_2})])$  is continuous;
- (2) the function  $h(s_3, s_2) : (\mathcal{S}_3 \times \mathcal{S}_2, \mathcal{T}_{\mathcal{S}_3} \times \mathcal{T}_{\mathcal{S}_2}) \rightarrow (\mathbb{R}, \mathcal{T}_{\mathbb{R}})$  is continuous and bounded.

Then

- (a)  $\int_{\mathcal{S}_2} h(s_3, s_2) \gamma(ds_2|s_1)$  is  $\mathcal{T}_{\mathcal{S}_3} \times \mathcal{T}_{\mathcal{S}_1}$ -continuous. If  $(\mathcal{S}_3, \mathcal{T}_{\mathcal{S}_3}) = (\mathcal{S}_1, \mathcal{T}_{\mathcal{S}_1})$ , it is understood as  $\mathcal{T}_{\mathcal{S}_1}$ -continuous;
- (b) with  $\lambda \in \mathcal{P}(\mathcal{S}_2)$ ,  $\int_{\mathcal{S}_2} h(s_3, s_2) \lambda(ds_2)$  is  $\mathcal{T}_{\mathcal{S}_3} \times \mathcal{V}[C_b(\mathcal{S}_2; \mathcal{T}_{\mathcal{S}_2})]$ -continuous.

*Proof.* Consider a sequence  $(s_3^n, s_1^n)$  converging to  $(s_3, s_1)$  under the product topology  $\mathcal{T}_{\mathcal{S}_3} \times \mathcal{T}_{\mathcal{S}_1}$ . Equip  $\mathcal{S}_1$ ,  $\mathcal{S}_2$ , and  $\mathcal{S}_3$  with some complete compatible metrics.  $B := \{(s_3^n, s_1^n)\}_{n=1}^\infty \cup \{(s_3, s_1)\}$  is a compact set. Moreover, the uniform continuity is defined under these metrics.

Fix an arbitrary  $\varepsilon > 0$ . Since the product topology is used,  $s_1^n \rightarrow s_1$  under  $\mathcal{T}_{\mathcal{S}_1}$ . With the assumption that  $\gamma(ds_2|s_1)$  is continuous in  $s_1$ ,  $\gamma(ds_2|s_1^n)$  converges weakly to  $\gamma(ds_2|s_1)$ . Thus  $\{\gamma(ds_2|s_1^n)\}_{n=1}^\infty$  is tight by Prokhorov's theorem. We can find a compact subset  $A \subset \mathcal{S}_2$  such that  $\sup_n \gamma(\mathcal{S}_2 \setminus A|s_1^n) \leq \varepsilon$ .

Since  $h$  is uniformly continuous on the compact set  $B \times A$ , there exists  $N > 0$  such that

$$\sup_{n > N, s_2 \in A} |h(s_3, s_2) - h(s_3^n, s_2)| \leq \varepsilon. \quad (\text{A.1})$$

We have

$$\left| \int_{\mathcal{S}_2} h(s_3^n, s_2) \gamma(ds_2|s_1^n) - \int_{\mathcal{S}_2} h(s_3, s_2) \gamma(ds_2|s_1) \right| \leq \text{I} + \text{II} + \text{III},$$

where

$$\begin{aligned} \text{I} &= \left| \int_{\mathcal{S}_2} h(s_3, s_2) [\gamma(ds_2|s_1^n) - \gamma(ds_2|s_1)] \right|, \\ \text{II} &= \left| \int_A [h(s_3^n, s_2) - h(s_3, s_2)] \gamma(ds_2|s_1^n) \right|, \\ \text{III} &= \left| \int_{\mathcal{S}_2 \setminus A} [h(s_3^n, s_2) - h(s_3, s_2)] \gamma(ds_2|s_1^n) \right|. \end{aligned}$$

Since  $h$  is bounded and continuous, the term I converges to zero thanks to the weak convergence. As the set  $A$  is compact, when  $n > N$ , we have  $\text{II} \leq \varepsilon$  by the uniform continuity.  $\text{III} \leq C\varepsilon$  for a generic constant  $C$ , since  $h$  is bounded and  $\sup_n \gamma(\mathcal{S}_2 \setminus A|s_1^n) \leq \varepsilon$ . As  $\varepsilon > 0$  is arbitrary, we obtain the continuity as desired.

Claim (b) can be proved similarly. □

*Proof of Lemma 3.3.* Recalling the  $\pi^{t,\gamma}$  in Definition 2.2 but with a generic bicausal  $\pi$  after  $t + 1$ , we can show a recursive relationship for the objective  $J$  in (3.1):

$$\begin{aligned} J(x_t, y_t; \pi^{t,\gamma}) &= \left[ \int \left( c_{t+1}(x_t, y_t, x_{t+1}, y_{t+1}) + J(x_{t+1}, y_{t+1}; \pi) \right) \gamma(dx_{t+1}, dy_{t+1}) \right. \\ &\quad - \int G(x_{t+1}, y_{t+1}, \int h(x_T, y_T) \pi(dx_T, dy_T|x_{t+1}, y_{t+1})) \gamma(dx_{t+1}, dy_{t+1}) \\ &\quad \left. + G(x_t, y_t, \int \int h(x_T, y_T) \pi(dx_T, dy_T|x_{t+1}, y_{t+1})) \gamma(dx_{t+1}, dy_{t+1}) \right) \\ &\quad - \int \int \sum_{k=t+2}^T c_k(x_{t+1}, y_{t+1}, x_k, y_k) \pi(dx_{t+2:T}, dy_{t+2:T}|x_{t+1}, y_{t+1}) \gamma(dx_{t+1}, dy_{t+1}) \\ &\quad \left. + \int \int \sum_{k=t+2}^T c_k(x_t, y_t, x_k, y_k) \pi(dx_{t+2:T}, dy_{t+2:T}|x_{t+1}, y_{t+1}) \gamma(dx_{t+1}, dy_{t+1}) \right]. \end{aligned}$$

The proof is similar to the discrete case. Hence, if an equilibrium transport  $\pi^*$  exists and set  $\pi = \pi^*$  for  $t + 1, \dots, T - 1$ , we can derive the extended DP equation (3.2) in terms of  $g_{t+1}$  and  $b_k$ . Next, we

proceed by backward induction to show that the extended DP equation (3.2) is well-defined and  $V_t$ ,  $g_{t+1}$ , and  $b_k$  are continuous under a finer Polish topology.

Consider time  $t = T - 1$ . Since  $\nu(dy_T|y_{T-1})$  is Borel measurable, Kechris (2012, Theorem 13.11) shows that there exists a finer Polish topology  $\mathcal{T}_{\mathcal{Y}_{T-1}}^{(1)} \supseteq \mathcal{T}_{\mathcal{Y}_{T-1}}$  with the same Borel sets  $\mathcal{B}(\mathcal{T}_{\mathcal{Y}_{T-1}}^{(1)}) = \mathcal{B}(\mathcal{T}_{\mathcal{Y}_{T-1}})$ , such that  $\nu(dy_T|y_{T-1}) : (\mathcal{Y}_{T-1}, \mathcal{T}_{\mathcal{Y}_{T-1}}^{(1)}) \rightarrow (\mathcal{P}(\mathcal{Y}_T), \mathcal{V}[C_b(\mathcal{Y}_T; \mathcal{T}_{\mathcal{Y}_T})])$  is continuous. Since previous open sets are still open,  $\mathcal{T}_{\mathcal{Y}_{T-1}}$ -continuous functions are still  $\mathcal{T}_{\mathcal{Y}_{T-1}}^{(1)}$ -continuous. We check that the Borel measurable selection theorem (Brown and Purves, 1973, Corollary 1) is applicable to our problem. By Lemma A.2 and Assumption 3.1, the objective at time  $T - 1$ , given by

$$f(x_{T-1}, y_{T-1}, \gamma) := \int c_T(x_{T-1}, y_{T-1}, x_T, y_T) \gamma(dx_T, dy_T) \\ + G\left(x_{T-1}, y_{T-1}, \int h(x_T, y_T) \gamma(dx_T, dy_T)\right),$$

is  $\mathcal{T}_{\mathcal{X}_{T-1}} \times \mathcal{T}_{\mathcal{Y}_{T-1}}^{(1)} \times \mathcal{V}[C_b(\mathcal{X}_T \times \mathcal{Y}_T; \mathcal{T}_{\mathcal{X}_T} \times \mathcal{T}_{\mathcal{Y}_T})]$ -continuous.

By Lemma A.1, the graph of the correspondence

$$D : (\mathcal{X}_{T-1} \times \mathcal{Y}_{T-1}, \mathcal{T}_{\mathcal{X}_{T-1}} \times \mathcal{T}_{\mathcal{Y}_{T-1}}^{(1)}) \rightarrow (\mathcal{P}(\mathcal{X}_T \times \mathcal{Y}_T), \mathcal{V}[C_b(\mathcal{X}_T \times \mathcal{Y}_T; \mathcal{T}_{\mathcal{X}_T} \times \mathcal{T}_{\mathcal{Y}_T})]) \\ \text{that maps } (x_{T-1}, y_{T-1}) \mapsto \Pi(\mu(dx_T|x_{T-1}), \nu(dy_T|y_{T-1})),$$

is closed and thus Borel. Therefore, the objective at time  $T - 1$  is defined on a Borel set. Moreover, for each  $(x_{T-1}, y_{T-1})$ , the section  $\Pi(\mu(dx_T|x_{T-1}), \nu(dy_T|y_{T-1}))$  is compact. Hence, by Brown and Purves (1973, Corollary 1), there is a Borel measurable optimizer  $\pi^*(dx_T, dy_T|x_{T-1}, y_{T-1})$  such that

$$f(x_{T-1}, y_{T-1}, \pi^*(dx_T, dy_T|x_{T-1}, y_{T-1})) = \inf_{\gamma \in \Pi(\mu(dx_T|x_{T-1}), \nu(dy_T|y_{T-1}))} f(x_{T-1}, y_{T-1}, \gamma),$$

which is also the value function  $V_{T-1}(x_{T-1}, y_{T-1})$ .

As a preparation for applying Brown and Purves (1973, Corollary 1) at time  $T - 2$ , we refine the topology on  $\mathcal{Y}_{T-1}$  again. Since  $\mathcal{X}_{T-1}$  is finite, we suppose  $\mathcal{X}_{T-1} = \{1, \dots, n\}$  without loss of generality. For a given  $i \in \mathcal{X}_{T-1}$ , we apply Kechris (2012, Theorem 13.11) recursively to

$$\pi^*(dx_T, dy_T|i, y_{T-1}) : (\mathcal{Y}_{T-1}, \mathcal{T}_{\mathcal{Y}_{T-1}}^{(i)}) \rightarrow (\mathcal{P}(\mathcal{X}_T \times \mathcal{Y}_T), \mathcal{V}[C_b(\mathcal{X}_T \times \mathcal{Y}_T; \mathcal{T}_{\mathcal{X}_T} \times \mathcal{T}_{\mathcal{Y}_T})]).$$

There exists a stronger Polish topology  $\mathcal{T}_{\mathcal{Y}_{T-1}}^{(i+1)} \supseteq \mathcal{T}_{\mathcal{Y}_{T-1}}^{(i)}$  with  $\mathcal{B}(\mathcal{T}_{\mathcal{Y}_{T-1}}^{(i+1)}) = \mathcal{B}(\mathcal{T}_{\mathcal{Y}_{T-1}}^{(i)}) = \mathcal{B}(\mathcal{T}_{\mathcal{Y}_{T-1}})$ , such that  $\pi^*(dx_T, dy_T|i, y_{T-1})$  is  $\mathcal{T}_{\mathcal{Y}_{T-1}}^{(i+1)}$ -continuous in  $y_{T-1}$ . We claim that  $\pi^*(dx_T, dy_T|x_{T-1}, y_{T-1})$  is jointly continuous in  $(x_{T-1}, y_{T-1})$  under the product topology  $\mathcal{T}_{\mathcal{X}_{T-1}} \times \mathcal{T}_{\mathcal{Y}_{T-1}}^{(n+1)}$ . Consider a complete compatible metric  $d_{\mathcal{Y}}$  for  $\mathcal{T}_{\mathcal{Y}_{T-1}}^{(n+1)}$  and the discrete metric  $d_{\mathcal{X}}$  on  $\mathcal{X}_{T-1}$ , that is,  $d_{\mathcal{X}}(x, x') = 0$  if  $x = x'$  and  $d_{\mathcal{X}}(x, x') = 1$  if  $x \neq x'$ .  $(\mathcal{X}_{T-1} \times \mathcal{Y}_{T-1}, \mathcal{T}_{\mathcal{X}_{T-1}} \times \mathcal{T}_{\mathcal{Y}_{T-1}}^{(n+1)})$  is a Polish space with the metric  $d_{\mathcal{X}}(x, x') + d_{\mathcal{Y}}(y, y')$ , where we omitted the time subscript for simplicity. Denote  $d_{\mathcal{P}}$  as a complete compatible metric for  $(\mathcal{P}(\mathcal{X}_T \times \mathcal{Y}_T), \mathcal{V}[C_b(\mathcal{X}_T \times \mathcal{Y}_T; \mathcal{T}_{\mathcal{X}_T} \times \mathcal{T}_{\mathcal{Y}_T})])$ . Given  $(x, y)$ , for every  $\varepsilon > 0$ , we want to show that there exists  $\delta > 0$ , such that if  $d_{\mathcal{X}}(x, x') + d_{\mathcal{Y}}(y, y') < \delta$ , then  $d_{\mathcal{P}}(\pi^*(\cdot|x, y), \pi^*(\cdot|x', y')) < \varepsilon$ . In fact, since for each  $i \in \mathcal{X}_{T-1}$ , we can find  $\delta_i > 0$ , such that if  $d_{\mathcal{Y}}(y, y') < \delta_i$ , then  $d_{\mathcal{P}}(\pi^*(\cdot|i, y), \pi^*(\cdot|i, y')) < \varepsilon$ . Therefore, we can take  $\delta = \min\{\min_i\{\delta_i\}, 1\}$ , which guarantees  $x = x'$  when  $d_{\mathcal{X}}(x, x') + d_{\mathcal{Y}}(y, y') < \delta$  and then apply the continuity on  $y$  under a fixed  $x$  to show  $d_{\mathcal{P}}(\pi^*(\cdot|x, y), \pi^*(\cdot|x', y')) < \varepsilon$ .

Moreover, by Lemma A.2,

$$\begin{aligned} g_{T-1}(x_{T-1}, y_{T-1}) &:= \int h(x_T, y_T) \pi^*(dx_T, dy_T | x_{T-1}, y_{T-1}), \\ b_T(x_{T-1}, y_{T-1}, x_{T-1}, y_{T-1}) &:= \int c_T(x_{T-1}, y_{T-1}, x_T, y_T) \pi^*(dx_T, dy_T | x_{T-1}, y_{T-1}), \end{aligned}$$

and the value function  $V_{T-1}(x_{T-1}, y_{T-1})$  are  $\mathcal{T}_{\mathcal{X}_{T-1}} \times \mathcal{T}_{\mathcal{Y}_{T-1}}^{(n+1)}$ -continuous. For  $i \in \{0, \dots, T-2\}$ ,

$$b_T(x_i, y_i, x_{T-1}, y_{T-1}) := \int c_T(x_i, y_i, x_T, y_T) \pi^*(dx_T, dy_T | x_{T-1}, y_{T-1})$$

is  $\mathcal{T}_{\mathcal{X}_i} \times \mathcal{T}_{\mathcal{Y}_i} \times \mathcal{T}_{\mathcal{X}_{T-1}} \times \mathcal{T}_{\mathcal{Y}_{T-1}}^{(n+1)}$ -continuous.

At time  $t = T-2$ ,  $\mathcal{Y}_{T-1}$  is always endowed with  $\mathcal{T}_{\mathcal{Y}_{T-1}}^{(n+1)}$ . By Bertsekas and Shreve (1978, Proposition 7.25) or Kechris (2012, Theorem 17.24),  $(\mathcal{P}(\mathcal{Y}_{T-1}), \mathcal{V}[C_b(\mathcal{Y}_{T-1}; \mathcal{T}_{\mathcal{Y}_{T-1}})])$  and  $(\mathcal{P}(\mathcal{Y}_{T-1}), \mathcal{V}[C_b(\mathcal{Y}_{T-1}; \mathcal{T}_{\mathcal{Y}_{T-1}}^{(n+1)})])$  have the same collection of Borel sets, since  $\mathcal{B}(\mathcal{T}_{\mathcal{Y}_{T-1}}^{(n+1)}) = \mathcal{B}(\mathcal{T}_{\mathcal{Y}_{T-1}})$ . Hence,  $\nu(dy_{T-1} | y_{T-2}) : (\mathcal{Y}_{T-2}, \mathcal{T}_{\mathcal{Y}_{T-2}}) \rightarrow (\mathcal{P}(\mathcal{Y}_{T-1}), \mathcal{V}[C_b(\mathcal{Y}_{T-1}; \mathcal{T}_{\mathcal{Y}_{T-1}}^{(n+1)})])$  is still Borel measurable. Similarly, by Kechris (2012, Theorem 13.11), there exists a finer Polish topology  $\mathcal{T}_{\mathcal{Y}_{T-2}}^{(1)} \supseteq \mathcal{T}_{\mathcal{Y}_{T-2}}$  with the same Borel sets  $\mathcal{B}(\mathcal{T}_{\mathcal{Y}_{T-2}}^{(1)}) = \mathcal{B}(\mathcal{T}_{\mathcal{Y}_{T-2}})$ , such that  $\nu(dy_{T-1} | y_{T-2}) : (\mathcal{Y}_{T-2}, \mathcal{T}_{\mathcal{Y}_{T-2}}^{(1)}) \rightarrow (\mathcal{P}(\mathcal{Y}_{T-1}), \mathcal{V}[C_b(\mathcal{Y}_{T-1}; \mathcal{T}_{\mathcal{Y}_{T-1}}^{(n+1)})])$  is continuous.

By Lemma A.2 and continuity results of  $V_{T-1}$ ,  $g_{T-1}$ , and  $b_T$  above, the objective at time  $T-2$ , given by

$$\begin{aligned} f(x_{T-2}, y_{T-2}, \gamma) &:= \int \left( c_{T-1}(x_{T-2}, y_{T-2}, x_{T-1}, y_{T-1}) + V_{T-1}(x_{T-1}, y_{T-1}) \right) \gamma(dx_{T-1}, dy_{T-1}) \\ &\quad - \int G(x_{T-1}, y_{T-1}, g_{T-1}(x_{T-1}, y_{T-1})) \gamma(dx_{T-1}, dy_{T-1}) \\ &\quad + G\left(x_{T-2}, y_{T-2}, \int g_{T-1}(x_{T-1}, y_{T-1}) \gamma(dx_{T-1}, dy_{T-1})\right) \\ &\quad - \int b_T(x_{T-1}, y_{T-1}, x_{T-1}, y_{T-1}) \gamma(dx_{T-1}, dy_{T-1}) \\ &\quad + \int b_T(x_{T-2}, y_{T-2}, x_{T-1}, y_{T-1}) \gamma(dx_{T-1}, dy_{T-1}), \end{aligned}$$

is  $\mathcal{T}_{\mathcal{X}_{T-2}} \times \mathcal{T}_{\mathcal{Y}_{T-2}}^{(1)} \times \mathcal{V}[C_b(\mathcal{X}_{T-1} \times \mathcal{Y}_{T-1}; \mathcal{T}_{\mathcal{X}_{T-1}} \times \mathcal{T}_{\mathcal{Y}_{T-1}}^{(n+1)})]$ -continuous.

By Lemma A.1, the correspondence

$$\begin{aligned} D : (\mathcal{X}_{T-2} \times \mathcal{Y}_{T-2}, \mathcal{T}_{\mathcal{X}_{T-2}} \times \mathcal{T}_{\mathcal{Y}_{T-2}}^{(1)}) &\rightarrow (\mathcal{P}(\mathcal{X}_{T-1} \times \mathcal{Y}_{T-1}), \mathcal{V}[C_b(\mathcal{X}_{T-1} \times \mathcal{Y}_{T-1}; \mathcal{T}_{\mathcal{X}_{T-1}} \times \mathcal{T}_{\mathcal{Y}_{T-1}}^{(n+1)})]) \\ &\text{that maps } (x_{T-2}, y_{T-2}) \mapsto \Pi(\mu(dx_{T-1} | x_{T-2}), \nu(dy_{T-1} | y_{T-2})), \end{aligned}$$

has a closed graph and is compact-valued.

Again, Brown and Purves (1973, Corollary 1) proves that there exists a Borel measurable optimizer  $\pi^*(dx_{T-1}, dy_{T-1} | x_{T-2}, y_{T-2})$  such that

$$f(x_{T-2}, y_{T-2}, \pi^*(dx_{T-1}, dy_{T-1} | x_{T-2}, y_{T-2})) = \inf_{\gamma \in \Pi(\mu(dx_{T-1} | x_{T-2}), \nu(dy_{T-1} | y_{T-2}))} f(x_{T-2}, y_{T-2}, \gamma),$$

which also gives the value function  $V_{T-2}(x_{T-2}, y_{T-2})$ .

Without loss of generality, suppose  $\mathcal{X}_{T-2} = \{1, \dots, n\}$ . There exists a finer topology  $\mathcal{T}_{\mathcal{Y}_{T-2}}^{(n+1)} \supseteq \mathcal{T}_{\mathcal{Y}_{T-2}}$  with  $\mathcal{B}(\mathcal{T}_{\mathcal{Y}_{T-2}}^{(n+1)}) = \mathcal{B}(\mathcal{T}_{\mathcal{Y}_{T-2}})$ , such that  $\pi^*(dx_{T-1}, dy_{T-1}|x_{T-2}, y_{T-2})$  is jointly continuous in  $(x_{T-2}, y_{T-2})$  under the product topology  $\mathcal{T}_{\mathcal{X}_{T-2}} \times \mathcal{T}_{\mathcal{Y}_{T-2}}^{(n+1)}$ . Moreover,

$$\begin{aligned} g_{T-2}(x_{T-2}, y_{T-2}) &:= \int g_{T-1}(x_{T-1}, y_{T-1}) \pi^*(dx_{T-1}, dy_{T-1}|x_{T-2}, y_{T-2}), \\ b_{T-1}(x_{T-2}, y_{T-2}, x_{T-2}, y_{T-2}) &:= \int c_{T-1}(x_{T-2}, y_{T-2}, x_{T-1}, y_{T-1}) \pi^*(dx_{T-1}, dy_{T-1}|x_{T-2}, y_{T-2}), \\ &\int b_T(x_{T-1}, y_{T-1}, x_{T-1}, y_{T-1}) \pi^*(dx_{T-1}, dy_{T-1}|x_{T-2}, y_{T-2}), \\ &\int b_T(x_{T-2}, y_{T-2}, x_{T-1}, y_{T-1}) \pi^*(dx_{T-1}, dy_{T-1}|x_{T-2}, y_{T-2}), \end{aligned}$$

and the value function  $V_{T-2}(x_{T-2}, y_{T-2})$  are  $\mathcal{T}_{\mathcal{X}_{T-2}} \times \mathcal{T}_{\mathcal{Y}_{T-2}}^{(n+1)}$ -continuous. For  $i \in \{0, \dots, T-3\}$ ,

$$\begin{aligned} b_{T-1}(x_i, y_i, x_{T-2}, y_{T-2}) &:= \int c_{T-1}(x_i, y_i, x_{T-1}, y_{T-1}) \pi^*(dx_{T-1}, dy_{T-1}|x_{T-2}, y_{T-2}) \\ \text{and } \int b_T(x_i, y_i, x_{T-1}, y_{T-1}) \pi^*(dx_{T-1}, dy_{T-1}|x_{T-2}, y_{T-2}) \end{aligned}$$

are  $\mathcal{T}_{\mathcal{X}_i} \times \mathcal{T}_{\mathcal{Y}_i} \times \mathcal{T}_{\mathcal{X}_{T-2}} \times \mathcal{T}_{\mathcal{Y}_{T-2}}^{(n+1)}$ -continuous.

Therefore, we can prove the result by backward induction.  $\pi^*(dx_{t+1}, dy_{t+1}|x_t, y_t)$  and  $V_t(x_t, y_t)$  are Borel measurable. Indeed, there is a finer Polish topology such that they are continuous.  $\square$

The proof of Theorem 3.5 needs the following properties of l.s.c. functions.

**Lemma A.3.** *Consider Polish topological spaces  $(\mathcal{S}_1, \mathcal{T}_{\mathcal{S}_1})$ ,  $(\mathcal{S}_2, \mathcal{T}_{\mathcal{S}_2})$ , and  $(\mathcal{S}_3, \mathcal{T}_{\mathcal{S}_3})$ . Suppose*

- (1) *the stochastic kernel  $\gamma(ds_2|s_1) : (\mathcal{S}_1, \mathcal{T}_{\mathcal{S}_1}) \rightarrow (\mathcal{P}(\mathcal{S}_2), \mathcal{V}[C_b(\mathcal{S}_2; \mathcal{T}_{\mathcal{S}_2})])$  is continuous;*
- (2) *the function  $h(s_3, s_2) : (\mathcal{S}_3 \times \mathcal{S}_2, \mathcal{T}_{\mathcal{S}_3} \times \mathcal{T}_{\mathcal{S}_2}) \rightarrow (\mathbb{R}, \mathcal{T}_{\mathbb{R}})$  is l.s.c. and bounded from below;*
- (3) *the function  $g(s_2) : (\mathcal{S}_2, \mathcal{T}_{\mathcal{S}_2}) \rightarrow (\mathbb{R}, \mathcal{T}_{\mathbb{R}})$  is l.s.c. The function  $G(s_1, g) : (\mathcal{S}_1 \times \mathbb{R}, \mathcal{T}_{\mathcal{S}_1} \times \mathcal{T}_{\mathbb{R}}) \rightarrow (\mathbb{R}, \mathcal{T}_{\mathbb{R}})$  is l.s.c. Moreover,  $G(s_1, \cdot)$  is nondecreasing for each  $s_1$ .*

Then

- (a)  $\int_{\mathcal{S}_2} h(s_3, s_2) \gamma(ds_2|s_1)$  is  $\mathcal{T}_{\mathcal{S}_3} \times \mathcal{T}_{\mathcal{S}_1}$ -l.s.c. and bounded from below. If  $(\mathcal{S}_3, \mathcal{T}_{\mathcal{S}_3}) = (\mathcal{S}_1, \mathcal{T}_{\mathcal{S}_1})$ , it is understood as  $\mathcal{T}_{\mathcal{S}_1}$ -l.s.c. and bounded from below;
- (b) with  $\lambda \in \mathcal{P}(\mathcal{S}_2)$ ,  $\int_{\mathcal{S}_2} h(s_3, s_2) \lambda(ds_2)$  is  $\mathcal{T}_{\mathcal{S}_3} \times \mathcal{V}[C_b(\mathcal{S}_2; \mathcal{T}_{\mathcal{S}_2})]$ -l.s.c. and bounded from below;
- (c)  $G(s_1, g(s_2)) : (\mathcal{S}_1 \times \mathcal{S}_2, \mathcal{T}_{\mathcal{S}_1} \times \mathcal{T}_{\mathcal{S}_2}) \rightarrow (\mathbb{R}, \mathcal{T}_{\mathbb{R}})$  is l.s.c.

*Proof.* By Bertsekas and Shreve (1978, Lemma 7.14), there exists a sequence  $h_k(s_3, s_2)$  of continuous and bounded functions such that  $h_k$  converges increasingly to  $h$ . By monotone convergence theorem,

$$\int_{\mathcal{S}_2} h(s_3, s_2) \gamma(ds_2|s_1) = \int_{\mathcal{S}_2} \sup_k h_k(s_3, s_2) \gamma(ds_2|s_1) = \sup_k \int_{\mathcal{S}_2} h_k(s_3, s_2) \gamma(ds_2|s_1).$$

Hence, claim (a) follows since  $\int_{\mathcal{S}_2} h(s_3, s_2) \gamma(ds_2|s_1)$  is a supremum of continuous functions in  $(s_3, s_1)$ , by Lemma A.2. Claim (b) can be proved similarly.

For claim (c), we consider a sequence  $(s_1^n, s_2^n)$  converging to  $(s_1, s_2)$  under the product topology  $\mathcal{T}_{S_1} \times \mathcal{T}_{S_2}$ . Then

$$\liminf_{n \rightarrow \infty} G(s_1^n, g(s_2^n)) \geq \liminf_{n \rightarrow \infty} G(s_1^n, \inf_{k \geq n} g(s_2^k)) \geq G(s_1, \lim_{n \rightarrow \infty} \inf_{k \geq n} g(s_2^k)) \geq G(s_1, g(s_2)).$$

The first inequality uses the fact that  $g(s_2^n) \geq \inf_{k \geq n} g(s_2^k)$  and  $G(s_1^n, \cdot)$  is nondecreasing. The second inequality holds since  $G(\cdot, \cdot)$  is l.s.c. The last inequality is due to  $\lim_{n \rightarrow \infty} \inf_{k \geq n} g(s_2^k) = \liminf_{n \rightarrow \infty} g(s_2^n) \geq g(s_2)$ . □

*Proof of Theorem 3.5.* The proof is a modification for the case of Lemma 3.3.

Consider time  $t = T - 1$ .  $\nu(dy_T|y_{T-1}) : (\mathcal{Y}_{T-1}, \mathcal{T}_{\mathcal{Y}_{T-1}}^{(1)}) \rightarrow (\mathcal{P}(\mathcal{Y}_T), \mathcal{V}[C_b(\mathcal{Y}_T; \mathcal{T}_{\mathcal{Y}_T})])$  is continuous. By Lemma A.3 and Assumption 3.4, the objective at time  $T - 1$ , given by

$$f(x_{T-1}, y_{T-1}, \gamma) := \int c_T(x_{T-1}, y_{T-1}, x_T, y_T) \gamma(dx_T, dy_T) + G\left(x_{T-1}, y_{T-1}, \int h(x_T, y_T) \gamma(dx_T, dy_T)\right),$$

is  $\mathcal{T}_{\mathcal{X}_{T-1}} \times \mathcal{T}_{\mathcal{Y}_{T-1}}^{(1)} \times \mathcal{V}[C_b(\mathcal{X}_T \times \mathcal{Y}_T; \mathcal{T}_{\mathcal{X}_T} \times \mathcal{T}_{\mathcal{Y}_T})]$ -l.s.c. Indeed,  $\int c_T(x_{T-1}, y_{T-1}, x_T, y_T) \gamma(dx_T, dy_T)$  is l.s.c. in  $(x_{T-1}, y_{T-1}, \gamma)$  by Lemma A.3 (b). Similarly,  $\int h(x_T, y_T) \gamma(dx_T, dy_T)$  is l.s.c. in  $\gamma$ .  $G(x_{T-1}, y_{T-1}, \int h(x_T, y_T) \gamma(dx_T, dy_T))$  is l.s.c. in  $(x_{T-1}, y_{T-1}, \gamma)$  by Lemma A.3 (c).

Hence, by Brown and Purves (1973, Corollary 1), there is a Borel measurable optimizer  $\pi^*(dx_T, dy_T|x_{T-1}, y_{T-1})$ . It is jointly continuous in  $(x_{T-1}, y_{T-1})$  under a finer product topology  $\mathcal{T}_{\mathcal{X}_{T-1}} \times \mathcal{T}_{\mathcal{Y}_{T-1}}^{(n+1)}$  by Kechris (2012, Theorem 13.11). We note that l.s.c. functions are still l.s.c. under a finer topology. Then  $g_{T-1}(x_{T-1}, y_{T-1})$  and  $b_T(x_i, y_i, x_{T-1}, y_{T-1})$  are still l.s.c. when  $\mathcal{X}_{T-1} \times \mathcal{Y}_{T-1}$  is endowed with  $\mathcal{T}_{\mathcal{X}_{T-1}} \times \mathcal{T}_{\mathcal{Y}_{T-1}}^{(n+1)}$ .

At time  $T - 2$ , the objective is given by

$$\begin{aligned} f(x_{T-2}, y_{T-2}, \gamma) &:= \int c_{T-1}(x_{T-2}, y_{T-2}, x_{T-1}, y_{T-1}) \gamma(dx_{T-1}, dy_{T-1}) \\ &\quad + G\left(x_{T-2}, y_{T-2}, \int g_{T-1}(x_{T-1}, y_{T-1}) \gamma(dx_{T-1}, dy_{T-1})\right) \\ &\quad + \int b_T(x_{T-2}, y_{T-2}, x_{T-1}, y_{T-1}) \gamma(dx_{T-1}, dy_{T-1}). \end{aligned}$$

It is  $\mathcal{T}_{\mathcal{X}_{T-2}} \times \mathcal{T}_{\mathcal{Y}_{T-2}}^{(1)} \times \mathcal{V}[C_b(\mathcal{X}_{T-1} \times \mathcal{Y}_{T-1}; \mathcal{T}_{\mathcal{X}_{T-1}} \times \mathcal{T}_{\mathcal{Y}_{T-1}}^{(n+1)})]$ -l.s.c., by Lemma A.3 and Assumption 3.4. The remaining proof follows similarly as in Lemma 3.3. □

## A.2 The continuous and non-Markovian case

Lemma A.4 extends Lemma A.2 to unbounded functions. We note that Lemma A.4 relies on the metric used to define the growth rate.

**Lemma A.4.** *Consider metric spaces  $(S_1, d_1)$ ,  $(S_2, d_2)$ , and  $(S_3, d_3)$  that are Polish. Moreover,  $S_2$  is a finite dimensional vector space. With a given  $p \in [1, \infty)$ , suppose*

- (1) *the stochastic kernel  $\gamma(ds_2|s_1) : (S_1, d_1) \rightarrow \mathcal{P}_p(S_2)$  is continuous;*
- (2) *the function  $h(s_3, s_2) \in C_p(S_3 \times S_2)$ .*

Then

(a)  $\int_{\mathcal{S}_2} h(s_3, s_2) \gamma(ds_2|s_1)$  is continuous in  $(s_3, s_1)$ ;

(b) if  $(\mathcal{S}_3, d_3) = (\mathcal{S}_1, d_1)$  and  $\gamma(ds_2|s_1)$  satisfies  $\int_{\mathcal{S}_2} d_2(s_2, \bar{s}_2)^p \gamma(ds_2|s_1) \leq C(1 + d_1(s_1, \bar{s}_1)^p)$  for all  $s_1 \in \mathcal{S}_1$ , then  $\int_{\mathcal{S}_2} h(s_1, s_2) \gamma(ds_2|s_1) \in C_p(\mathcal{S}_1)$ ;

(c) with  $\lambda \in \mathcal{P}_p(\mathcal{S}_2)$ ,  $\int_{\mathcal{S}_2} h(s_3, s_2) \lambda(ds_2)$  is continuous in  $(s_3, \lambda)$ .

*Proof.* For the claim (a), consider a sequence  $(s_3^n, s_1^n)$  converging to  $(s_3, s_1)$ .  $B := \{(s_3^n, s_1^n)\}_{n=1}^\infty \cup \{(s_3, s_1)\}$  is a compact set. Fix an arbitrary  $\varepsilon > 0$ . Similar to Lemma A.2, we can find a compact subset  $A \subset \mathcal{S}_2$  such that  $\sup_n \gamma(\mathcal{S}_2 \setminus A | s_1^n) \leq \varepsilon$ . Without loss of generality, we can assume that there is a sufficiently large radius  $R$  such that the ball with radius  $R$  is contained by  $A$ :

$$K_R := \{s_2 | d_2(s_2, \bar{s}_2) \leq R\} \subset A. \quad (\text{A.2})$$

Indeed, since  $\mathcal{S}_2$  is finite dimensional, the closed ball  $K_R$  is compact (Charalambos and Aliprantis, 2013, Theorem 5.26). We can use  $K_R \cup A$  to replace  $A$  if needed.

Similarly, we have

$$\left| \int_{\mathcal{S}_2} h(s_3^n, s_2) \gamma(ds_2|s_1^n) - \int_{\mathcal{S}_2} h(s_3, s_2) \gamma(ds_2|s_1) \right| \leq \text{I} + \text{II} + \text{III},$$

where

$$\begin{aligned} \text{I} &= \left| \int_{\mathcal{S}_2} h(s_3, s_2) [\gamma(ds_2|s_1^n) - \gamma(ds_2|s_1)] \right|, \\ \text{II} &= \left| \int_A [h(s_3^n, s_2) - h(s_3, s_2)] \gamma(ds_2|s_1^n) \right|, \\ \text{III} &= \left| \int_{\mathcal{S}_2 \setminus A} [h(s_3^n, s_2) - h(s_3, s_2)] \gamma(ds_2|s_1^n) \right|. \end{aligned}$$

Since  $h(s_3, \cdot)$  satisfies the growth rate condition, the term I converges to zero when  $n \rightarrow \infty$  by Villani (2009, Definition 6.7 (iv)). As the set  $B \times A$  is compact, when  $n > N$ , we have  $\text{II} \leq \varepsilon$  by the uniform continuity. For III, since  $A$  contains a large enough ball with radius  $R$ ,

$$\begin{aligned} \text{III} &\leq \int_{\mathcal{S}_2 \setminus A} (|h(s_3^n, s_2)| + |h(s_3, s_2)|) \gamma(ds_2|s_1^n) \\ &\leq C \sup_n [1 + d_3(s_3^n, \bar{s}_3)^p] \varepsilon + C [1 + d_3(s_3, \bar{s}_3)^p] \varepsilon + 2C \int_{\mathcal{S}_2 \setminus K_R} d_2(s_2, \bar{s}_2)^p \gamma(ds_2|s_1^n). \end{aligned}$$

For the second inequality, we have used the growth rate condition of  $h$ , the inequality  $\sup_n \gamma(\mathcal{S}_2 \setminus A | s_1^n) \leq \varepsilon$ , and the fact that the ball  $K_R \subset A$ . By Villani (2009, Definition 6.7 (iii)), the last term is less than  $2C\varepsilon$  when  $n \rightarrow \infty$  and  $R$  is sufficiently large. In summary,

$$\limsup_{n \rightarrow \infty} \text{I} + \text{II} + \text{III} \leq C\varepsilon,$$

with a generic constant that is independent of  $\varepsilon$ . As  $\varepsilon > 0$  is arbitrary, we obtain the continuity as desired.

Claim (b) is direct. Claim (c) can be proved similarly to (a).  $\square$

Another useful result is the concatenation of continuous kernels is still continuous.

**Lemma A.5.** Consider metric spaces  $(\mathcal{S}_1, d_1)$ ,  $(\mathcal{S}_2, d_2)$ , and  $(\mathcal{S}_3, d_3)$  that are Polish. Moreover,  $\mathcal{S}_2$  and  $\mathcal{S}_3$  are finite dimensional vector spaces. With a given  $p \in [1, \infty)$ , suppose

- (1) the stochastic kernel  $\pi(ds_2|s_1) : (\mathcal{S}_1, d_1) \rightarrow \mathcal{P}_p(\mathcal{S}_2)$  is continuous and  $\int_{\mathcal{S}_2} d_2(s_2, \bar{s}_2)^p \pi(ds_2|s_1) \leq C(1 + d_1(s_1, \bar{s}_1)^p)$ ;
- (2) the stochastic kernel  $\pi(ds_3|s_1, s_2) : (\mathcal{S}_1 \times \mathcal{S}_2, (d_1^p + d_2^p)^{1/p}) \rightarrow \mathcal{P}_p(\mathcal{S}_3)$  is continuous and  $\int_{\mathcal{S}_3} d_3(s_3, \bar{s}_3)^p \pi(ds_3|s_1, s_2) \leq C(1 + d_1(s_1, \bar{s}_1)^p + d_2(s_2, \bar{s}_2)^p)$ .

Then there exists a unique kernel

$$\pi(ds_{2:3}|s_1) = \pi(ds_3|s_1, s_2)\pi(ds_2|s_1) \quad (\text{A.3})$$

from  $(\mathcal{S}_1, d_1)$  to  $\mathcal{P}_p(\mathcal{S}_2 \times \mathcal{S}_3)$ . It is continuous in  $s_1$ .

*Proof.* By Bertsekas and Shreve (1978, Proposition 7.28), there exists a unique  $\pi(ds_{2:3}|s_1)$  defined by (A.3). We only need to prove the continuity.

Consider a sequence  $\{s_1^n\}$  converging to  $s_1$ . By Villani (2009, Definition 6.7 and Theorem 6.8), we need to show that for all continuous functions  $\varphi$  with a growth rate of  $|\varphi(s_2, s_3)| \leq C(1 + d_2(s_2, \bar{s}_2)^p + d_3(s_3, \bar{s}_3)^p)$ , one has

$$\lim_{n \rightarrow \infty} \int_{\mathcal{S}_2 \times \mathcal{S}_3} \varphi(s_2, s_3) \pi(ds_{2:3}|s_1^n) = \int_{\mathcal{S}_2 \times \mathcal{S}_3} \varphi(s_2, s_3) \pi(ds_{2:3}|s_1). \quad (\text{A.4})$$

By Lemma A.4 (b),  $\Phi(s_1^n, s_2) := \int_{\mathcal{S}_3} \varphi(s_2, s_3) \pi(ds_3|s_1^n, s_2)$  is in  $C_p(\mathcal{S}_1 \times \mathcal{S}_2)$ . Thus, we can apply Lemma A.4 (b) again to  $\int_{\mathcal{S}_2} \Phi(s_1^n, s_2) \pi(ds_2|s_1^n)$ . It belongs to  $C_p(\mathcal{S}_1)$ . Then the convergence (A.4) holds. □

*Proof of Theorem 4.5.* The recursive relationship for  $V_t(x_{1:t}, y_{1:t})$  in (4.5) is direct. We prove that  $g_{t+1}$  and  $b_{t+1}$  are continuous and  $\theta_{t+1}^*(x_{1:t}, y_{1:t})$  exists.

First, we have  $V_T \in C_p(\mathcal{X} \times \mathcal{Y})$  by the boundary condition and Assumption 4.1.

Next, consider time  $t = T - 1$ . Thanks to Assumption 4.4(1), Assumption 4.1 and Lemma A.4, the objective functional

$$\begin{aligned} f(x_{1:T-1}, y_{1:T-1}, \theta_T) = & G\left(x_{T-1}, y_{T-1}, \int h(x_{1:T}, y_{1:T}) \gamma(dx_T, dy_T | \theta_T)\right) \\ & + \int c(x_{T-1}, y_{T-1}, x_{1:T}, y_{1:T}) \gamma(dx_T, dy_T | \theta_T) \end{aligned}$$

is  $\mathcal{T}_{\mathcal{X}_{1:T-1}} \times \mathcal{T}_{\mathcal{Y}_{1:T-1}} \times \mathcal{T}_{\Theta_T}$ -continuous. Moreover, by Assumption 4.4(3),  $f(x_{1:T-1}, y_{1:T-1}, \theta_T)$  is strictly quasiconvex in  $\theta_T$ . Assumption 4.4(2) imposes the required properties of the correspondence  $D_{T-1}$ . By a version of Berge's maximum theorem with strict quasiconcavity, see Sundaram (1996, Theorem 9.14 and Corollary 9.20) or Charalambos and Aliprantis (2013, Theorem 17.31),  $V_{T-1}$  given by

$$V_{T-1}(x_{1:T-1}, y_{1:T-1}) = \inf_{\theta_T \in D_{T-1}(x_{1:T-1}, y_{1:T-1})} f(x_{1:T-1}, y_{1:T-1}, \theta_T)$$

is  $\mathcal{T}_{\mathcal{X}_{1:T-1}} \times \mathcal{T}_{\mathcal{Y}_{1:T-1}}$ -continuous and the infimum is attained. There exists a unique and continuous optimizer  $\theta_T^*(x_{1:T-1}, y_{1:T-1}) : (\mathcal{X}_{1:T-1} \times \mathcal{Y}_{1:T-1}, d) \rightarrow (\Theta_T, d_{\Theta_T})$ , which is a function instead of correspondence. As a composition,  $\gamma(dx_T, dy_T | \theta_T^*(x_{1:T-1}, y_{1:T-1})) : (\mathcal{X}_{1:T-1} \times \mathcal{Y}_{1:T-1}, d) \rightarrow \mathcal{P}_p(\mathcal{X}_T \times \mathcal{Y}_T)$  is also continuous.

For the growth rate, we note the marginal constraint

$$\gamma(dx_T, dy_T | \theta_T^*(x_{1:T-1}, y_{1:T-1})) \in \Pi(\mu(dx_T | x_{1:T-1}), \nu(dy_T | y_{1:T-1}))$$

together with Assumption 4.2 (2). Then

$$\begin{aligned} & \left| \int_{\mathcal{X}_T \times \mathcal{Y}_T} c(x_{T-1}, y_{T-1}, x_{1:T}, y_{1:T}) \gamma(dx_T, dy_T | \theta_T^*(x_{1:T-1}, y_{1:T-1})) \right| \\ & \leq \int_{\mathcal{X}_T \times \mathcal{Y}_T} C \left[ 1 + \sum_{t=1}^T d_{\mathcal{X}_t}(x_t, \bar{x}_t)^p + \sum_{t=1}^T d_{\mathcal{Y}_t}(y_t, \bar{y}_t)^p \right] \gamma(dx_T, dy_T | \theta_T^*(x_{1:T-1}, y_{1:T-1})) \\ & = C + C \int_{\mathcal{X}_T} \sum_{t=1}^T d_{\mathcal{X}_t}(x_t, \bar{x}_t)^p \mu(dx_T | x_{1:T-1}) + C \int_{\mathcal{Y}_T} \sum_{t=1}^T d_{\mathcal{Y}_t}(y_t, \bar{y}_t)^p \nu(dy_T | y_{1:T-1}) \\ & \leq C \left[ 1 + \sum_{t=1}^{T-1} d_{\mathcal{X}_t}(x_t, \bar{x}_t)^p + \sum_{t=1}^{T-1} d_{\mathcal{Y}_t}(y_t, \bar{y}_t)^p \right]. \end{aligned}$$

Similarly, with Assumption 4.1, one has

$$\begin{aligned} & \left| G \left( x_{T-1}, y_{T-1}, \int_{\mathcal{X}_T \times \mathcal{Y}_T} h(x_{1:T}, y_{1:T}) \gamma(dx_T, dy_T | \theta_T^*(x_{1:T-1}, y_{1:T-1})) \right) \right| \tag{A.5} \\ & \leq C \left( 1 + \left| \int_{\mathcal{X}_T \times \mathcal{Y}_T} h(x_{1:T}, y_{1:T}) \gamma(dx_T, dy_T | \theta_T^*(x_{1:T-1}, y_{1:T-1})) \right|^{pr} + d((x_{T-1}, y_{T-1}), (\bar{x}_{T-1}, \bar{y}_{T-1}))^p \right) \\ & \leq C \left( 1 + \int_{\mathcal{X}_T \times \mathcal{Y}_T} |h(x_{1:T}, y_{1:T})|^{pr} \gamma(dx_T, dy_T | \theta_T^*(x_{1:T-1}, y_{1:T-1})) + d((x_{T-1}, y_{T-1}), (\bar{x}_{T-1}, \bar{y}_{T-1}))^p \right) \\ & \leq C [1 + d((x_{1:T-1}, y_{1:T-1}), (\bar{x}_{1:T-1}, \bar{y}_{1:T-1}))^p]. \end{aligned}$$

Therefore,  $V_{T-1} \in C_p(\mathcal{X}_{1:T-1} \times \mathcal{Y}_{1:T-1})$ .

By Lemma A.4 and  $1/r \leq p$ , the following functions are continuous in  $(x_{1:T-1}, y_{1:T-1})$ :

$$\begin{aligned} g_{T-1}(x_{1:T-1}, y_{1:T-1}) & := \int h(x_{1:T}, y_{1:T}) \gamma(dx_T, dy_T | \theta_T^*(x_{1:T-1}, y_{1:T-1})), \\ b_{T-1}(x_i, y_i, x_{1:T-1}, y_{1:T-1}) & := \int c(x_i, y_i, x_{1:T}, y_{1:T}) \gamma(dx_T, dy_T | \theta_T^*(x_{1:T-1}, y_{1:T-1})), \quad i \in \{0, \dots, T-1\}. \end{aligned}$$

In each step of backward induction, we also use Lemma A.5 that the successive concatenation of continuous conditional kernels  $\gamma(dx_T, dy_T | \theta_T^*(x_{1:T-1}, y_{1:T-1})), \dots, \gamma(dx_{t+1}, dy_{t+1} | \theta_{t+1}^*(x_{1:t}, y_{1:t}))$  induces a unique continuous conditional probability measure  $\gamma(dx_{t+1:T}, dy_{t+1:T} | \theta_{t+1:T}^*(x_{1:t}, y_{1:t}))$ .  $\square$

*Proof of Corollary 4.7.* With  $\Theta_{t+1} = \mathcal{P}_p(\mathcal{X}_{t+1} \times \mathcal{Y}_{t+1})$ , we only need to show the correspondence  $D_t$  satisfies Assumption 4.4 (2) in Lemma A.6. Then Corollary 4.7 follows directly from Theorem 4.5. Compared with Neufeld and Sester (2021), Lemma A.6 considers the  $W_p$  metric and does not have martingale constraints.  $\square$

Denote the sum of Wasserstein distances between  $\mu, \mu' \in \mathcal{P}(\mathcal{X})$  and  $\nu, \nu' \in \mathcal{P}(\mathcal{Y})$  as

$$W_p^\oplus((\mu, \nu), (\mu', \nu')) := W_p(\mu, \mu') + W_p(\nu, \nu').$$

**Lemma A.6.** Consider the metric spaces and Wasserstein distances in Section 4.1. For a given  $t$ , denote a correspondence as

$$D : \mathcal{X}_{1:t} \times \mathcal{Y}_{1:t} \rightarrow \mathcal{P}_p(\mathcal{X}_{t+1} \times \mathcal{Y}_{t+1}) \text{ that maps } (x_{1:t}, y_{1:t}) \mapsto \Pi(\mu(dx_{t+1}|x_{1:t}), \nu(dy_{t+1}|y_{1:t})).$$

Suppose Assumption 4.2 Condition (1) holds. Then  $D$  is a continuous correspondence and  $D(x_{1:t}, y_{1:t})$  is non-empty, convex, and compact, under the product topology of  $\mathcal{T}_{\mathcal{X}_{1:t}}$ ,  $\mathcal{T}_{\mathcal{Y}_{1:t}}$ , and the topology induced by the Wasserstein distance on  $\mathcal{P}_p(\mathcal{X}_{t+1} \times \mathcal{Y}_{t+1})$ .

*Proof.* With the metric  $d$  on  $\mathcal{X}_{1:t} \times \mathcal{Y}_{1:t}$  and the metric  $W_p$  on  $\mathcal{P}_p(\mathcal{X}_{t+1})$ ,  $\mathcal{P}_p(\mathcal{Y}_{t+1})$ , and  $\mathcal{P}_p(\mathcal{X}_{t+1} \times \mathcal{Y}_{t+1})$ , we first show that the correspondence  $(\alpha, \beta) \mapsto \Pi(\alpha, \beta)$  is continuous with  $W_p^\oplus$  metric on the domain and  $W_p$  on the range.

**Compactness and upper hemicontinuity:** The idea is similar to Lemma A.1. We show that if a sequence  $\{(\alpha^n, \beta^n, \gamma^n)\}$  is in the graph of  $D$  and

$$\lim_{n \rightarrow \infty} W_p^\oplus((\alpha^n, \beta^n), (\alpha, \beta)) = 0, \tag{A.6}$$

then the sequence  $\{\gamma^n\}$  has a limit point in  $\Pi(\alpha, \beta)$ .

By Villani (2009, Definition 6.7), the convergence in (A.6) implies the usual weak convergence. With the same argument in Lemma A.1, we can prove that a subsequence  $\{\gamma^{n_k}\}_{k=1}^\infty$  converges weakly in the usual sense to some  $\gamma \in \Pi(\alpha, \beta)$ . Furthermore,

$$\begin{aligned} & \lim_{k \rightarrow \infty} \int_{\mathcal{X}_{t+1} \times \mathcal{Y}_{t+1}} d((x_{t+1}, y_{t+1}), (\bar{x}_{t+1}, \bar{y}_{t+1}))^p \gamma^{n_k}(dx_{t+1}, dy_{t+1}) \\ &= \lim_{k \rightarrow \infty} \int_{\mathcal{X}_{t+1} \times \mathcal{Y}_{t+1}} [d_{\mathcal{X}_{t+1}}(x_{t+1}, \bar{x}_{t+1})^p + d_{\mathcal{Y}_{t+1}}(y_{t+1}, \bar{y}_{t+1})^p] \gamma^{n_k}(dx_{t+1}, dy_{t+1}) \\ &= \lim_{k \rightarrow \infty} \left( \int_{\mathcal{X}_{t+1}} d_{\mathcal{X}_{t+1}}(x_{t+1}, \bar{x}_{t+1})^p \alpha^{n_k}(dx_{t+1}) + \int_{\mathcal{Y}_{t+1}} d_{\mathcal{Y}_{t+1}}(y_{t+1}, \bar{y}_{t+1})^p \beta^{n_k}(dy_{t+1}) \right) \\ &= \int_{\mathcal{X}_{t+1}} d_{\mathcal{X}_{t+1}}(x_{t+1}, \bar{x}_{t+1})^p \alpha(dx_{t+1}) + \int_{\mathcal{Y}_{t+1}} d_{\mathcal{Y}_{t+1}}(y_{t+1}, \bar{y}_{t+1})^p \beta(dy_{t+1}) \\ &= \int_{\mathcal{X}_{t+1} \times \mathcal{Y}_{t+1}} [d_{\mathcal{X}_{t+1}}(x_{t+1}, \bar{x}_{t+1})^p + d_{\mathcal{Y}_{t+1}}(y_{t+1}, \bar{y}_{t+1})^p] \gamma(dx_{t+1}, dy_{t+1}) \\ &= \int_{\mathcal{X}_{t+1} \times \mathcal{Y}_{t+1}} d((x_{t+1}, y_{t+1}), (\bar{x}_{t+1}, \bar{y}_{t+1}))^p \gamma(dx_{t+1}, dy_{t+1}). \end{aligned}$$

Therefore, conditions in Villani (2009, Definition 6.7 (i)) are verified and we obtain the convergence  $\lim_{k \rightarrow \infty} W_p(\gamma^{n_k}, \gamma) = 0$ .

**Lower hemicontinuity:** By Charalambos and Aliprantis (2013, Theorem 17.21), we have to prove the following claim: For any  $(\alpha, \beta) \in \mathcal{P}_p(\mathcal{X}_{t+1}) \times \mathcal{P}_p(\mathcal{Y}_{t+1})$ , if  $(\alpha^n, \beta^n)$  converges weakly to  $(\alpha, \beta)$  in the metric  $W_p^\oplus$ , then for each  $\gamma \in \Pi(\alpha, \beta)$ , there exists a subsequence  $(\alpha^{n_k}, \beta^{n_k})$  and  $\gamma^k \in \Pi(\alpha^{n_k}, \beta^{n_k})$  for each  $k$ , such that  $\gamma^k$  converges weakly to  $\gamma$  in  $\mathcal{P}_p(\mathcal{X}_{t+1} \times \mathcal{Y}_{t+1})$  (Villani, 2009, Definition 6.7). Indeed, this result has been proved in Beiglböck et al. (2022, Equations 2.1 and 2.2).

We have proved the continuity of the correspondence  $(\alpha, \beta) \mapsto \Pi(\alpha, \beta)$  and the compactness of  $\Pi(\alpha, \beta)$ . Moreover, Assumption 4.2 Condition (1) guarantees that

$$(x_{1:t}, y_{1:t}) \mapsto (\mu(dx_{t+1}|x_{1:t}), \nu(dy_{t+1}|y_{1:t}))$$

is continuous. By Charalambos and Aliprantis (2013, Theorem 17.23) on the continuity of the composition of correspondence,  $D$ , viewed as the composition

$$(x_{1:t}, y_{1:t}) \mapsto (\mu(dx_{t+1}|x_{1:t}), \nu(dy_{t+1}|y_{1:t})) \mapsto \Pi(\mu(dx_{t+1}|x_{1:t}), \nu(dy_{t+1}|y_{1:t})),$$

is also continuous. □

## B Supplement to the executive job market

### B.1 Data cleaning and summary statistics

The choice of a five-year time horizon 2017 – 2021 is motivated by the following factors. A longer time horizon incurs a heavy computational burden. Moreover, in our final dataset, the median tenure of a CEO is 4 years and the average tenure is 5.97 years. In the literature with different datasets, Taylor (2013, Table 1) reported the average CEO tenure as 7.9 years and the median as 6 years. Overall, a five-year time horizon is close to the CEO’s tenure. Besides, the job market can change significantly over a longer period.

To obtain and clean the data, we adopt the following steps:

- (1) We download the net sales data from Compustat and the executive compensation information from Execucomp. There are no restrictions on the net sales or market values of firms at this stage. The key variables are net sales (“sale” in Compustat) and total compensation (“tdc1” in Execucomp). In 2017 – 2021, we have data on 1998 firms from Execucomp and 11911 firms from Compustat. Execucomp primarily includes salary information for S&P 1500 components.
- (2) We remove firms with missing net sales data for the five-year period. Compensation data are usually available for the CEO, chief financial officer, and the three other most highly compensated executive officers. We use their mean salary as the representative wage paid to top executives by the firm. After merging the sale and wage datasets, there are 1590 firms remaining.
- (3) To further filter the firms, we restrict our analysis to companies with investment-grade credit ratings. We download the S&P Domestic Long-Term Issuer Credit Rating (variable name: “splticrm”) and remove firms with a rating of CCC+ or lower. We also remove firms without ratings.

Table 8 shows the descriptive statistics for the data.

Industry	GICS Code	Number of firms	Market value	Net sales	Compensation
Energy	10	48	22693.93	19713.07	4.82
Materials	15	66	12889.25	7301.68	3.79
Industrials	20	118	20781.59	12368.6	4.14
Consumer Discretionary	25	112	32048.23	16761.5	5.80
Consumer Staples	30	48	46617.8	34468.41	5.55
Health Care	35	63	51570.67	33801.81	6.07
Financials	40	110	24242.18	16041.93	5.38
Information Technology	45	79	75539.2	17750.21	7.25
Communication Services	50	30	78888.99	26807.29	9.02
Utilities	55	50	18192.87	7446.87	3.21
Real Estate	60	66	11529.68	1949.91	3.88

Table 8: Summary statistics of firms over 2017 – 2021. Values in the last three columns are measured in millions of USD.

## B.2 Estimated transition matrices

Figure 7 gives the estimated transition matrices for sale and wage ranks. Group 1 is the group with the highest wages or sales. To save space, we average the transition matrices across 11 sectors and summarize them in two figures. A common pattern in all sectors is that sale ranks are more stable than wage ranks. Wages are more stable for the highest and the lowest group. For the wage groups in the middle, the probability of a rise or fall in wage ranks is approximately equal.

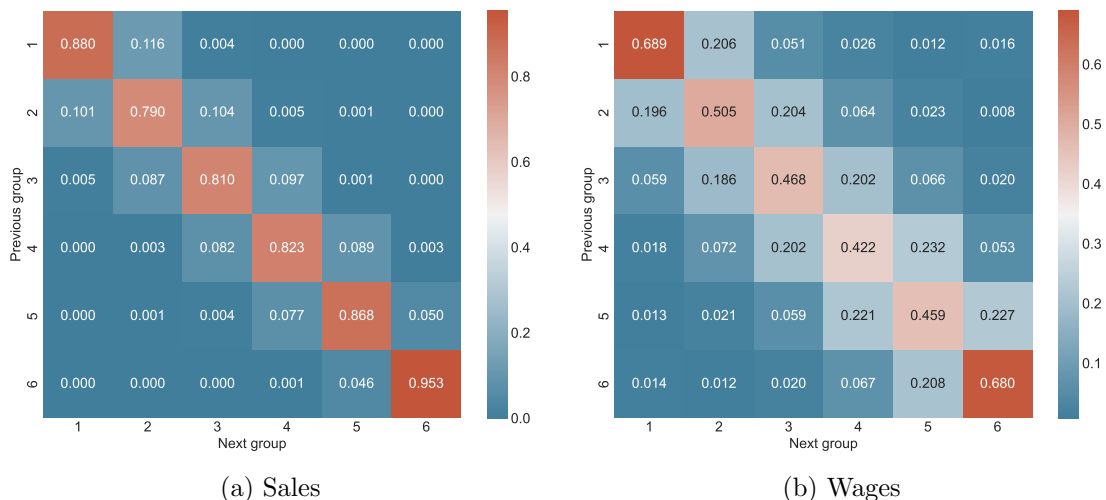


Figure 7: Transition matrices of wage and sale ranks. The matrices are averaged across 11 sectors.

### B.3 Robustness check with different number of clusters

As a robustness check, we examine the results in Section 7 with different numbers of clusters. The screening method in Figure 2b suggests that the choice of five clusters is also reasonable. All other specifications are kept the same. The first row of Table 9 shows that the systematic bias moves further toward the negative side as the number of clusters decreases, indicating that the outcomes may be more similar to the one-cluster case. When resampled real data are used, we obtain the same conclusion as in the six-cluster situation. Table 10 finds that the correlations are negative and the  $p$ -values are smaller than 5%.

Sector	10	15	20	25	30	35	40	45	50	55	60
Benchmark $\alpha$	-0.42	-0.12	-0.318	-0.324	-0.282	-0.366	-0.42	-0.21	-0.252	-0.222	-0.294
Raw $\alpha$	0.012	-0.072	-0.006	0.45	-0.132	-0.51	-0.444	-0.066	-0.492	-0.462	0.054
Adjusted $\alpha$	0.432	0.048	0.312	0.774	0.15	-0.144	-0.024	0.144	-0.24	-0.24	0.348

Table 9: Mean values of the optimal  $\alpha$  using five clusters. Other settings are the same as in the six-cluster counterpart.

Correlation	Spearman ( $p$ -value)	Kendall ( $p$ -value)
Raw $\alpha$	-0.709 (0.015)	-0.636 (0.006)
Adjusted $\alpha$	-0.700 (0.016)	-0.636 (0.006)

Table 10: Testing the association between job market efficiency and inertia when five clusters are adopted.

When seven clusters are used, the systematic bias shifts to the positive side, as shown in the first row of Table 11. The original and adjusted optimal  $\alpha$  tend to be larger than those obtained using five or six clusters. Although the correlations in Table 12 are still negative, the power of the test is much lower. One possible explanation is that Figure 2b shows that the choice of seven clusters results in a slightly worse correlation than the five and six clusters options. In addition, estimation errors in the transition matrices can be larger. Unfortunately, using a longer period of empirical data to estimate the transition matrices may not be a viable solution, as the job market may not be stationary over a long time horizon. Our parameter settings were fine-tuned for six clusters, so it is expected that the performance can be worse with a different number of clusters.

Sector	10	15	20	25	30	35	40	45	50	55	60
Benchmark $\alpha$	0.234	-0.06	0.33	0.324	-0.06	0.582	-0.096	0.198	-0.102	0.066	0.078
Raw $\alpha$	0.372	-0.06	0.756	0.42	0.222	0.636	0.054	0.438	0.204	0.264	0.666
Adjusted $\alpha$	0.138	0.0	0.426	0.096	0.282	0.054	0.15	0.24	0.306	0.198	0.588

Table 11: Mean values of the optimal  $\alpha$  using seven clusters. Other settings are the same as in the six-cluster counterpart.

Correlation	Spearman ( $p$ -value)	Kendall ( $p$ -value)
Raw $\alpha$	-0.345 (0.298)	-0.382 (0.121)
Adjusted $\alpha$	-0.245 (0.467)	-0.309 (0.218)

Table 12: Testing the association between job market efficiency and inertia when seven clusters are adopted.

University	Number of employees	Min wage	Median wage	Max wage
UC Berkeley	222	3000.0	250141.5	632257.0
UC Davis	164	1250.0	211538.0	472937.0
UC Irvine	172	2117.0	225990.0	609000.0
UC Los Angeles	195	1906.0	330058.0	778102.0
UC Merced	29	19401.0	207291.5	350160.0
UC Riverside	72	500.0	230418.5	412552.0
UC San Diego	181	12400.0	246321.0	586884.0
UC Santa Barbara	114	21667.0	258774.0	580967.0
UC Santa Cruz	66	6936.0	182750.0	379110.0

Table 13: Wage statistics of B/E/E professors in 2017 – 2021. The numbers of employees are in 2021 only. Min, median, and max wages (in U.S. dollars) are for five years from 2017 to 2021.

University	Number of employees	Min wage	Median wage	Max wage
UC Berkeley	73	11086.0	209901.0	582942.0
UC Davis	49	54768.0	160465.0	313901.0
UC Irvine	64	45856.0	171821.0	387084.0
UC Los Angeles	40	4057.0	261654.0	494989.0
UC Merced	27	62208.0	155763.0	230762.0
UC Riverside	44	10608.0	175183.0	301166.0
UC San Diego	60	11258.0	199728.0	436367.0
UC Santa Barbara	13	36633.0	176921.0	430169.0
UC Santa Cruz	22	10667.0	163482.0	235600.0

Table 14: Wage statistics of B/E/E associate professors. Numbers are reported in the same way as in Table 13.

University	Number of employees	Min wage	Median wage	Max wage
UC Berkeley	72	9992.0	172602.5	356679.0
UC Davis	51	1000.0	141866.0	262833.0
UC Irvine	74	10833.0	143116.0	331450.0
UC Los Angeles	82	8917.0	175874.5	408104.0
UC Merced	31	8450.0	129069.0	203730.0
UC Riverside	58	27775.0	132105.5	266866.0
UC San Diego	97	2386.0	155516.0	429625.0
UC Santa Barbara	48	1295.0	162483.0	302019.0
UC Santa Cruz	45	9017.0	138514.0	247281.0

Table 15: Wage statistics of B/E/E associate professors. Numbers are reported in the same way as in Table 13.

University	Number of employees	Min wage	Median wage	Max wage
UC Berkeley	1246	4.0	44151.0	197419.0
UC Davis	933	2.0	45978.0	137724.0
UC Irvine	524	40.0	43032.0	102079.0
UC Los Angeles	1056	10.0	48566.0	181982.0
UC Merced	89	1694.0	39271.5	100772.0
UC Riverside	299	42.0	44651.0	87372.0
UC San Diego	1394	14.0	46350.0	139683.0
UC Santa Barbara	430	54.0	47104.0	148142.0
UC Santa Cruz	184	106.0	45629.5	80133.0

Table 16: Wage statistics of postdocs. Numbers are reported in the same way as in Table 13.

## C Supplement to the academic job market

### C.1 Summary statistics

### C.2 Estimated transition matrices

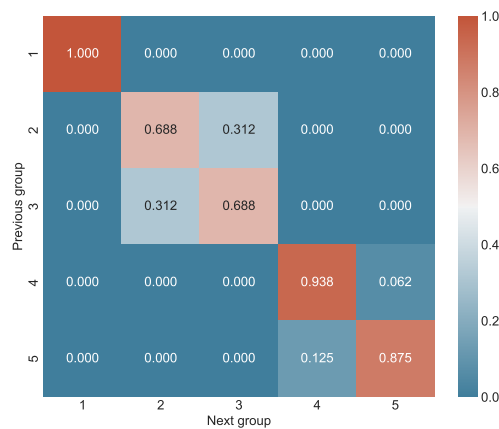
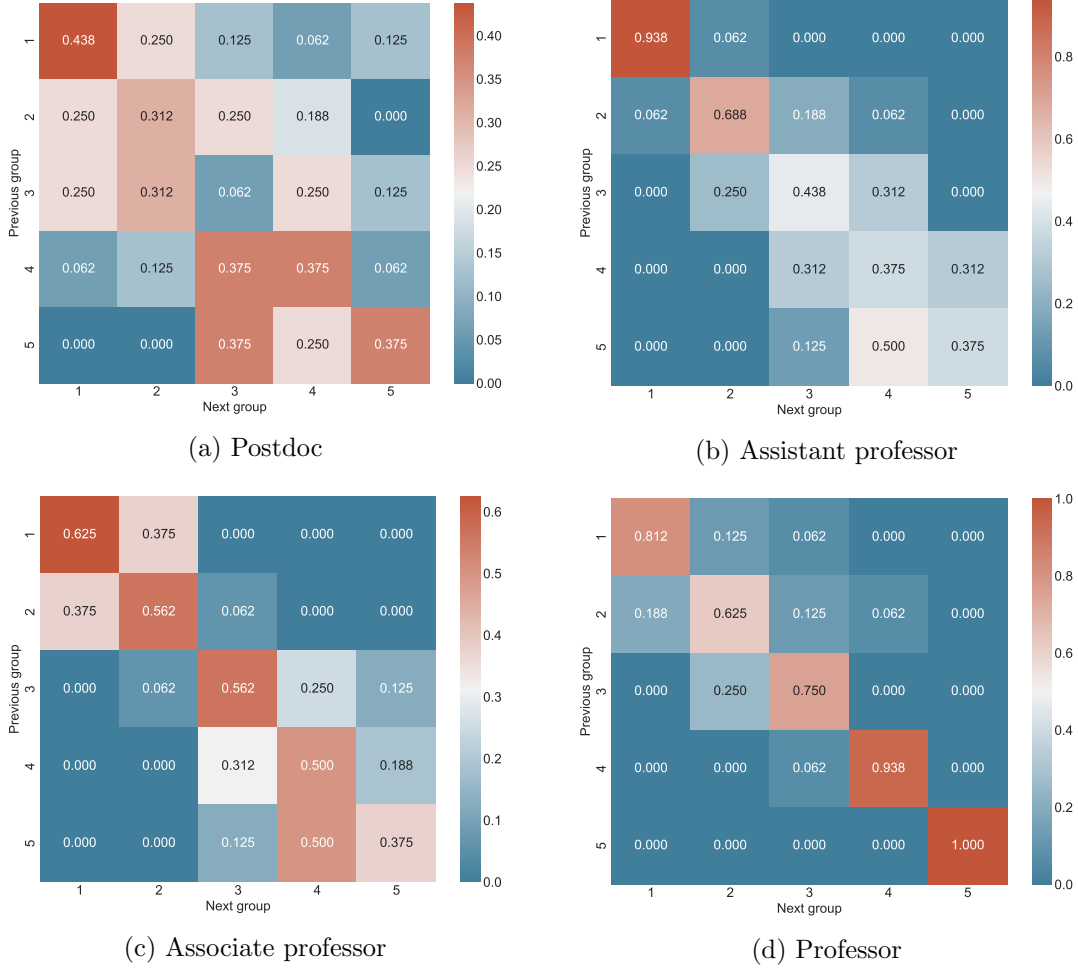


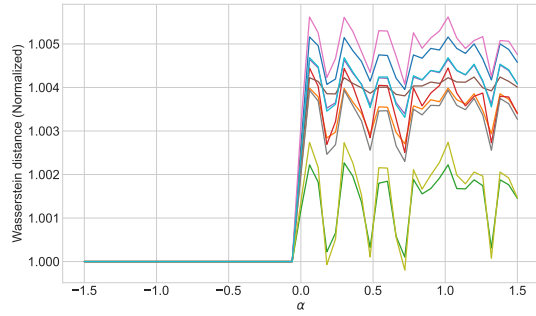
Figure 8: Transition matrices of university rankings.

Figure 9: Transition matrices of wages.

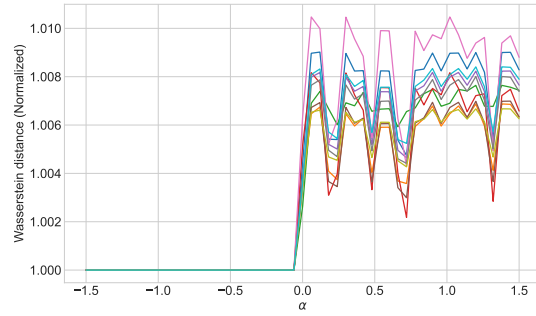


To estimate the transition matrices of wages and university rankings, we use data from 2013 to 2021, the longest period available for UC employee salaries on the Government Compensation in California website. Figure 8 shows that university rankings are stable in this time horizon. Most university ranking transitions happen between the second and the third group. For wages, Figure 9 demonstrates that postdoc wage ranks are relatively unstable over time. The transition matrices become more and more stable when the academic job ranks become higher. The first group with the highest wages is stable among tenure-track and tenured faculty, while it is unstable for postdoc employees.

### C.3 Calibration curves for assistant and associate professors

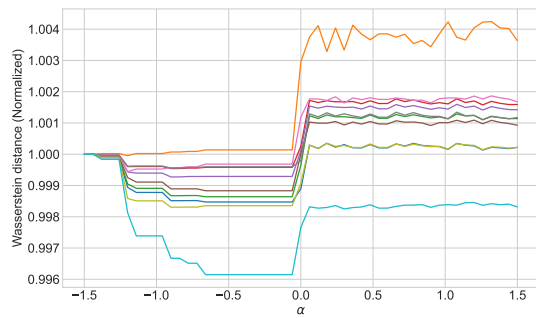


(a) Synthetic data with perfect matching

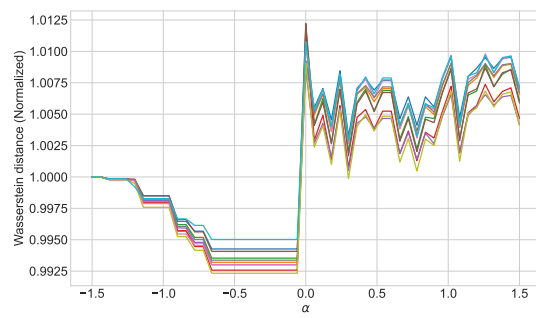


(b) Resampled real data

Figure 10: Calibration curves for B/E/E assistant professors.



(a) Synthetic data with perfect matching



(b) Resampled real data

Figure 11: Calibration curves for B/E/E associate professors.